Master

Distribution Category:
Nuclear Waste Management (UC-70)

ANL-79-99

ARGONNE NATIONAL LABORATORY
9700 South Cass Avenue
Argonne, Illinois 60439

CHEMICAL ENGINEERING DIVISION

FUEL CYCLE PROGRAMS
QUARTERLY PROGRESS REPORT

April-June 1979

by

M. J. Steindler, Milton Ader, R. E. Barletta, J. K. Bates,
C. H. Bean, R. A. Couture, K. F. Flynn, T. J. Gerding,
L. J. Jardine, D. K. Kroeck, Michael Krumpelt,
W. J. Mecham, J. H. Meisenhelder, K. M. Myles,
R. H. Pelto, M. G. Seitz, Seymour Vogler,
and Jacqueline Williams

September 1980

Previous reports in this series

ANL-78-76	April-June 1978
ANL-79-6	July-September 1978
ANL-79-29	October-December 1978
ANL-79-45	January-March 1979

TABLE OF CONTENTS

TABLE OF CONTENTS (contd)

LIST OF FIGURES

LIST OF FIGURES (contd)

LIST OF TABLES

LIST OF TABLES (contd)

CHEMICAL ENGINEERING DIVISION

FUEL CYCLE PROGRAMS
QUARTERLY PROGRESS REPORT

April-June 1979

by

M. J. Steindler, Milton Ader, R. E. Barletta, J. K. Bates,
C. H. Bean, R. A. Couture, K. F. Flynn, T. J. Gerding,
L. J. Jardine, D. K. Kroeck, Michael Krumpelt,
W. J. Mecham, J. H. Meisenhelder, K. M. Myles,
R. H. Pelto, M. G. Seitz, Seymour Vogler,
and Jacqueline Williams

ABSTRACT

In the program on pyrochemical and dry processing of nuclear fuel, work on materials development included the exposure to molten metal and salt followed (usually) by evaluation of the corrosion resistance of: a Mo-0.5% Ti-0.07% Ti-0.01% C alloy, a Mo-30% W alloy, SiC, Si_2ON_2, ZrB_2-SiC, $MgAl_2O_4$, Al_2O_3, AlN, HfB_2, Y_2O_3, BeO, Si_3N_4, nickel nitrate-infiltrated tungsten, tungsten-coated molybdenum, and tungsten metallized alumina-yttria. Work to obtain data for thorium-uranium salt transport processing included measurements of the solubility of thorium in liquid cadmium, defining the prominent features of the Cd-Th binary phase diagram, the obtaining of additional information on the Cd-Mg-Th phase diagram, thorium dioxide reduction experiments, and work on the electrolysis of CaO in molten salt. Work to develop pyrochemical processes and associated hardware for coprocessing uranium and plutonium contained in spent FBR fuels included: completion of a second-generation computer model of the transport process, completion of the turntable transport process design, experimental work on the U-Cu-Mg ternary system, and the determination of uranium and plutonium distribution coefficients between a molten salt and a molten metal. Refractory metal vessels are being service-life tested. The chloride volatility processing of thorium-based fuel was evaluated for its proliferation resistance, and a preliminary ternary phase diagram for the Zn-U-Pu system has been developed by computer calculation. Additional work was done on material characterization and process analysis of the Exportable Pyrochemical process (Pyro-Civex process). Review of literature data on the oxidation of fissile metals to oxides has been completed. Work was continued to establish chemical bases for the reprocessing of actinide oxides in molten salts. Flowsheets are being developed for the processing of nuclear fuel in molten tin.

Work on the encapsulation of solidified radioactive waste in a metal matrix included leach rate studies of crystalline waste materials and evaluation of the impact resistance of metal-matrix waste forms.

In work on the transport properties of nuclear waste in geologic media, the adsorption of strontium on oolitic limestone was studied, as well as the migration of cesium in basalt.

Fitting of data on the adsorption of iodate by hematite to a mathematical model was attempted.

SUMMARY

Materials Development for PDPM. Current experiments indicate that the more promising ceramics for use in PDPM environments are $MgAl_2O_4$, Al_2O_3, AlN, HfB_2, Y_2O_3, BeO, and possibly some Si_3N_4 formulations.

A piece of tube, formed by plasma-spraying tungsten, was nickel, $Ni(NO_3)_2$, infiltrated and heat-treated. Scanning electron microscopy on an earlier heat-treated specimen showed no identifiable surface attack and no intergranular penetration after 120 h of exposure to molten zinc-molten $CaCl_2$-KCl at 800°C.

Two other materials that appear promising for use in PDPM environments are (1) tungsten coatings chemically deposited as vapor and (2) tungsten-metallized alumina-yttria crucibles.

Thorium-Uranium Salt Transport Processing. Measurement of the solubility of thorium in liquid cadmium between 573 and 658°C yielded the linear solubility equation,

$$\log \text{ wt \% thorium} = 3.054 - 1850/T.$$

The slope of this line (log wt % vs. 1/T) differs sharply from that previously reported for thorium solubilities at lower temperatures. Intersection of the two curves occurs at 568°C, which is believed to be the temperature above which $ThCd_{11}$ decomposes peritectically.

Experiments are in progress to obtain data on the Cd-Th and Cd-Mg-Th phase diagrams. Electron microprobe analysis of various Cd-Th alloys annealed at different temperatures has confirmed the existence of $ThCd_{11}$ as an intermediate phase and indicates the probable existence of phases with Cd/Th ratios of 6/1 and 3-4/1. Three different regions of the Cd-Mg-Th system are being examined for information on liquidus contours, intermetallic compounds, and eutectic compositions. In the region represented by the composition

85 wt % Cd-10.5 wt % Mg-4.5 wt % Th,

thorium solubility measurements indicate that the equilibrium solid phase may be similar to $ThCd_{11}$.

A preliminary ternary phase diagram of the cadmium-magnesium-thorium system has been drawn, based on the available data.

The Differential Scanning Calorimeter has been calibrated for heat of fusion measurements, using high-purity metal samples. It will be used to determine the heat of reaction for the peritectic decomposition of $ThCd_{11}$.

In ThO_2 reduction experiments, the total amount of reduction (about 10%) has been less than expected; all reduction took place in the first hour.

Current/potential measurements in an all fluoride salt system (40 wt % LiF-22 wt % CaF_2-38 wt % SrF_2) yielded decomposition potentials which agreed reasonably well with the theoretical decomposition potentials derived from free energy data. Upon the addition of approximately 5 wt % CaO to the all-fluoride system, the decomposition potential on graphite anodes at 780°C was approximately 2.3 V, in very good agreement with earlier results obtained in a 15 wt % CaF_2-$CaCl_2$ salt.

U-Pu Salt Transport Processing. The literature search for the study of Non-Aqueous Separation of Zinc from Fuel Rod Cladding has been completed. A "Scope of Work for Hot Cell Experiments" has been prepared. The second generation computer model Salt II has been completed and debugged. Comparison surveys are being run to identify any differences between the earlier Salt I programs and the Salt II program. The turntable Transport Process (TTP) design is complete, and a topical report, which includes a discussion of the energy and material balances for this facility, is in preparation. With the Salt II program on hand, the Proliferation Study is proceeding rapidly. Experimental work is continuing on the U-Cu-Mg ternary system.

Sampling problems in the proof-of-principle studies have been resolved, and experimentation is under way. Preliminary results for uranium and plutonium distribution coefficients between a molten salt and molten metal phase agree with calculated values. However, the distribution coefficient for americium (an FP-3 stand-in) was an order of magnitude lower than the calculated distribution coefficient for cerium.

The Molten Salt Purification Laboratory has been supplying purified salts for both the Proof-of-Principle studies and the Vessel Fabrication Studies. The "black" salt survey is continuing, and ways of purifying $CaCl_2$ are being studied.

Fabrication of Process-size Refractory Metal Vessels. Work is being concentrated on completing the service-life testing of three crucibles so that a joint report summarizing two years of PDPM material development can be written by Rocky Flats and Argonne National Laboratory. The report on the literature search of tungsten fabrication has been distributed. Metallwerke Plansee estimates that a 14-ft-long transfer line of molybdenum - 30% tungsten tube would cost $12,000.

Heating of molybdenum crucibles that have been CVD-coated with tungsten to 1000°C stress-relieves the bond area without grain growth of the molybdenum. Sintering of nickel-impregnated, plasma-sprayed tungsten in 100% hydrogen or in 25% hydrogen - 75% nitrogen atmospheres results in the same consolidation. Electrochemical grinding of sintered tungsten is considered unsuccessful. The development of ceramic coatings continues at Rocky Flats in a program separate from PDPM.

Chloride Volatility Processing of Thorium-Based Fuels. In evaluating the proliferation resistance of this process, it was determined that altering the volatilization temperature or the condensation temperature could result in separation of fissile material from the fertile material. However, some highly radioactive fission products will be associated with the fissile material, thus making initial misappropriation of the material difficult.

A preliminary ternary phase diagram for the Zn-U-Pu system has been developed by computer calculation, derived from the three binary phase diagrams.

Material Characterization and Process Analysis. The engineering analysis on the Exportable Pyrochemical Process is continuing, and assumptions have been established for the fuel cycle cost analysis. Information has been obtained on fuel cycle costs associated with transportation, waste treatment and storage, fuel element fabrication, and plant decommissioning.

Literature has been obtained on the direct oxidation of uranium, plutonium, and their alloys. A preliminary evaluation of this information indicates that uranium-plutonium alloys probably can be readily oxidized, although very little data are available on the characteristics of the oxide product. If this oxide product has poor sintering characteristics, it appears that an oxidation-reduction treatment can improve its sinterability.

Both alpha boxes have been obtained for Exportable Pyrochemical Process product characterization. One of the alpha boxes has been installed in the mockup area of the hot cell facility, remote manipulators have been installed, and the checkout task has begun.

Molten Salt Processes Applied to Nuclear Fuels. Thermodynamic calculations demonstrate that the equilibrium constant for formation of $UCl_4 \cdot 2AlCl_3$ by UCl_4 in NH_3AlCl_3 is very small. Thus, formation of $UCl_4 \cdot 2AlCl_3$ during the recovery of purified uranium by distillative removal of NH_4AlCl_4 from $NH_4AlCl_4UCl_4$ solutions is not expected to be a problem, despite the volatility of the uranium complex.

Equilibrium measurements show that solutions containing about 50 mol % UCl_4 or $ThCl_4$, 47 mol % LiCl, and only about 3 mol % $AlCl_3$ can be obtained in the dissolution of UO_2 and of ThO_2 in $LiCl/AlCl_3$ melts at 610°C. Hence, thermodynamically, the reaction

$$3AnO_2 + 4AlCl_3(salt) = 3AnCl_4(salt) + 2Al_2O_3$$

is very favorable for the first step of the PROMEX process, the dissolution of oxide fuels in molten LiCl.

Sparging of the melt with a carbon chloride gas is proposed as a possibly useful way of reducing the amount of Al_2O_3 formed during the dissolution of oxide fuel in molten $LiCl/AlCl_3$.

Molten Tin Process for Reactor Fuels. Analysis of the nitride phase formed by nitriding a U/Pu mixture in molten tin shows an increase of the U/Pu ratio of 10.14 compared with a ratio of 4.88 in the initial molten tin. Thus uranium tends to become enriched in the nitride phase and plutonium in the tin phase. A subsequent stage of nitriding at an increased nitrogen pressure would be expected to remove the enriched plutonium in a separate nitride phase.

The rates of nitriding of uranium and thorium have been explored, both separately and as mixtures in molten tin; uranium nitrides at a more rapid rate than does thorium at 700 torr N_2 pressure and 1900 K. At reduced N_2 pressures, uranium does not nitride whereas thorium does, albeit slowly. Thus, conditions can be established whereby either uranium or thorium can be preferentially recovered from molten tin.

The molten tin process presents advantages in terms of nuclear waste disposal by separating out product streams containing (1) gaseous fission products, (2) fission products that are the major decay heat producers, (3) fuel-rich actinides, (4) fuel-depleted actinides, and (5) fission products that are low decay heat producers. These separate streams can be treated differently in terms of storage or end use concepts.

Metal Encapsulation of Radioactive Waste in Metal. High-pressure autoclaves have been used to determine leach rates in aqueous media at elevated temperatures (e.g., up to 300°C). Also, rock-equilibrated aqueous leaching media have been used in order to more nearly approach conditions extant in geologic repositories. Initial results indicate significant but not dramatic differences from results of similar studies using distilled water.

Leach rate studies of crystalline (i.e., SYNROC) waste materials have been initiated. Preliminary results indicate the need for more detailed investigations with more carefully simulated waste forms in order to identify any significant advantages of using crystalline materials.

In continuing work on the evaluation of impact resistance of metal-matrix waste forms, the calculational models developed in the earlier stages of this study were used to interpret preliminary experimental results of impact fracture tests of simulated waste-glass specimens. Surface-area and particle-size data were correlated with impact energy, and comparisons were made with such data on waste glass and similar materials.

Transport Properties of Nuclear Waste in Geologic Media. A porosimeter was employed to examine pore-size distributions in oolitic limestone and two basalts. Very little porosity exists in pores smaller than 20-μm diameter in any of the material studied. (From pores <20 μm diameter the porosity was about 0.25% in the limestone and <0.1% in the basalts.) Even so, the surface area of very fine pores may greatly exceed the fracture surface area of the granulated material; therefore, small-size pores might provide most of the surface for chemical adsorption of radionuclides.

Batch tests to investigate the adsorption of strontium by oolitic limestone revealed that the adsorption is not dependent on prior irradiation of the strontium-bearing groundwater solution or on concentration of strontium in the solution. These findings may considerably simplify a detailed treatment of strontium migration from a repository.

Column-infiltration experiments in which cesium dissolved in a synthetic groundwater solution was passed through basalt showed migration for cesium to be dependent on the cesium concentration in the range 10^{-4} to below 10^{-8}M. This behavior parallels the behavior observed by batch experiments for cesium adsorption on basalt in which partition coefficients were seen to increase with decreasing cesium concentrations.

Trace-Element Transport in Lithic Material by Fluid Flow at High Temperature. Earlier reported isotherms for adsorption of iodate by hematite are found not to be predicted accurately by a regular solution model. Because an ideal solution, which corresponds to a Langmuir isotherm, is a special case of a regular solution, an ideal solution model does not fit either.

I. PYROCHEMICAL AND DRY PROCESSING METHODS PROGRAM
(C. H. Bean, K. M. Myles, and M. J. Steindler)

A. Introduction

A Pyrochemical and Dry Processing Methods (PDPM) Program (Table 1) was established at the beginning of FY 1978 within the Chemical Engineering (CEN) Division, Fuel Cycle Section at Argonne National Laboratory (ANL). Upon redirection of the Fuel Cycle Development Program by DOE for FY 1979, the PDPM Program was included in the Consolidated Fuel Reprocessing Program under the direction of Oak Ridge Operations/Oak Ridge National Laboratory (ORO/ORNL). Under this arrangement, ANL continues to provide PDPM work plans, management plans, and cost plans to the Chicago Operations Regional Office (CORO) for approval as required by DOE. Additional work authorization and agreement forms for each of the PDPM Program subtasks are submitted to the Chicago Operations Office for approval by ORNL. The CEN Fuel Cycle Section continues to provide the technical direction of the PDPM Program.

The PDPM Program provides for the reprocessing of spent fuel by processes that reduce the risk of proliferation of nuclear weapons. The work on this program is being performed at ANL, by other DOE multipurpose laboratories, and by industrial contractors.

B. Management
(C. H. Bean, K. M. Myles, and Seymour Vogler)

The PDPM Management Plan for FY 1979 was completed and was submitted to CORO, ORO/ORNL, and DOE-NPD for review and approval. This plan provides a comprehensive review of the PDPM Program objectives, scope, technical program, organization, management functions, program controls, and supporting documents in conformance with DOE-NPD, CORO, ORO/ORNL, and ANL requirements.

Equipment procurements were reviewed for the PDPM Program for FY 1979, for all work packages at ANL and at all contractor facilities. Priorities were established for items procured at ANL to assure maximum utilization of the limited equipment funds.

A total of $52.8 K for capital equipment was accrued through May 16, 1979. The remaining FY 1979 equipment funds have been committed with the exception of $18 K for one item. This procurement is being postponed to assure budget control until all other items are closed or received.

Representatives from Rockwell International, Atomics International Division, Rocky Flats Plant and Energy Systems Group met with PDPM Management at ANL on June 19, 1979, to discuss criteria for the cost analysis of portions of a commercial zinc distillation process. This study extends the effort initiated by Bechtel Corp. in support of the ORNL evaluation of an exportable pyrochemical process.

Topical reports for the background studies and literature surveys for PDPM Work Packages supported in FY 1978 are being reviewed by PDPM Management. Following this review, the reports will be submitted for final editing and

Table 1. PDPM Work Packages

Work Package No.	ANL Activity	Work Package Title	Location
00	00	Management Planning, Reporting, Costing, and QA	ANL
01	AO	Materials Development for PDPM	ANL
02	BO	Carbide Fuel Processing	ANL
03	CO	Thorium-Uranium Salt-Transport Processing	ANL
04	DO	Uranium-Plutonium Salt-Transport Processing	RI-RF[a]
05	EO	Fabrication of Process-Size Refractory Metal Vessels	RI-RF
06	FO	Aluminum Alloy Processing of Thorium- and Uranium-Based Fuels	IRT[b]
07	GO	Chloride Volatility Processing of Thorium-Based Fuels	B&W[c]
08	HO	Material Characterization and Process Analysis	RI-AI[d]
09	JO	Molten Nitrate Salt Oxidation Processes	PNL[e]
10	KO	Molten Salt Processes Applied to Ceramic Fuels	ORNL[f]
11	LO	Reprocessing of Thoria-Urania Fuel in Molten Salts Containing $ThCl_4$	AMES[g]
12	MO	Molten-Tin Process for Reactor Fuels	LLL[h]
13	NO	Engineering Support for PDPM Processes	ANL

[a] Rockwell International - Rocky Flats.

[b] IRT Corporation.

[c] Babcock & Wilcox.

[d] Rockwell International - Atomics International.

[e] Pacific Northwest Laboratory.

[f] Oak Ridge National Laboratory.

[g] Ames Laboratory.

[h] Lawrence Livermore Laboratory.

publication as a series of ANL topical reports. Annual reports and final summary reports are scheduled for review following review of these topical reports.

The Nuclear Fuel Cycle Division and Materials Science and Technology Division of the American Nuclear Society cosponsored a special session on pyrochemical reprocessing at the 25th Annual Meeting in Atlanta on June 5, 1979. Six papers were presented based on work supported by DOE for the PDPM Program.

C. Engineering Analysis and Separations Process

1. Materials Development for PDPM

(R. M. Arons* and J. Y. N. Wang*)

The project objectives are (1) to anticipate, identify, and scope potential materials or materials fabrication problems that may limit the practical realization of candidate processes in the PDPM program; (2) to devise through analytical and experimental methods, means to resolve these problems; (3) to assess the refabricability of the fuel after reprocessing; and (4) to provide program support to the PDPM Program Office by coordinating materials activities and by lending technical assistance within the program.

a. Engineering Analysis

(R. M. Arons* and J. Y. N. Wang*)

The corrosion of molybdenum-tungsten alloys in liquid zinc at 455°C for one year has been examined recently in Austria [ECK]. The alloys were produced by one of two methods: (1) vacuum arc melting or (2) powder metallurgy pressing and sintering. The resistance of these alloys to molten zinc was independent of the method of production. Resistivity of Mo-30% W alloy is practically unlimited at this temperature. The Mo-10% W alloy shows measurable corrosion rates. The weight loss of pure molybdenum is about ten times that of Mo-10% W. The Mo-5% W alloy showed the highest corrosion rate of all specimens tested.

Recently, we have investigated tungsten sintering as an alternative method of fabricating large tungsten crucibles. The activation of sintering in tungsten by use of nickel or palladium was well studied 12 years ago by Toth and Lockington [TOTH] and supplemented earlier work by Brophy and coworkers (see, for example, [BROPHY]). In this work, Toth impregnated cold-pressed tungsten bars with alcohol solutions of $NiCl_2 \cdot 6H_2O$ or $PdCl_2 \cdot H_2O$, followed by a drying cycle and firing in pure hydrogen for times between 5 and 240 min at temperatures between 850 and 1200°C. It was found that increasing the amount of activator metal strongly increased the sintering rate, but that beyond a certain concentration of additive, the sintering rate was slightly lowered. The presumption was that the optimum activator concentration corresponded to a monoatomic layer of activator on the surface of the

---

*Materials Science Division, Argonne National Laboratory.

tungsten particles. Thus, they concluded that the mechanism of sintering enhancement was the movement of tungsten atoms through a series of steps in which surface diffusion of tungsten on the surface of the activator was rate-controlling. This conclusion was supported by the observation that the activation energy measured for activator-enhanced sintering was well below that for tungsten volume diffusion and lay between that of surface diffusion and grain-boundary diffusion. It is not known why nickel or palladium has the power to extensively modify the surface of tungsten or the surface diffusivity. [TOTH] also observed segregation of the activators to the grain boundary and an embrittlement of the metal, leading to intergranular fracture.

b. Experimental

(1) PDPM Environmental Test Facility (PETF)
(R. M. Arons,* D. J. Dorman,* J. Y. N. Wang,* R. R. Schlueter,* and L. J. Marek*)

As reported in the preceding quarterly progress report [STEINDLER-1979C], a final pump design has been successful in the two-phase (liquid metal and fused salt) corrosion testing of potential PDPM hardware construction materials. This new design, comprising a graphite pump housing, tantalum drive shaft and impellers, and polished alumina journal bearings, has been operated for 120-h tests, with little apparent degradation. We expect to make additional tests of coupons using this type of apparatus.

A second type of apparatus has been designed for the service testing of crucibles. The crucible test rig is identical to the coupon testing apparatus [STEINDLER-1978B, -1979A], except that the housing or shroud does not extend into the melt, but instead extends to just above the melt, providing support for the rotating impeller shaft. Operation of this apparatus has been relatively trouble-free, owing to both its simplicity (compared to the coupon tester) and the design experience gained in the fabrication of the coupon tester.

A rocking furnace which was used in an earlier ANL Materials Science Division project has been converted for PDPM corrosion testing. The furnace can rock about 180°C and then return to its original position to expose an entire specimen to both molten metal and salts at a rate of six cycles per minute.

A 3/4-in.-ID seamless tantalum tube was chosen as the container capsule for two reasons: (a) it is presently available in our stock and (b) prior testing [STEINDLER-1979C] has shown it to be resistant to molten metal and salts at the temperatures of interest. Weighed amounts of furnace-dried $CaCl_2$, KCl, and zinc are loaded along with the molybdenum test specimens into the container tube in a helium-filled dry glove box. The tantalum tube is sealed under a helium-purged partial vacuum and then encapsulated in a Type 304 stainless steel tube under an argon atmosphere to protect the tantalum from air oxidation.

---

*Materials Science Division, Argonne National Laboratory.

(2) Metallic Materials
(J. Y. N. Wang* and L. J. Marek*)

Both as-rolled and recrystallized TZM (Mo-0.5% Ti-0.07% Zr-0.01% C) specimens were exposed to a mixture of molten zinc and $CaCl_2$-50 wt % KCl salt at about 800°C. The as-rolled material contains a dispersion of fine precipitates. After about 120 h of testing under an argon atmosphere, both specimens displayed higher corrosion rates than pure molybdenum under similar test conditions. Deep grain-boundary penetrations in the recrystallized specimen were clearly visible. TZM alloy will not be further considered as PDPM material.

Energy-dispersive X-ray emission spectrometry has been widely used for analysis of posttest corrosion specimens. Because of problems caused by overlapping of adjacent spectral lines, ambiguous results are often obtained. In the later part of this quarter (June 1979), the evaluation of penetration and diffusion of molten metal species into the base metal using wavelength-dispersive X-ray emission spectrometry was attempted. This technique permits the desired peaks to be clearly separated owing to extremely high wavelength resolution.

A Mo-30% W alloy was exposed to molten zinc and $CaCl_2$-50 wt % KCl at 800°C for 120 h. The specimen was sectioned and the newly exposed area was analyzed by the wavelength technique to determine zinc diffusion as a function of distance from the surface exposed to molten zinc. A pure zinc standard was used as reference (100% Zn). Each analysis was calibrated against the zinc standard and recorded as wt % Zn actually present at the location analyzed. Despite some minor difficulties, the initial results were encouraging. This work will be continued.

Recrystallized and as-rolled molybdenum and molybdenum alloys were encapsulated with zinc and KCl-50 wt % $CaCl_2$ mixture and assembled in the rocking furnace (described above) during the final week of June. This test will continue for a minimum of 500 h.

(3) Ceramic Materials
(R. M. Arons* and D. J. Dorman*)

As previously reported [STEINDLER-1979C], five SiC samples were tested for 120 h at 800°C in a tungsten vessel containing an agitated mixture of molten zinc and fused $CaCl_2$-KCl eutectic. Of the five, one had been prepared by chemical vapor deposition (CVD) and the others by four variations of hot pressing. The CVD sample and three of the hot-pressed samples showed negligible weight loss. SEM microscopy showed no evidence of corrosion or infiltration of the corrodents into the SiC. The fifth sample showed a 1% weight gain. SEM analysis showed some porosity, but no apparent corrosion products. The weight gain may have been due to slight infiltration by corrodents or moisture; however, X-ray analysis showed no evidence of Zn, Ca, or K, and moisture retention is unlikely since the sample was baked at 120°C in vacuum prior to weighing.

---

*Materials Science Division, Argonne National Laboratory.

A similarly tested Si_2ON_2 specimen showed a considerable weight loss (5%), corresponding to a corrosion rate of 2 mils/120 h or an extrapolated equivalent of 146 mpy. Visual observation of the surface showed a color change from light gray in the virgin material to dark brown in the corrosion-tested material. SEM and X-ray analysis showed a corrosion product rich in either Cu or Ta (the two elements are virtually indistinguishable in energy-dispersive analysis). Since there is no potential source for Cu, one must conclude that tantalum from the corrosion test apparatus hardware formed a compound or solution with the Si_2ON_2.

A wide range of other ceramic materials have been tested in the previously described zinc and salt systems, and the results are outlined in Table 2. As indicated in the table, all ZrB_2 or ZrB_2-SiC composite materials formed thick surface corrosion layers, which readily spalled in four cases. All specimens with spalling surface layers showed multiple spallation layers, as graphically indicated in Fig. 1. The existence of more than one spalled layer indicates that spallation took place in the corrosive bath and not on cooldown or other thermomechanical transients. This repetitive spallation under steady-state conditions is characteristic of a very unstable system because the product layer affords no protection to the bulk, and is indicative of a system in which the specific volume of the surface product differs from that of the bulk. SEM examination of the ZrB_2-SiC specimens with X-ray analysis shows the scale to be richer in zirconium than the bulk,

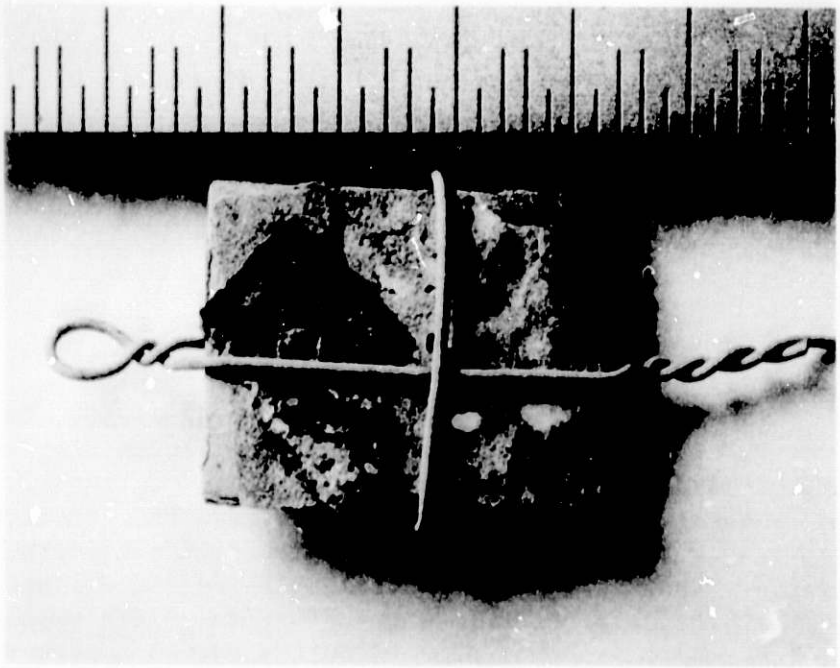

Fig. 1. $ZrBr_2$-SiC Specimen after Exposure at 800°C for 120 h to Zn and $CaCl_2$-KCl. Wire wrapped around specimen is used to fixture specimen during testing. (Scale marker is 1 mm per division.) ANL Neg No. 306-79-689

Table 2. Corrosion at 800°C for Selected Ceramics in Agitated Mixtures of Molten Salt and Metal

Material	Form	Weight Loss, %	mils/120 h	mpy	Comments
$MgAl_2O_4$	Hot Pressed	0.18	0.10	7.3	
MgO	Sintered	24.38	a	a	Gross surface attack
MgO	Hot Pressed	3.25	3.5	252	Gross surface attack
Al_2O_3	Refractory Brick	0.44[b]	0.24	17.2	
Al_2O_3	Hot Pressed	0.047	0.059	4.3	
Al_2O_3	Hot Pressed	0.083	0.057	4.2	
ZrO_2	Sintered	3.86	2.1	155	
ZrB_2	Hot Pressed	7.49	3.5	258	Spalling surface product
ZrB_2-SiC	Hot Pressed	2.49	1.2	85.8	Spalling surface product
ZrB_2-SiC	Hot Pressed	8.61	4.9	359	Spalling surface product
ZrB_2-SiC	Hot Pressed	5.73	3.6	263	Spalling surface product
Zrb_2-SiC	Hot Pressed	65.1	30.8	2245	Thick surface product
Si_3N_4	MgO Hot Pressed	2.77	1.5	111	
Si_3N_4	Y_2O_3 Hot Pressed	1.08	0.7	52.9	
AlN	Hot Pressed	0.10	0.045	3.3	
HfB_2	Hot Pressed	0.77	0.45	33.1	Spalling surface product
Y_2O_3	Hot Pressed	0.0013	0.001	0.056	
BeO	Hot Pressed	3.16	0.50	36.4	

[a] Gross pitting and internal attack; surface loss rate meaningless.

[b] Sample was friable; some weight loss may be mechanically induced.

suggesting that a silicon compound is selectively leached. This is not understood at present since SiC is known to be stable in the environment in question.

The experiments performed this quarter show that the more promising ceramics are $MgAl_2O_4$, Al_2O_3, AlN, HfB_2, Y_2O_3, BeO, and possibly some Si_3N_4 formulations.

Tests performed in the preceding quarter [STEINDLER-1979C] showed that SiC and graphite are also resistant to the zinc and salt environment.

(4) Plasma-sprayed Tungsten
(R. M. Arons*)

Two 7.62-cm by 7.62-cm (3-in. by 3-in.) cylindrical crucibles were formed by plasma-spraying tungsten on a graphite mandrel and then were sent to Rocky Flats for heat treating. These crucibles were infiltrated with nickel nitrate (in contrast to nickel chloride in previously reported experiments [STEINDLER-1979C]) and heat-treated in pure H_2 for 1 h at 1000°C and for 3 h at 1300°C. After they were heat-treated, these crucibles were returned to ANL for critical evaluation and corrosion testing. Dimensional changes upon firing were as follows: height change ranged from 3.51 to 4.16% shrinkage, diameter change ranged from 3.35 to 3.46% shrinkage, and wall thickness change ranged from 25.7 to 31.4% shrinkage. These results are in agreement with the previous findings [STEINDLER-1979C] that most consolidation occurs in the direction of prior spraying.

A 1-in.-OD tungsten tube was also sent to Rocky Flats to test the effect on consolidation of the atmosphere composition during firing. This tube was infiltrated with nickel nitrate and fired under a similar heating schedule as described above, but in a 25% H_2-Ar atmosphere. Metallography at ANL indicates that this tube was also fully consolidated and that 25% H_2 is apparently an acceptable heat-treating atmosphere.

A piece of tungsten tube heat-treated at ANL and previously described [STEINDLER-1979C] was tested in a zinc and $CaCl_2$-KCl environment for 120 h at 800°C. This tube shows no apparent attack metallographically, and a negligible weight gain. SEM examination of a polished cross section of this piece (Fig. 2) shows no identifiable surface attack and no intergranular penetration. (Existing surface roughness is an artifact of fabrication.) In addition, no corrodent species could be found in the tungsten by X-ray analysis.

One of the 7.6-cm by 7.6-cm crucibles described above was also corrosion-tested as a container for an agitated mixture of molten zinc and fused $CaCl_2$-KCl at 800°C for 225 h. After the crucible was cleaned in water and HCl to remove the salt and zinc, no evidence of attack other than minor surface staining was observed. Weight loss of the crucible was equivalent to an attack of 0.096 mil/225 h or an extrapolated equivalent of 3.7 mpy.

---

*Materials Science Division, Argonne National Laboratory.

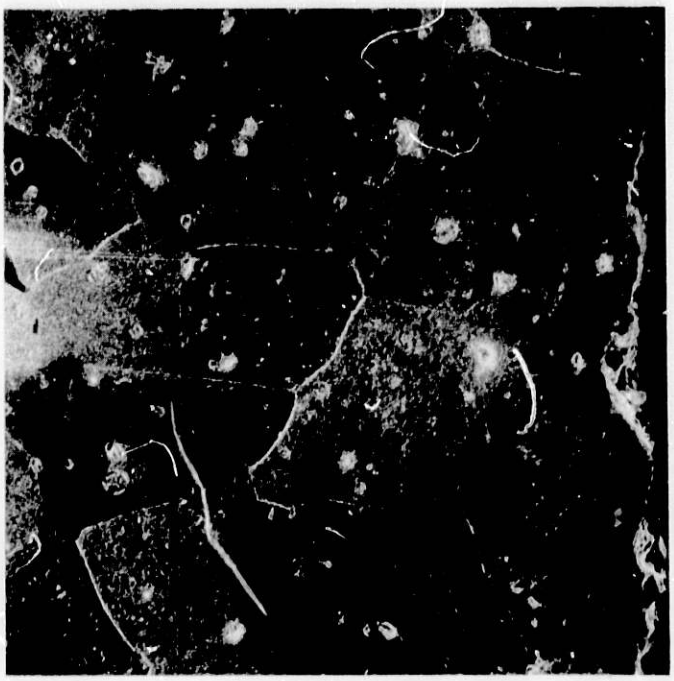

Fig. 2. SEM Micrograph of Polished Cross Section of Plasma-sprayed and Nickel-treated Tungsten after Exposure to Zn and $CaCl_2$-KCl at 800°C for 120 h. Magnification, 1200X. ANL Neg. No. 306-79-690

These results appear to be most promising and to indicate that plasma spraying can be used to fabricate both protective coatings and monolithic components such as crucibles and tubing for use in PDPM environments.

(5) Tungsten CVD Coatings
(R. M. Arons* and C. Edstrom†)

Segments of molybdenum spin-formed crucibles were sent to an outside vendor by C. Edstrom of Rocky Flats for the deposition of a tungsten liner by chemical vapor deposition (CVD) methods after which a series of six specimens (portions of these segments) with various thermomechanical histories was then sent to ANL for metallographic examination in order to allow recommendation of an optimum fabrication schedule. Parameters of interest were surface finish prior to tungsten deposition and heat-treatment temperatures after deposition. The heat treatments used included (1) no treatment, (2) annealing in vacuum at 1000°C for 16-20 h, and (3) annealing in vacuum at 1200°C for 16-20 h.

---

*Materials Science Division, Argonne National Laboratory.

†Rockwell International - Rocky Flats.

It was found that the tungsten layer is not affected by prior surface finish or heat treatment. This layer consisted of large grains of high grain aspect ratio (GAR) parallel to the deposition direction. In some cases, these grains may extend the entire coating thickness.

The effect of prior surface finish was unobservable metallographically except that one specimen of high interfacial roughness displayed some minor interfacial porosity. One may surmise that high surface roughness may promote tungsten adhesion, but this hypothesis was not tested.

Heat treatment had a profound effect on the molybdenum substrate. The nonheat-treated specimens showed an as-drawn grain structure of moderately sized grains, slightly elongated in the circumferential direction, with fine highly disturbed grains at the interface where the molybdenum had been machined prior to tungsten deposition. The specimens treated at 1000°C showed somewhat coarser equiaxed grains, with complete relief of the disturbed machined surface. The 1200°C specimens showed gross grain growth, indicating excessive heat treatment.

It is our recommendation that the intermediate anneal, i.e., 1000°C for 16-20 h, is optimal. The somewhat finer grain size should provide a strengthening effect and the lesser extent of grain growth will possibly enhance intergranular strength (due to less "sweeping" of impurities to the grain boundaries). The untreated condition is probably undesirable due to the high apparent strains at the interface, which may promote delamination of the coating.

(6) Tungsten Metallization

(R. M. Arons* and J. T. Dusek*)

Two tungsten-metallized alumina-yttria crucibles were fabricated for corrosion testing in zinc and $CaCl_2$-KCl at 800°C. One crucible was sectioned, and a coupon was tested in the zinc and salt environment for 120 h. The observed weight change (after testing, cleaning in water, and cleaning in dilute HCl) was negligible and no degradation was observed. Figure 3 shows a cross section of the exposed surface of this coupon after testing. No attack of the tungsten layer is observed; no permeation of the zinc or salt into the coating has taken place. Posttest integrity of the coating and the coating-substrate interface is excellent.

A second crucible was tested in its original configuration as a container for an agitated zinc and salt mixture at 800°C for 250 h. The crucible was cooled, then rinsed in water to remove the salt layer, then sectioned without zinc removal. Macroscopic examination showed the crucible to be in excellent condition, and no degradation in the form of cracking or spallation of the coating was observed. SEM examination (Fig. 4) showed no apparent surface degradation and no permeation of corrodents into the coating. A zinc X-ray map of the same area shows all zinc to be at the outer surface and the tungsten coating.

---

*Materials Science Division, Argonne National Laboratory.

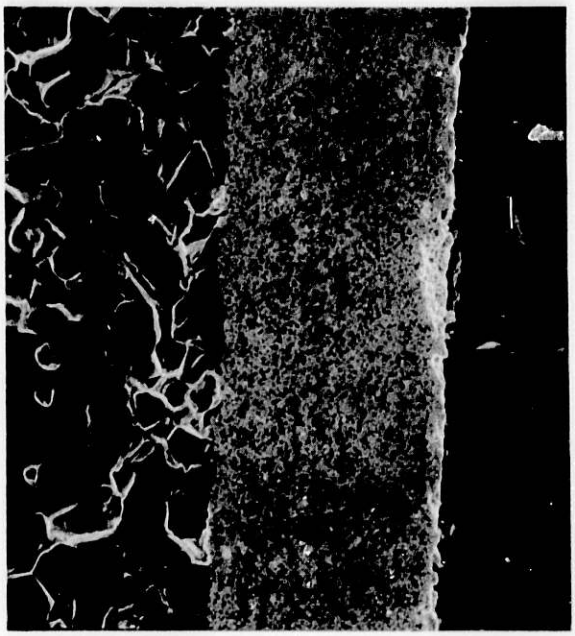

Fig. 3. Cross Section of Tungsten Metallized Layer (Center) on Alumina-Yttria Substrate (Left) after Exposure to Zn and $CaCl_2$-KCl for 120 h at 800°C. (Area on the right is mounting material.) Magnification, 600X. ANL Neg. No. 306-79-691

(7) Publications

R. M. Arons and J. W. Hafstrom, Ceramic Hardware for Use in the Pyrochemical Reprocessing of Nuclear Fuels, presented at the 81st Annual Meeting, American Ceramic Society (paper). Abstract published in Ceram. Bull. 58, 3 (1979).

R. M. Arons, J. T. Dusek, and J. W. Hafstrom, Development of Tungsten Coatings for the Corrosion Protection of Ceramics, presented at the International Symposium on Metallurgical Coatings held at the Sixth International Vacuum Metallurgy Conference in San Diego, CA, April 23-27, 1979.

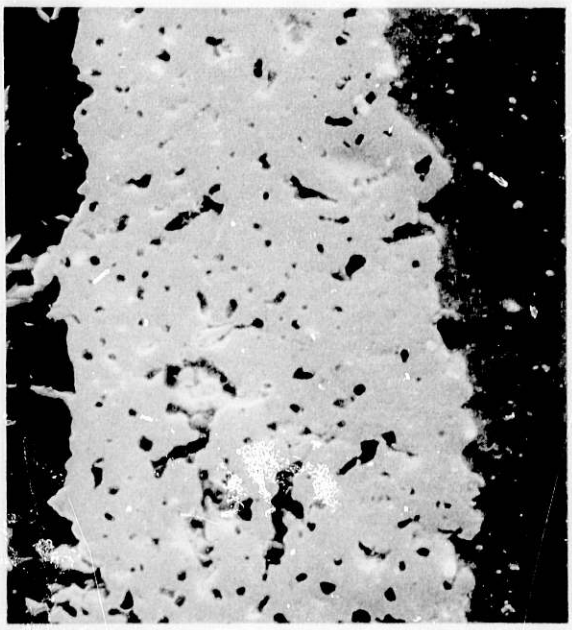

(a)

(b)

Fig. 4. (a) Tungsten-Metallized Layer (Middle) on Alumina-Yttria Substrate (Far Left) after Exposure to Zinc and $CaCl_2$-KCl at 800°C for 120 h. Solidified zinc (right) is still in contact with the tungsten. (b) Zinc X-ray Map Illustrating the Lack of Zinc Permeation into the Tungsten Layer. (a) Magnification, 1500X. (b) Magnification, 1500X. ANL Neg. No. 306-79-691

2. Thorium-Uranium Salt-Transport Processing

(M. Krumpelt, Milton Ader, R. E. Barletta, J. K. Bates, T. J. Gerding, D. K. Kroeck, and J. H. Meisenhelder)

Pyrochemical processes involving salt-transport and metal precipitation steps are currently being investigated for use in projected thorium-based fuel cycles. The reference flowsheet (Fig. 5) has been designed to meet proliferation standards and is applicable to plutonium-thorium transmuter and undenatured thorium-uranium breeder fuels. The necessary criteria are that the fissile and fertile streams be coprocessed (Th:Pu-U of 4:1) and be diversion resistant as a result of the inclusion of some fission products.

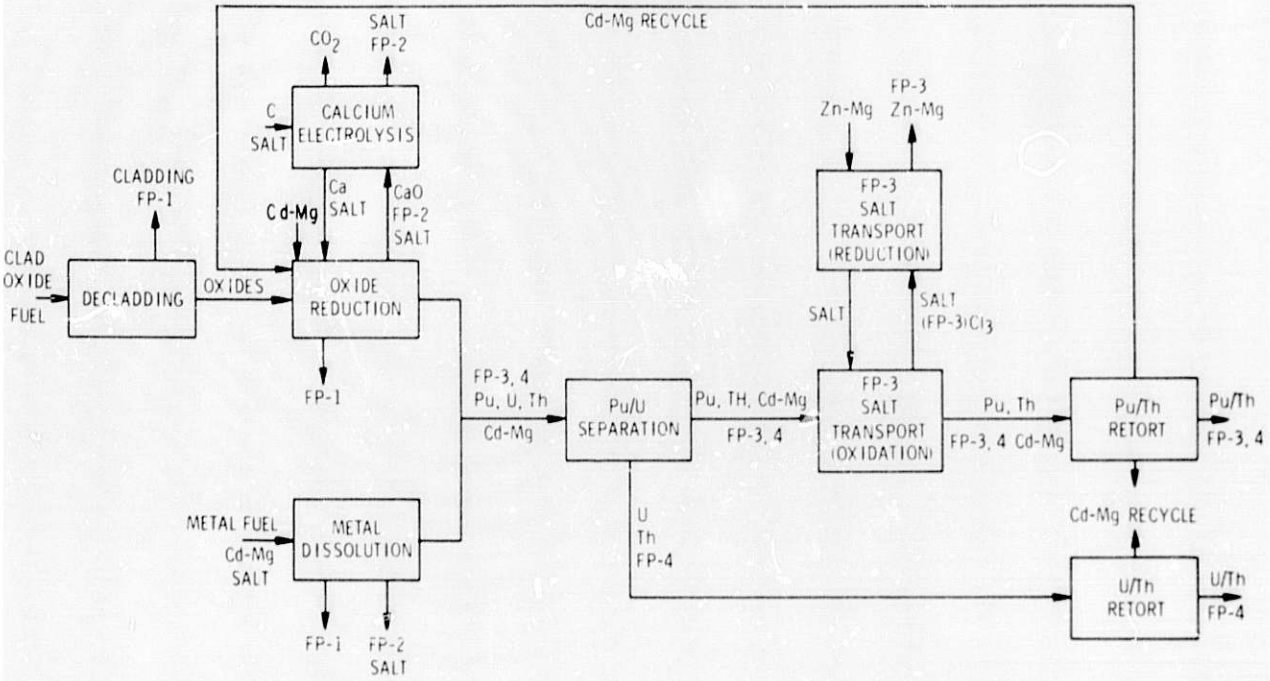

Fig. 5. Conceptual Flowsheet for Thorium-Based Fuels. FP-1: Xe, Kr, ^3H; FP-2: I, Br, Cs, Rb, Ba, Sr, Sm, Eu, Se, Te; FP-3: trivalent rare earths, Y; FP-4: Zn, Nb, Mo, Tc, Ru, Rh, Pd, Hg, Cd, In, Sn, Sb

a. Solubility Studies

The main process separation step requires that thorium be partitioned between the plutonium (which is soluble in Cd/Mg alloys) and the uranium (which is insoluble in Cd/Mg alloys). Thorium solubility measurements have been made for the ternary system, Th-Mg-Cd, to permit selection of the proper process conditions. Studies to identify the solid phases precipitating from solutions of different compositions continue, with the ultimate aim of defining the phase diagram.

(1) Solubility of Thorium in Cadmium
(Milton Ader and J. H. Meisenhelder)

Measurements of thorium solubility in liquid cadmium between 327 and 568°C were reported by Bates in [STEINDLER-1979C]. These solubilities represent liquidus compositions of the binary phase diagram, the equilibrium solid phase being $ThCd_{11}$. The solubility data have now been extended to 658°C and show that $ThCd_{11}$ decomposes peritectically at about 568°C to yield a less cadmium-rich intermediate phase, which has not yet been identified.

The current measurements (Exp. MA-2) were carried out in tantalum equipment under helium pressure (1-2 atm). The procedure involved stirring an initial mixture of 720 g of cadmium and 30 g of thorium at about 550°C for about 1 h and then stirring at the first sampling temperature, 508°C, for about 1.3 h. Stirring was stopped, and the liquidus phase was sampled by pressurization through a tantalum frit (35-μm porosity) press-fitted into a temperature-equilibrated tantalum tube. Then, a routine of adding more thorium, stirring at different temperatures for 1.3 to 1.8 h, and sampling the liquid phase was repeated several times. Equilibrium was approached from both higher and lower temperatures, and the nominal concentration of thorium always exceeded its solubility. The first two determinations were made at relatively low temperatures (508 and 536°C) to test the agreement of our measurements with those previously reported.

The experimental results are listed in Table 3 and are plotted as log wt % thorium solubility versus reciprocal absolute temperature in Fig. 6. A dashed straight line* representing the least-squared solubility data of Bates is also included. The six data points between 573 and 658°C were least-squared to yield the linear solubility equation,

$$\log \text{ wt \% thorium} = 3.054 - 1855.0/T \quad (\text{std. dev.} = 3.6\%)$$

The intersection of this line with the lower-temperature dashed line in Fig. 6 is calculated to occur at 568°C. This result agrees fairly well with (a) a thermal halt at 566 ± 2°C observed several times during the solubility experiment and (b) previously reported thermogravimetric experiments [STEINDLER-1979C] in which $ThCd_{11}$ was found to decompose at 569 ± 2°C. From earlier work at Argonne [LAWROSKI] the equilibrium solid phase in this region of the Cd-Th system between 321 and 568°C appears to be $ThCd_{11}$. If $ThCd_{11}$ behaves like $NpCd_{11}$ [KRUMPELT], $PuCd_{11}$ [JOHNSON-1965], and $CeCd_{11}$ [JOHNSON-1966], the above-mentioned termal halts at 566 and 569°C could be attributed to the peritectic reaction

$$ThCd_{11}(c) \rightleftarrows ThCd_6(c) + 5\ Cd(l, satd)$$

Efforts are being made to verify this reaction and to identify other intermediate phases in the Cd-Th system.

---

*Calculated from Table 3 of [STEINDLER-1979C] as log wt % thorium = 7.445 - 5548.9/T.

Table 3. Solubility of Thorium in Cadmium. Experiment MA-2

Sample	Temp, °C[a]	Thorium Solubility	
		Wt %[b]	At. %[b]
2A	508	2.01	0.98
3B	536	3.78	1.87
5A	598	8.03	4.06
6A	573	7.49	3.77
7A	637	10.04	5.13
8B	615	9.43	4.80
9A	644	10.93	5.61
11A	658	11.74	6.05

[a]Estimated accuracy, ±2°C.

[b]Mass isotopic dilution analysis; estimated accuracy, ±2% relative.

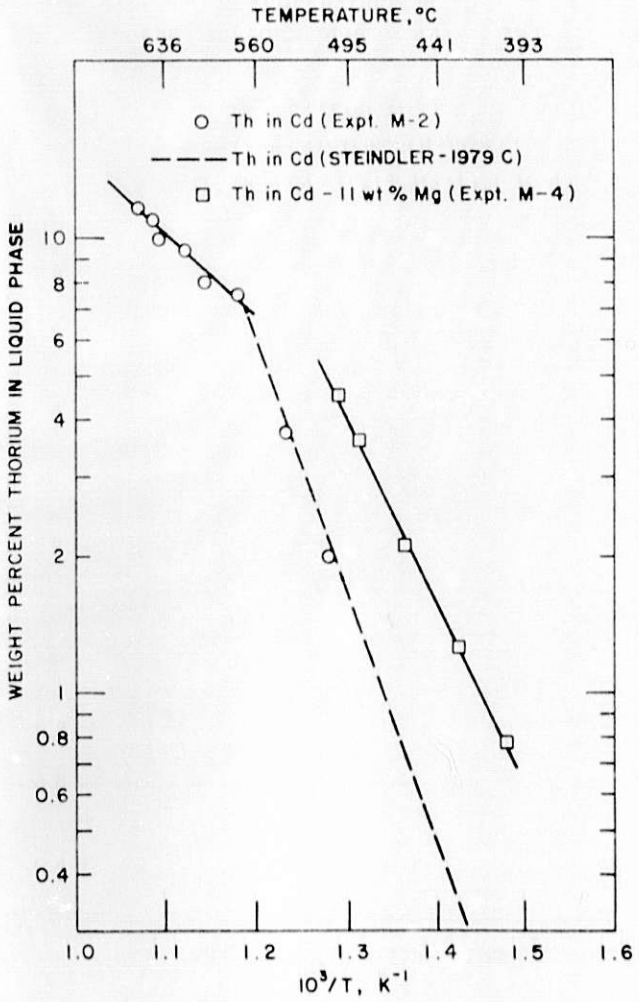

Fig. 6. Thorium Solubilities in Cadmium and Cadmium-Magnesium

(2) Intermediate Phases in the Cd-Th System
(Milton Ader)

Experiments to define prominent features of the Cd-Th binary phase diagram are in progress. Electron microprobe analysis* has been used to obtain preliminary information concerning the compositions of intermediate phases.

An initial attempt to identify the solid phase resulting from the decomposition of $ThCd_{11}$ above about 568°C was made during Exp. MA-2. A duplicate of sample MA2-11 (see Table 3) taken at 658°C was cooled over a 1-h interval to 580°C (i.e., about 12 centigrade degrees above the peritectic decomposition temperature) and then quickly quenched to room temperature. The solidified melt was sectioned, cast into an epoxy mold, polished, and examined with the electron microprobe. The analysis revealed a crystalline phase which had a Cd/Th atomic ratio of 3.3 to 3.7 and was surrounded by Cd and $ThCd_{11}$ (matrix) phases. The absence of $ThCd_6$ and the presence of about $ThCd_{3.5}$ were unexpected.

Next, mixtures of cadmium and thorium, with Cd/Th atomic ratios ranging from 13 to 2, were sealed in 1.3-cm-dia by 7.6-cm long tantalum capsules under 1-atm helium pressure. The capsules were heated at different temperatures for various intervals without agitation. At the end of the heating periods, the melts were quenched to about 300°C within about 3 to 4 min and then slowly cooled to room temperature. Finally, the capsules were sectioned and prepared for electron microprobe analysis (Table 4). It should

Table 4. Electron Microprobe Analysis of Cd-Th Alloys

Capsule No.	Cd/Th Atomic Ratio	Equilibrium Temp, °C	Heating Time	Phase, Cd (wt %) - Th (wt %)
5	13	545	17 d	1, Cd(84) - Th(16) 2, Cd(100) - Th(<0.5) 3, Cd(64-75) - Th(36-25)
1	7	1000	21 h	1, Cd(83) - Th(16) 2, Cd(59-64) - Th(40-36)
7	4	650	14 d	1, Cd(<0.2) - Th(100)[unreacted Th] 2, Cd(100) - Th(<0.4) 3, Cd(74-66) - Th(26-34)

*Analysis by W. A. Shinn, Fuels and Materials Chemistry Group, Chemical Engineering Division, Argonne National Laboratory.

be noted that, except for capsule 5, essentially no crystalline material was observed in these preparations presumably because of the rapid quenching. In general, capsules heated below 1000°C still contained untreated thorium metal; this is indicative of slow reaction and slow diffusion. It was also observed during grinding and polishing that the Cd-Th alloys, especially mixtures having Cd/Th ratios of 7 or less, were sensitive to moisture and air. Unfortunately, no inert-atmosphere facility where radioactive samples could be polished was available. Therefore, an inert coolant (kerosene) and extender (Hyprez Oil) were used during grinding and polishing, and polished specimens were stored in an evacuated or a helium-filled desiccator. The results of three of the capsule experiments are discussed below.

Capsule 5. The predominant phase is phase 1, whose composition approximates $ThCd_{11}$ (15.8% Th, 84.2% Cd). Also present are phase 2, pure cadmium and phase 3, a phase of variable composition (Cd/Th = 3 to 6). The compositions of phases 1 and 2 are those that would be expected from the starting Cd/Th ratio and the equilibration temperature.

Capsule 1. Phase 1 is apparently the matrix and has a Cd/Th ratio of about 10.5. This is possibly the $ThCd_{11}$ phase showing a wide homogeneity range. Within this matrix are grains of phase 2 with Cd/Th ratios between 3.1 and 3.7. The phase of these grains may be that observed in solubility experiment MA-2.

Capsule 7: The center of the alloy contained a long sliver of the original unreacted thorium metal, phase 1. Around it was a very fine-grained reaction layer which was not analyzed because of difficulty of keeping the electron beam focused on the tiny grains. Surrounding this reaction layer were stringers of cadmium, phase 2, parallel to the unreacted thorium. Beyond the stringers of cadmium were numerous grains, namely, phase 3, having Cd/Th ratios close to those of $ThCd_6$ and $ThCd_4$.

The electron microprobe data indicate the existence of $ThCd_{11}$, $ThCd_6$, and $ThCd_{3-4}$ as intermediate phases in the Th-Cd system, although some of the results are difficult to reconcile with the experimental conditions. Additional experiments of this type are being carried out under conditions which, it is hoped, will promote the attainment of equilibrium. X-ray diffraction analysis will be used to supplement the microprobe results.

(3) Cadmium-Magnesium-Thorium System
(Milton Ader and J. H. Meisenhelder)

Additional information is being obtained on the Cd-Mg-Th ternary phase diagram. Three different regions of the ternary system were selected for studies of liquidus contours, equilibrium intermetallic compounds, and eutectic compositions. An initial, representative composition for each region was prepared by stirring the three components (using tantalum equipment and a helium atmosphere) at a high enough temperature to solubilize the metals. The melt was then gradually cooled with stirring, and filtered samples of the liquid phase were removed at several temperatures for compositional

analysis. Finally, the freezing-point range of the solidifying (eutectic) liquid was noted. The conditions and results of the experiments are listed in Table 5. Precipitation of a thorium-containing phase in each of the selected regions was achieved, although in Expt. MA-5, probably only the last or last two liquid samples were saturated with thorium.

Table 5. Liquidus Compositions in the Cadmium-Magnesium-Thorium System

Sample	Temp, °C	Time at Temp, min	Liquid Phase Composition,[a] wt %			
			Cd	Mg	Th	Total
Expt. MA-4						
1	551	120	86.7	10.5	4.53[b]	101.7
2A	501	51	86.7	10.3	4.51	101.5
3A	488	42	87.6	10.5	3.58	101.7
4B	459	60	88.3	11.3	2.12	101.7
5F	428	161	88.8	11.4	1.27	101.5
6F	402	126	88.0	11.6	0.78	100.4
Freezing point range, 396-391°C.						
Expt. MA-5						
2A	697	102	15.0	52.3	32.7[b]	100.0
3B	673	54	14.5	50.7	32.2[b]	97.4
4B	632	68	14.9	52.5	32.2[b]	99.6
5A	605	75	14.2	51.8	32.0	98.0
6A	581	71	14.2	59.2	29.0	102.4
Freezing point range, 575-570°C.						
Expt. MA-6						
1B	695	90	45.1	36.9	18.3[b]	100.3
2B	673	75	45.1	35.3	18.3[b]	98.7
3B	652	45	46.6	36.2	18.4[b]	101.2
4A	631	40	45.9	36.3	18.2	100.4
5A	605	80	45.2	36.8	17.9	99.9
6B	579	65	46.1	37.3	17.1	100.5
7B	549	120	45.8	39.0	15.2	100.0
8A	536	20	46.0	39.0	14.6	99.6
Freezing point range, 525-519°C.						

[a] Estimated accuracy, ±3%.

[b] Unsaturated with respect to thorium.

A semilog plot of the thorium solubility data of Expt. MA-4 vs. reciprocal temperature is shown in Fig. 6 as a straight line (log wt % thorium = 5.811 - 4001.4/T). The slope of this line approximates that for thorium solubility in pure cadmium. This suggests that, despite the presence of about 11 wt % Mg, the solid phase precipitating in this region of the ternary diagram may be $ThCd_{11}$. A similar plot for Expt. MA-6 (not shown) gives a curved line.

The solidified melts from Expts. MA-4 and MA-6 will be examined metallographically and by electron microprobe; results are not yet available.

(4) Cadmium-Magnesium-Thorium Phase Diagram
(Michael Krumpelt)

A preliminary ternary phase diagram for the cadmium-magnesium-thorium system has been drawn (Fig. 7) based on the available information. In the Th-Mg binary system, only one compound ($ThMg_5$) is known [YAMAMOTO]. In the Th-Cd binary system, $ThCd_{11}$ has been positively identified, and preliminary evidence has been obtained for three other compounds: $ThCd_6$, $ThCd_{3.5}$, and $ThCd_2$. No compounds have been reported for the Cd-Mg

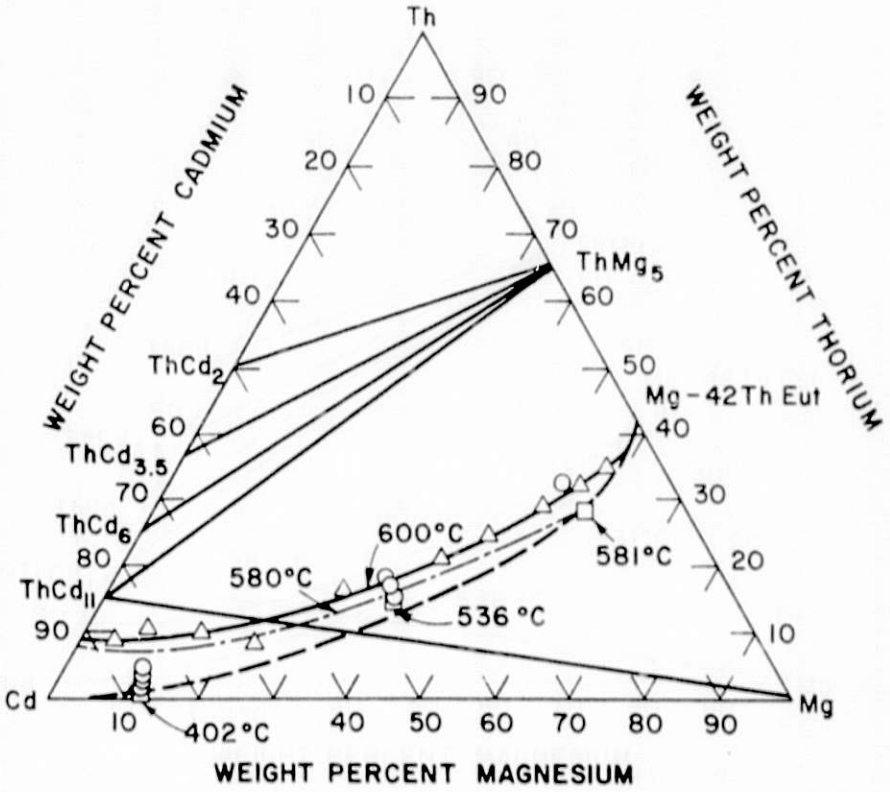

Fig. 7. Preliminary Phase Diagram for the Cadmium-Magnesium-Thorium System

system. Since the slope of the thorium solubility line for Expt MA-4 data is similar to the one for $ThCd_{11}$ in the binary system (Fig. 6), indicating that $ThCd_{11}$ was precipitating, a tie-line has been drawn between $ThCd_{11}$ and Mg. Other tie-lines have been tentatively drawn between $ThMg_5$ and the various Th-Cd compounds. In Fig. 7, the ternary eutectic compositions reported in Table 5 are indicated by squares. The dashed line connects these three points and also the known eutectic points in the Th-Cd and Th-Mg system. This line is a first-order estimate of ternary eutectic compositions. The circles represent liquidus compositions in the ternary system at different temperatures. The line running above the eutectic line represents a 580°C liquidus contour, and the line above it, which runs through the triangles, represents a 600°C liquidus contour. The phase diagram, as outlined, indicates that thorium solubility increases with increasing magnesium content of the ternary alloy, as reported earlier [STEINDLER-1979B].

(5) Differential Scanning Calorimetry
(J. K. Bates and J. H. Meisenhelder)

The thermogravimetric-differential thermal analysis (TG-DTA) unit is still not properly installed, but can be used to measure the heats of transition ΔH_t by differential scanning calorimetry (DSC) and note the heat changes using differential thermal analysis (DTA). However, problems exist in measuring the temperatures of these events. The instrument has been calibrated for each mode of operation measuring melting temperature (T_m) and measuring heats of fusion (ΔH_f). NBS reference standards were used in the temperature calibrations, and high-purity metal samples were used for the ΔH_f calibrations (Table 6).

The melting temperatures were consistently lower than the literature values, with the deviation increasing at higher temperatures. The determined ΔH_{fusion} values were consistently higher than the literature values and led to an instrument constant of 1.21. Thus, to obtain the actual value for ΔH_f from that measured by DSC, the following equation is used:

$$\Delta H = \frac{\Delta H(exp)}{1.21}$$

Currently, the instrument is being used to determine $\Delta H_{reaction}$ for the peritectic decomposition of $ThCd_{11}$ and in establishing the Th/Cd/Mg and Th/Cd phase diagrams.

b. Reduction of Thorium Oxide

The reduction of thorium oxide is an essential step in the reprocessing of oxide fuels (Fig. 5). Previous studies have demonstrated that low-fired thoria pellets are difficult to reduce and that at most, 5 wt % of an initial charge is reduced after 4 h at 675°C [STEINDLER-1979C]. Reduction of material obtained from a reactor is probably of intermediate difficulty; a better understanding of the reduction mechanism is needed.

Table 6. Calibration of TG/DTA/DSC Instrument

Sample	Literature Values[a]		Sample Mass, mg	Rel. Peak Area	Experimental Values		Instrument Constant
	T_m, °C	ΔH_f, cal/g			T_m, °C	ΔH_f, cal/g	
In	156.4	6.8	9.7	346.6	155.0	8.53	1.25
Sn	231.9	14.2	22.8	819.84	230.6	17.26	1.21
Cd	320.9	12.9	17.4	550.34	319.8	15.18	1.18
Pb	327.4	5.51	16.5	450.6	326.0	6.55	1.19
Zn	419.5	24.4	11.4	704.5	417.0	29.66	1.21
						Avg.	1.21

[a] JANAF TABLES [STULL].

In a review of previous reduction studies on ThO_2, UO_2, and PuO_2, seven factors have been identified that must be considered when evaluating the reduction process. These factors are (a) alloy composition, (b) fuel type, (c) flux composition, (d) process temperature, (e) mixing parameters, (f) metal loading, and (g) oxide loading.

Two types of experiments were planned to identify the factors that are the most important in controlling the reduction rate. The first set of experiments is discussed in this report. The second set of reduction experiments will be done with low-fired ThO_2 pellets obtained from Westinghouse. These experiments are designed to study the mass transfer between the salt and alloy and between the salt and pellet.

(1) Analysis of Salt for Calcium and Calcium Oxide

The extent of reduction can be determined either by monitoring CaO buildup in the salt or by monitoring the amount of thorium in the alloy. Because alloy samples may become contaminated with salt, the most reliable measure of thorium concentration is the ratio, Th:Mg.

The procedure for analyzing for calcium and calcium oxide content in the presence of calcium salts consists of dissolving a known weight of the salt mixture in 10 mL of 0.1N HCl by heating to boiling with stirring.

$$Ca + 2HCl \rightarrow CaCl_2 + H_2\uparrow + \text{excess HCl}$$

$$CaO + 2HCl \rightarrow CaCl_2 + H_2O + \text{excess HCl}$$

Excess or unreacted HCl is then back-titrated with standard NaOH. The end point is taken at pH 7 with a Sargent-Welch pH meter.

The amount of CaO in the salt is determined by subtracting the amount of calcium in the salt, as determined by hydrogen gas evolution, from the total amount of CaO plus calcium as determined by acid-base titration. As a test of this procedure, a standard containing 5.46 wt % calcium and calcium oxide (0.75 wt % Ca, 4.71 wt % CaO) dissolved in $CaCl_2$-15 wt % CaF_2 eutectic salt was submitted to the Analytical Laboratory. Analysis yielded 3.6 wt % for a filtered sample and 5.2 wt % for an unfiltered sample.

To determine whether any factor in the experimental method, such as sampling through tantalum frits, was responsible for the low values, several analyses using the acid-base titration procedure were done by the Analytical Laboratory. Three standards containing calcium oxide and in one instance calcium were analyzed (Table 7) to demonstrate the reliability of the technique. The results of analyses of filtered samples taken from experiments 11-E and 11-ER in the thoria reduction series (discussed below) are shown in Table 8. The samples were taken at different stages of the experiment and consist of premelted salt (ER-1), premelted salt + ThO_2 (E-2, ER-3), and the salt layer at the beginning and end of the reduction (ER-5 and ER-9), respectively.

Preweighed standards and actual samples were analyzed. Samples that had been filtered through tantalum frits into tubes were dissolved from the tubing by cutting off the frit end only, so that the tantalum tubes could be reused. Dissolution of the salt from one end of the tube proved to be extremely slow. When the beaker containing the solution and tube was placed in an ultrasonic cleaner, the agitation produced complete dissolution in about one-half hour, but also resulted in fine grey particles being removed from the tantalum tube and a colored (instead of white) precipitate being formed during titration.

The results indicate that:

(1) Analysis of the standards was straightforward, and the experimental error was within acceptable limits. However, the standard solution containing Ca and CaO analyzed about 10% too high.

(2) Filtered samples of the premelted salt contained some calcium oxide. This has been confirmed by the Analytical Laboratory.

(3) In one experiment, 11-ER, filtered samples of salt and ThO_2 showed additional reactant. The amount was less when a fine tantalum frit was used. Since the average particle size of the ThO_2 was 0.5 μm, and the pore sizes of the two frits were 40 and 5 μm, respectively, it is possible that some ThO_2 was passing through the frit. A blank run with about 100 mg ThO_2 showed that neither ThO_2 nor any impurity that it might contain reacted with the 0.1N HCl, even slightly. At this point, we are not certain what caused this effect.

Table 7. Analysis for Calcium and Calcium Oxide in Prepared Standards

Standard	Wt of Sample	Millimoles of CaO Present[a]	Millimoles of Ca Present	Total Millimoles of Ca + CaO Present	Total Millimoles Ca or Ca + CaO Found	Error, %
CaO[b] (Mallinkrodt Analytical)	20.0 mg	0.345	--	--	0.341	1.0
	23.8 mg	0.410	--	--	0.406	1.0
5 wt % CaO-78 wt % $CaCl_2$-17 wt % CaF_2[c]	0.423 g	0.374	--	--	0.376	0.5
Standard Solution[d] of Ca and CaO in in $CaCl_2$-15 wt % CaF_2-0.75 wt % Ca-4.71 wt % CaO						
Filtered	1.0939 g	0.931	0.206	1.137 (1.039 mmol/g)	1.272 (1.163 mmol/g)	11.6
Unfiltered	0.6388 g	0.543	0.120	0.663 (1.039 mmol/g)	0.721 (1.29 mmol/g)	8.7

[a] Corrected for Analytical Laboratory assay of CaO and for CaO content of $CaCl_2$ and CaF_2.

[b] Assay by Analytical Laboratory, 96.7 wt %.

[c] Chemical compounds were separately weighed into the beaker.

[d] The solution was prepared by weighing the chemicals into a stainless steel crucible, heating to 775°C, and stirring for 3 h at 675°C. The Analytical Laboratory found 0.94 mmol/g of unfiltered sample and 0.675 mmol/g of filtered sample. Calculated total Ca + CaO in the standard solution is 1.039 mmol/g.

Table 8. CaO Analyses of Filtered Salt Samples

Sample No.	Temp, °C	Tantalum Frit	Wt of Sample, g	CaO Content, mmol	CaO Content, wt %
11-E-2[a]	743	Fine	1.4375	0.173	0.67
11-ER-1[b]	714	Coarse	0.9571	0.087	0.51
11-ER-3[c]	652	Coarse	1.0825	0.382	1.98
11-ER-5[d]	795	Fine	0.4624	0.134	1.63
11-ER-9[e]	799	Fine	0.6395	0.186	1.63
			0.7125	0.219	1.72
			0.7414	0.212	1.60

[a]Sample taken at the beginning of experiment 11-E in the thoria reduction series, before stirring, after addition of ThO_2.

[b]Sample taken before the addition of ThO_2 in preparation of salt mixture for experiment 11-ER in the thoria reduction series.

[c]Sample taken after ThO_2 addition to salt mixture for 11-ER. No sample was obtained with a fine frit.

[d]Sample taken at the beginning of experiment 11-ER, before stirring.

[e]Sample taken at the end of experiment 11-ER, after 4 h of stirring. This sample tube was cut into three pieces; two 1/2-in. pieces were dissolved without the use of ultrasonic cleaner. The sample in the third piece (0.7125) had only one end open; this sample was dissolved with the aid of the ultrasonic cleaner.

(4) The method of dissolution selected (use of an ultrasonic cleaner or boiling and stirring) was not a factor.

(5) No reduction of ThO_2 by Ca to yield CaO was detected by analysis of the salt layer in Experiment 11-ER.

We concluded that when oxide percentages were below about 3%, analysis of the salt layer in the thoria reduction experiments yielded no information useful in determining the extent of reaction.

(2) Thoria Reduction Experiments

The first set of experiments using thoria powder was designed to determine the effects of final thorium loading in the metal alloy, final CaO loading in the salt, and temperature on the reduction of thorium oxide by calcium. These parameters became the independent variables in a

factorial experiment with the other factors being held constant. High, intermediate, and low values were selected for the three parameters. The rate of reduction was the dependent variable. Nine experiments at the following conditions were planned:

Experiment No.	Temp, °C	Final Th in Alloy, wt %	Final CaO in Salt, wt %
11-A	800	15	9.7
11-B	650	3.94	9.7
11-C	800	3.94	9.7
11-D	650	3.94	2.5
11-E	800	3.94	2.5
11-F	725	9.47	6.1
11-G	800	15	2.5
11-H	650	15	9.7
11-I	650	15	2.5

Mixing: 800 rpm
Salt: $CaCl_2$-15 wt % CaF_2
Alloy: Cd-50 wt % Mg + twice the stoichiometric amount of Ca
Fuel Type: Powder

Samples of the salt and alloy were taken at the beginning and completion of each experiment. In the initial experiment, samples were taken every hour to determine when reduction was complete. However, in subsequent runs, few samples were taken.

Of the nine experiments planned, five experiments (11-A, 11-D, 11-E, 11-ER, and 11-F) have been completed and the results, given in Table 9 are discussed below.

11-A. This was the initial experiment performed--to ascertain whether experiments operated with the most strenuous conditions (high temperature and high loadings) were feasible. The metals and salts were prepared and added to the crucible. Metal preparation involved acid cleaning, and the salts were premelted to form a eutectic mixture (m.p., about 630°C). The combined alloy-salt mixture was then brought to temperature with stirring (300 rpm); after 1/2 h of settling, samples were taken from the upper (salt) and lower (metal) liquid layers (samples 11A-1, 11A-2, and 11A-3). The ThO_2 was added through a hollow tantalum tube inserted so that its end was just above the melt. After ThO_2 addition was complete, stirring at 800 rpm commenced. Samples were taken from the bottom of the melt at 1-h intervals until four samples were obtained (11A-4 to -7). A 5-min settling time was allowed before each sampling. After 5 h, Sample 11A-8 was taken from the top of the melt and the experiment was concluded. Unfortunately none of the samples appeared to be salt. The melt was allowed to settle overnight at 730°C and an additional sample was taken at the bottom (11A-10) of the melt. The entire melt was then cooled and removed for inspection. Visual inspection showed

Table 9. Factorial Set of Experiments to Study the Reduction of ThO_2 by Calcium

Exp. No.	Independent Variables: Temp, °C	Final CaO in Salt, wt %	Final Th in Alloy, wt %	Initial Quantities of Constituents, g (%): Mg	Cd	Ca	Salt[a]	ThO_2	Stirring Rate, rpm	Sample Analysis, wt %: Sample No. and Reduction Time	Mg	Cd	Ca	Th	Th/Mg Ratio x100
11-A	800°C (high)[b]	9.7 (high)	15 (high)	126.16 (44.65)	126.54 (44.78)	29.87 (10.57)	195.0	50	800	11A-2 start	41.6	45.4	10.3		
										11A-3 start	43.9	44.6	10.3		
										11A-4 1 h	45.5			1.12	2.46
										11A-5 2 h	43.3			1.12	2.59
										11A-6 4 h	43.4			1.12	2.58
										11A-7 5 h	44.7	42.5		1.23	2.75
										11A-8 5 h	42.8		10.2	1.24	2.90
										11A-10 metal	35.9			0.87	2.42
11-D	650 (low)	2.5 (low)	3.94 (low)	127.42 (48.37)	126.78 (48.12)	9.25 (3.51)	189.10	11.90	800	11D-1 start	43.2			<0.01	
										11D-2 1 h	47.3			0.3	0.63
										11D-3 2 h	39.5			0.32	0.81
										11D-4 3-3/4 h	41.7			0.20	0.48
										11D-5 (salt)			1.42 (CaO)		
11-F	725 (intermediate)	6.1 (intermediate)	9.47 (intermediate	124.65 (46.11)	126.58 (46.82)	19.11 (7.07)	195.43	31.06	800	11F-1 (salt)				<0.05	
										11F-3 2 h	0.11	0.11	35.9	<0.05	
										11F-8 4-1/2 h	47.8	48.5	5.5	0.80	1.67
11-E	800 (high)	2.5 (low)	3.94 (low)	127.52 (48.49)	126.23 (48.00)	9.25 (3.52)	192.25	11.26	1000	11E-1 start	48.3	49.9	2.18	0.07	0.14
										11E-3 24 h	50.6	46.8	2.01	0.43	0.85
11-ER	800 (high)	2.5 (low)	3.94 (low)	117.75 (39.31)	172.74 (57.67)	9.02 (3.01)	194.74	11.87	1000	11ER-4 start	39.1	57.7	2.91	<0.02	
										11ER-6[d] 1 h	39.0	53.3	2.90	0.16	0.41
										11ER-7 2 h	39.2	54.5	2.85	0.15	0.38
										11ER-8[d] 4 h	38.3	51.1	2.90	0.13	0.34

[a] 15 wt % CaF_2-$CaCl_2$.

[b] Refers to high, low, and intermediate values for the factorial experiment.

[c] Phases settled overnight before sampling.

[d] Samples contained salt and presented percentages have been corrected to reflect sample with salt subtracted.

the salt layer to be on top of the solidified mass. The solid mass was then sequentially dissolved and consisted of the top salt layer and under it, a hard dark grey collar of metal on the outside bottom of the crucible. The inside bottom of the solid mass consisted of grey sand-like pieces of soft material, with dark-grey particles dispersed throughout.

Sample analyses indicated that about 8.2% of the ThO_2 initially there had been reduced, but that almost all of the reduction had occurred in the first hour.

11-D. The procedure used for this experiment was the same as for experiment 11A, except that operating conditions were different. Difficulty was again experienced in obtaining a salt sample. The salt sample submitted for analysis was obtained by chipping the frozen salt layer. Reduction reached 5% in 1 h and did not increase thereafter.

11-F. The procedure for this run was altered in that the metals were premelted and ThO_2 was added to the premelted salt before the salt and alloy were melted together. Samples were taken as before, but this time all samples appeared to be salt. The melt was then cooled and examined; the salt layer was on top. The melt was reheated, and more salt samples were taken. At this point, a metal sample was obtained from the bottom (11F-8). Reduction was 8.4%.

11-E. In experiment 11E, the procedure followed in 11-F was used; however, the melt could not be stirred with the paddle in or near the alloy layer. This was brought about by the inadvertent addition of an extra piece of stainless steel to the melt. Thus, stirring at 1000 rpm could be accomplished only with the paddle entirely in the salt layer. Stirring was continued for 24 h before sampling. Reduction was 11%.

11-ER. Owing to the problem of locating the salt and alloy layers, the alloy composition was changed to Cd-40 wt % Mg. In addition, the stirring rate was 1000 rpm. Otherwise the procedure was the same as that in 11-F. Salt-alloy separation was somewhat improved, although some samples did consist of salt-alloy mixtures. Settling time before each sampling was 5 min. A reduction of 4% was observed.

Conclusions. In each series of experiments, the total amount of reduction was less than expected. Previous ThO_2 reductions with calcium, using a Cu-Mg alloy and a low stirring rate, achieved at least 60% reduction [AMECKE]. Additionally, in the present experiments, all reduction appeared to occur during the first hour. This may indicate that in reality, no reduction occurred and that the thorium which appeared in the alloy was due to ThO_2 that had not been filtered out. The average, ThO_2 particle was 0.5 μm, whereas the filter pore size was about 40 μm. Samples 11E-4 and 11ER-1 were each taken at the beginning of these experiments after the salt and alloy had been melted together. Neither sample showed that ThO_2 had passed through the filter; however, neither sample had been stirred. No explanation for the seeming lack of reduction is available at this time.

c. Molten Salt Recycle, Electrolysis of CaO in Molten Salt
(R. E. Barletta, L. J. Jardine, T. J. Gerding, D. K. Kroeck, and Michael Krumpelt)

Because of the termination of the PDPM program, it seems appropriate to summarize the experimental work on molten salt recycle.

(1) Introduction

In pyrochemical reprocessing methods, the spent oxide fuel is reduced with metallic calcium and dissolved in a liquid alloy. The resulting calcium oxide is removed by dissolving it in a cover salt. An example of such a process is the Salt Transport Process for UO_2-PuO_2 fuels [KNIGHTON-1978]. This process involves the reduction of actinide and fission product oxides, RO_2 by calcium metal at 600 to 800°C using a Mg-Cu alloy as the liquid alloy and a CaF_2-$CaCl_2$ cover salt:

$$RO_2 + 2Ca(salt/alloy) \rightarrow 2CaO(salt) + R(alloy)$$

After the reduction, the cover salt contains CaO, alkali and alkaline earth fission product chlorides, iodine, and low concentrations of actinides. This salt is a major waste stream which must be discarded as a high-level waste. The volume of this stream would be about 850 L/Mg of spent fuel [BATES]. Owing to the high dispersion potential (e.g., high water solubility of the salt, further processing would probably be required before an acceptable waste form is obtained.

Methods for complete or partial recycle of both cover salt and calcium are advantageous for sound waste management--particularly because they represent a large waste volume. One such method is electrolytic decomposition of CaO into calcium and CO_2, using a liquid metal cathode and a consumable graphite anode [BATES]. The calcium so prepared may be recycled, and the cover salt could then be either partially or totally reused, depending on fission product buildup. Ignoring the actinides and fission products present in the cover salt, three compounds can, in principle, be decomposed electrolytically: CaO, $CaCl_2$, and CaF_2. If unit activities are assumed, the calculated decomposition potentials, E_d, of these compounds at 975 K (calculated from the free energies of formation) are:

$$CaO \rightarrow Ca + 1/2\ O_2(g) \qquad E_d = 2.75\ V \qquad (1)$$

$$CaCl_2 \rightarrow Ca + Cl_2(g) \qquad E_d = 3.41\ V \qquad (2)$$

$$CaF_2 \rightarrow Ca + F_2(g) \qquad E_d = 5.34\ V \qquad (3)$$

With a consumable carbon anode, however, another reaction is possible:

$$CaO + 1/2\ C \rightarrow Ca + 1/2\ CO_2(g),\ E_d = 1.73\ V \qquad (4)$$

The E_d of reaction 4 is low enough compared to those of reactions (2) and (3) to allow selective decomposition of CaO in molten $CaCl_2$-CaF_2 salt.

Reaction 4 has been shown to occur for CaO electrolysis in $CaCl_2$ at 774-857°C [THREADGILL]. In these experiments, calcium metal was deposited on a water-cooled aluminum bar which was gradually drawn out of molten $CaCl_2$ salt. The cell was operated at current densities of 20-40 A/cm^2 and at potentials of 13 to 15 V with oxide concentrations of 0.68 to 12 wt %. Although the cell potential was well above the decomposition potential of $CaCl_2$ (reaction 2), Threadgill reports that the gas evolved did not contain chlorine. Numerous problems were encountered with this electrolysis, however--especially at CaO concentrations greater than 2 wt %. Examples were cell overheating, spattering of the electrolyte, arcing of the cell, and melting and burning of the calcium metal product during experiments. These problems are directly attributable to the rather extreme cell operating conditions (current and voltage).

In contrast to these extreme conditions, [BATES] reported electrolysis of 5 wt % CaO in 15 wt % CaF_2-$CaCl_2$ at 700°C, a current density of 0.5 A/cm^2, and a potential of 2 V, using a graphite anode and a liquid cadmium cathode. During electrolysis, the off-gas was monitored, and CO_2 and CO were detected. Also, chemical analysis of the salt and alloy phases indicated that the CaO concentration in the salt decreased from 5% to 1 wt % and that the calcium concentration in the alloy increased from 0 to 3 wt %. The authors report none of the difficulties in operating their cell which were reported by [THREADGILL], although neither stoichiometry nor a material balance was obtained, and the CO/CO_2 concentrations in the off-gas were low.

On the basis of these earlier studies into the chemistry of the process [BATES, THREADGILL] this investigation concentrated on determining cell operating conditions such as cell potential and current efficiencies. In experiments to determine cell potentials in the system of interest, a salt containing CaO in 15 wt % CaF_2-$CaCl_2$ and a cathode of 35 wt % Mg-Cu were used. This alloy was chosen since it is also a metal solvent in the Salt Transport Process [KNIGHTON-1978]. The use of this alloy also provides a cell arrangement in which the calcium metal is removed from the cell by dissolution in the liquid metal at the bottom of the cell rather than from the top of the cell as pure calcium metal, as was the case with the experiments of Threadgill.

(2) Experimental

The electrochemical experiments used a cylindrical 1/2-L (about 6.4-cm-dia) cell (Fig. 8). The cell was operated in a sealed furnace tube in a glove box purged with high-purity, dried argon. A separate purge of argon flowed over the cell proper. The cyclindrical graphite cathode 1.9 cm in diameter by 5 cm high) was baked out at 800°C under vacuum prior to use. The liquid metal cathode (35 wt % Mg-Cu) was prepared under dry conditions prior to electrolysis.

The CaO and CaF_2 used in these experiments were reagent grade materials heated to 800°C for two hours and stored under dry argon. The $CaCl_2$ was anhydrous ultra-high-purity calcium chloride, which was used without further treatment.

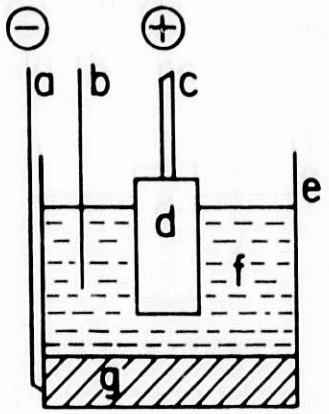

Fig. 8. Electrolytic Cell Used for CaO Electrolysis Study. (a) cathode connector; (b) thermocouple; (c) anode connector; (d) graphite anode; (e) stainless steel container; (f) fused salt electrolyte; (g) molten metal cathode

Power was supplied to the cell by a continuously adjustable power supply operated in either a constant-current or a constant-voltage mode. The cell voltage was monitored by a high-impedance digital voltmeter, and the current was measured across a calibrated shunt in series with the power supply.

(3) Current-Potential Curves

Steady-state currents at fixed potentials were measured in melts of 5 wt % CaO in 15 wt % CaF_2-$CaCl_2$ and in CaF_2-$CaCl_2$ containing no CaO. A graphite or platinum anode and a Mg-Cu cathode were used. The salt mixture plus the alloy were heated under vacuum to 600°C, argon was added, and the temperature raised to 800°C. The mixture was stirred intermittently for approximately one hour to ensure oxide dissolution. The stirring rod was then removed, and the preheated anode was lowered into the melt to about 1.3 cm above the alloy-salt interface.

Data were taken at various temperatures from 675 to 800°C with the power supply in the constant voltage mode, while the current was allowed to stabilize. The potential was then manually reduced to a new value, and another data point taken. This procedure was followed until zero current was reached. A complete curve was obtained in about 45 min. This procedure removed any trace impurities by electrolysis at high potentials during the early part of the experiment, preventing their having an effect on the current at low potentials.

(4) Current Efficiency Experiments

Oxide-salt mixtures containing 10, 9, 8, 6, and 4 wt % CaO were prepared by mixing CaO with CaF_2-$CaCl_2$ at 800°C for 5-7 h with intermittent stirring. The fused mixture was allowed to cool and was stored under argon.

Before the start of an electrolysis, 210 g of the premixed salt along with 100 g of the Mg-Cu were added to the electrolysis cell. The remaining 40 g of salt was reserved for chemical analysis. The cell was heated to about 685°C. The preheated graphite electrode was then lowered into the salt phase to about 1.3 cm above the alloy/salt interface. To measure current efficiencies, the cell was run at constant current. This operating current was determined by finding the current corresponding to a voltage between the decomposition potentials for CaO (reaction 4) and $CaCl_2$ (reaction 2) in order to minimize $CaCl_2$ decomposition. The power supply was operated in the constant-current mode for a known time, and thus the total integrated current could be determined. During electrolysis, the voltage was monitored to ensure that it did not exceed the $CaCl_2$ decomposition potential (about 3V).

At the conclusion of electrolysis, the power was turned off, the graphite anode was raised, and the cell was cooled to room temperature. Samples of the solid salt phase were taken from (1) the middle of the salt and (2) near the alloy/salt interface. Samples of the post-electrolysis alloy were also taken. Salt samples were analyzed for CaO and calcium metal, and metal samples were analyzed for total calcium content.*

The accuracy of the sampling procedure was tested by preparing a sample containing 5.16 wt % CaO in CaF_2-$CaCl_2$, and sampling the molten salt at 700°C using tantalum tubes and frits. The mixture was then cooled to room temperature, and solid-salt samples were taken at the top and bottom of the salt. Chemical analysis for CaO of these samples revealed a concentration of 4.71 ± 0.21 wt % CaO for filtered samples and 5.08 ± 0.02 wt % CaO for samples taken from the solid salt. No variation was apparent for samples taken near the top or bottom of the solidified salt. The solid-salt sampling method was chosen in preference to the molten salt sampling procedure because it gave results nearer the preweighed value.

(5) Results and Discussion

The current-potential data obtained for temperatures between 675°C and 800°C were plotted to determine the decomposition potentials. Typical results at 700°C are given in Fig. 9. Decomposition potentials were derived by linear extrapolation of the voltage data to zero current. The derived decomposition potentials are given in Table 10. To make assignments to the possible reactions, the observed data were compared with the theoretical values for reactions 1 through 4. As an example, Table 11 compares the experimental decomposition potentials for the reactions 1, 2, and 4 with those derived from free energy of formation data at 775°C. For reactions 1 and 2, agreement between theory and experiments is within about 0.3 V. There is a larger (0.5 V) difference for reaction 4. The discrepancy for reactions 1 and 2 may be accounted for by unknown deviations from unit activity for various species in the molten salt. However, information currently available in the literature and data obtained in these experiments do not allow quantitative

*Analysis performed by the Analytical Chemistry Laboratory of the Chemical Engineering Division.

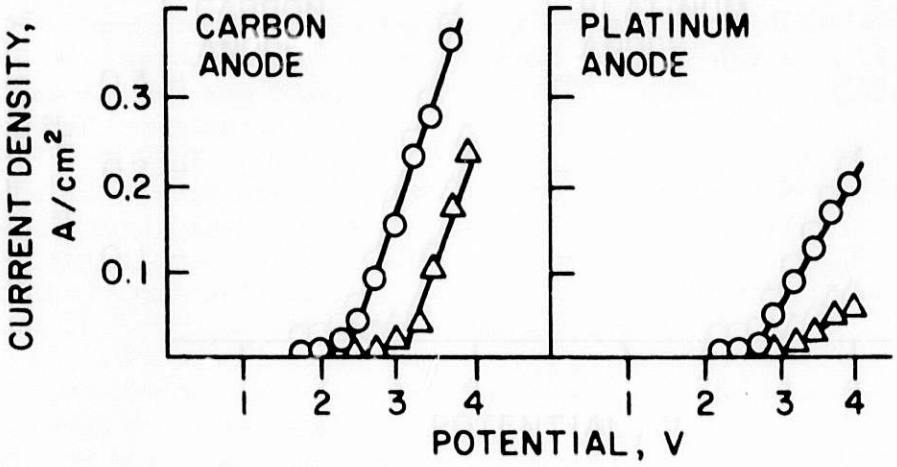

Fig. 9. Current-Potential Curves for CaF_2-$CaCl_2$ at 700°C. Circles represent salts containing 5 wt % CaO; triangles represent salts containing no CaO.

Table 10. Decomposition Potential, E_d, for the CaO-CaF_2-$CaCl_2$ System, 675-800°C (Cathode, 35 wt % Mg-Cu)

Salt Phase Composition	Anode Material	E_d, V					
		675°C	700°C	725°C	750°C	775°C	800°C
CaF_2-$CaCl_2$[a]	C	3.14	3.13	3.10	3.08	3.04	2.98
CaF_2-$CaCl_2$[a]	Pt	2.77	2.92	3.07	--	2.92	2.77
CaF_2-$CaCl_2$[a] + 5 wt % CaO	C	2.39	2.37	2.33	2.29	2.26	2.18
CaF_2-$CaCl_2$[a] + 5 wt % CaO	Pt	2.70	2.67	2.67	2.63	2.63	2.67

[a] 15 wt % CaF_2-$CaCl_2$.

estimates of activities to be made. It can be noted that of the various species present as either reactants or products in reactions 1, 2, and 4, CaO and Ca metal are present in low concentrations, and are thus likely to have chemical activities which deviate significantly from unity.

This discrepancy between the observed and theoretical decomposition potentials of reaction 4 is similar to the electrolysis of alumina in fused cryolite, in which an overpotential of 0.5 V for CO_2 evolution is observed. This overpotential has been explained by [THONSTEAD], who concluded that the rate-limiting reactions responsible for the overpotential

Table 11. Comparison of Observed and Calculated Decomposition Potentials for CaF_2-$CaCl_2$ with and without CaO at 775°C

Reaction	E_d, V	
	Experimental	Calculated (all activities unity)
$CaO \rightarrow Ca + 1/2\ O_2$	2.63[a]	2.73
$CaCl_2 \rightarrow Ca + Cl_2$	3.04[b]	3.35
	2.92[a]	
$CaO + 1/2\ C \rightarrow Ca + 1/2\ CO_2$	2.26[b]	1.71

[a]Platinum anode.

[b]Carbon anode.

are oxygen transfer through the electric double layer and formation of CO_2 from chemisorbed oxygen. It is likely that a similar mechanism could explain the observed overpotential in the CaO electrolysis on graphite. It should be noted, however, that no overvoltage was observed by [THOMPSON] for the E_d of reaction 4 in a molten calcium fluoride-sodium fluoride salt at 900-1100°C, using a graphite anode.

Based on the results of these decomposition potential experiments, it can be concluded that the potential range in which only CaO may be decomposed using a carbon anode is smaller than is anticipated from thermodynamic considerations alone (1.68 V). The practical potential range for CaO electrolysis is from about 2.7 to 3.0 V.

The current efficiencies for this range were determined by measuring the decrease in CaO concentration in the salt phase and the increase in calcium concentration in the metal phase and comparing these values with the integrated current. The results of chemical analyses of samples from which these efficiencies were calculated are given in Table 12 and the resulting current efficiencies are listed in Table 13. The current efficiencies in Table 13 are substantially less than 100%, which suggests that cell operating conditions and cell design were not optimum. Further, efficiencies based on CaO depletion do not correlate well with those based on calcium metal increase.

The fact that current efficiencies based on calcium metal in the alloy are consistently lower than those based on oxide analyses indicates that calcium did not readily transfer into the liquid alloy. Calcium metal in the salt phase (produced by electrolysis) was determined by analyzing various portions of the salt phase for calcium metal content. Limited solubility of the metal in the salt was expected since the reported solubility of calcium in $CaCl_2$ at 800°C is about 1 wt % [DESAJ, WADE]. Chemical analysis of postelectrolysis salt samples revealed bulk concentrations of

Table 12. Analytical Results for Samples taken during Current-Efficiency Measurements

Experiment No.	CaO and Ca in Salt[a]			Concentration of Ca Metal in Alloy[c] (final), wt %
	Starting CaO Concentration, wt %	Final CaO Concentration, wt %	Final Ca Concentration,[b] wt %	
1	10.1 ± 0.1	7.9 ± 0.3	0.41	0.38 ± 0.03
2	10.0 ± 0.5	8.02 ± 0.03	0.40	0.58 ± 0.23
3[d]	9.11 ± 0.88	7.76 ± 0.08	0.13	0.53 ± 0.02
4	7.93 ± 0.32	6.81 ± 0.34	2.00	1.90 ± 1.55
5	6.00 ± 0.24	5.05 ± 0.48	0.48	0.70 ± 0.15
6	4.00 ± 0.05	3.17 ± 0.28	0.15	0.44 ± 0.26

[a] 210 g total salt.

[b] Value based on single analysis of the salt phase near the alloy/salt interface.

[c] 100 g total alloy.

[d] Anode-cathode distance is approximately one-half the value (1.3 cm) of that in the other current-efficiency experiments.

Table 13. Current Efficiencies Based on CaO Decrease in Salt and Ca Increase in Alloy, Using Data from Table 12

Experiment	Integrated Current, A-h	Current Efficiency Based on CaO Decrease in Salt, %	Current Efficiency Based on Ca Increase in Alloy, %
1	8.04	54.9 ± 7.9	6.3 ± 0.5
2	4.02	98.8 ± 25.0	19.3 ± 7.6
3[a]	4.02	67.4 ± 44.0	17.7 ± 0.7
4	8.04	27.9 ± 11.6	31.6 ± 25.8
5	8.04	23.7 ± 13.4	11.6 ± 2.5
6	8.04	20.7 ± 7.1	7.3 ± 4.3

[a] Anode-cathode distance is approximately one-half the value of that in the other current-efficiency measurements.

calcium of about 50 ppm, but concentrations of calcium metal (given in Table 12) in salt samples taken near the salt/alloy interface were much greater. The fact that in experiment 4, the calcium metal content exceeded the solubility of calcium in $CaCl_2$ indicates that the metal-rich portion of the salt, i.e., the salt near the alloy/salt interface, is inhomogeneous and calcium metal is present as a suspended solid. That calcium metal was present is confirmed by observation of hydrogen evolution upon dissolution of the salt in acid.

High concentrations of calcium metal at the interface between the carbon anode and the liquid metal cathode point to a mechanism that might account for the observed low current efficiencies. Calcium metal cycling between anode and cathode could cause loss of efficiency. This hypothesis is supported by the work of [DESAJ] on thermodynamic properties of calcium metal in molten calcium chloride.

(6) Conclusions

An overvoltage of about 0.5 V for the electrolysis of CaO with a graphite anode was observed. Thus, the region of selective electrolysis of CaO is smaller than had been anticipated from decomposition potential estimates based on free energy of formation data.

Also, the presence of metallic calcium in the salt phase provides a complication to the electrolysis of CaO in CaF_2-$CaCl_2$ which could well account for the observed low current efficiencies. Not all of the calcium dissolved in the cathode alloy. This difficulty may be overcome by a modification of cell design.

These experimental measurements of decomposition potentials and current efficiencies were performed on a cell design which was not optimized.

3. U-Pu Salt Transport Processing

(J. B. Knighton,* C. Baldwin,* T. D. Santa Cruz,* W. A. Averill,* M. Bracco,* M. F. Boyle,* S. J. Dyer,* R. F. Fitzpatrick,* J. E. Hicks,* G. A. Lambert,* D. Olson,* R. L. Sandvig,* S. P. Sontag,* T. Whipple,* R. D. Wing,* and J. L. Zoellner*)

a. Introduction

The purpose of this work is to develop pyrochemical processes and associated hardware for coprocessing uranium and plutonium contained in spent FBR reactor fuels. The primary objective is to develop a process capable of producing a proliferation-resistant product suitable for reactor use. This proliferation resistance can be accomplished by coprocessing and/or by producing fission-product-contaminated plutonium. In addition, waste management of by-product for both interim and ultimate disposal will be explored.

---

* Rockwell International, Rocky Flats.

The technical goals of this work are (a) to develop a viable flowsheet for producing by pyrochemical means through coprocessing, a proliferation-resistant product suitable for reactor use, (b) to identify key problems and conduct early proof-of-principle experiments on key problems that challenge the feasibility of the flowsheet, (c) to prepare a process description and design criteria for a conceptual Pyrochemical Processing Facility (PPF), (d) to examine and integrate design concepts for the unit operations of the salt transport process, and (e) to evaluate containment of fission products and management of waste products.

b. Engineering Analysis

(1) Waste Management Studies
(S. P. Sontag*)

The argon supply line and the 220 V electrical outlet have been installed for the furnace to be used for calcium oxide reduction studies, and the controller has been wired for operation. This completes the necessary laboratory modifications. Final approval of the Operational Safety Analysis has been obtained.

Experimental work will not be started until additional funding becomes available.

The "Scope of Work for Hot Cell Experiments" is complete and is presented in the Appendix.

The TRU Program tasks at Rocky Flats, which have been reduced in scope due to reduced funding, will be completed.

(2) Zinc/Cladding Separation (Literature Search)
(R. L. Sandvig,* G. A. Lambert,* and S. J. Dyer*)

A topical report of the literature search on the nonaqueous separation of zinc from fuel rod cladding has been completed and will be issued as a separate document.

Some uncertainty was encountered concerning the diffusion step in the vapor-phase zinc recovery process described in the report, namely, the nature (porosity) of the process residue and the mechanism of the diffusion. During the final stage of the vapor-phase recovery process, the zinc is removed from the zinc-cladding melt by diffusion. Two extremes appear to be possible:

(1) The zinc molecules diffuse through an iron layer one or two molecules thick and enter a vapor pore in the residue.

(2) The zinc molecules diffuse through the nonporous melt and are not vaporized until they arrive at the solid-vapor interface. If this extreme occurs, either an extremely long time (on the order of 10^8 years) or a very thin (1 to 2 μm) section is required.

---

*Rockwell International, Rocky Flats.

In the topical report, the latter extreme was assumed to be unlikely. The first assumption was modified slightly, and a time for recovery of 6.8 h was estimated. Extensive experimental work will probably be required to determine the diffusion rate.

(3) Computer Model
(W. A. Averill*)

The second-generation computer model of the transport process has been completed; this version has been dubbed "SALT-II." There are some significant improvements incorporated into this version that were not addressed previously.

The first major improvement is the method of equilibrating the solid alloy phases with liquid alloy phases. In SALT-I (the first-generation model), the calculations which determined the mass balance between the solid and liquid alloys were performed after salt-alloy equilibration was complete. This was actually accomplished in two separate routines, one performed before the other. This is not a time-realistic representation of the process as it actually occurs, but it was felt that for the first generation, this model would be a fairly close approximation.

The second-generation version performs these calculations simultaneously. That is, the routine which equilibrates the salt and alloy also contains the calculation for the liquid/solid alloy equilibration. First, the first iterative step of salt/alloy equilibration is performed, then the first iterative step of the liquid/solid equilibration is performed. Both sets of algorithm converge at the same time and at the same rate. This incorporation would have meant a significant increase in run time for the entire program, but the many time-saving innovations that were instituted in this second-generation model have kept the over-all run time about the same for SALT-II as for SALT-I.

The second feature of improvements of SALT-II is the allowance for heels in the process vessels. This will allow the model to simulate actual process operation when material is transferred from one vessel to another and small amounts of material are left behind, either because of necessity or desire. These heel volumes are variable and can be explored along with the other process operating parameters. Finally, the third feature is the allowance for multiple passes. This will allow examination of transient start-up behavior and steady-state behavior of the system after parameters have been varied. This feature also allows the system configuration to be altered. With only slight modification, the system order of tasks can be changed to determine whether the system is truly nonproliferable.

(4) Design
(J. E. Hicks*)

The Turntable Transport Process design is complete except for a few small details. Detailed material and energy balances will be generated in the coming months while a topical report is being written. Work is presently centered on the design section of this report.

---

*Rockwell International, Rocky Flats.

The flow pattern for the Mixer-Settler Continuous Process (MSC)* has been developed, and equipment to provide the desired flow pattern has been designed. This equipment is quite complex, and some fabrication difficulties exist. The most promising construction material appears to be brazed or welded molybdenum-tungsten alloy, coated with tungsten by chemical vapor deposition after fabrication. A nine-stage mixer-settler train designed to be used for the MSC process in a square furnace is shown in Fig. 10. Each stage consists of two mixers and two settlers. Salt make-up and bleed channels are provided. The cutaway illustrates the mixing chamber and the exterior of a pump used to transfer the mixed material into the settling chambers.

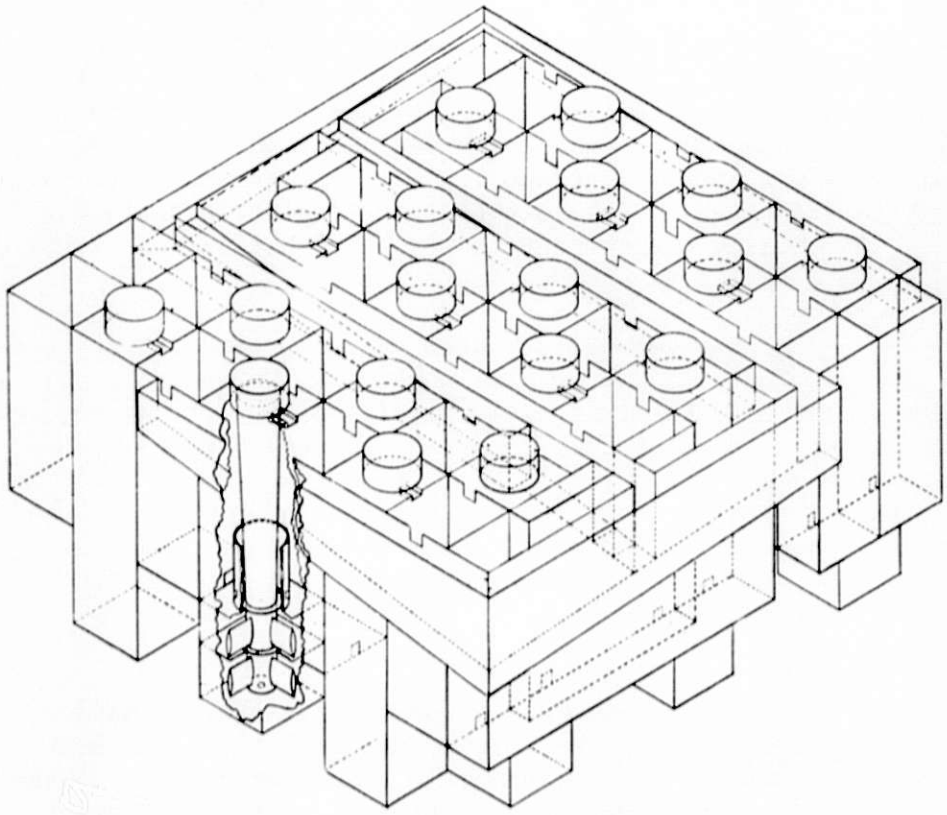

Fig. 10. Nine-Stage Mixer-Settler

The flow pattern in one stage of the MSC process is shown in Fig. 11. (a clearer version of [Fig. 20., STEINDLER-1979C]). Each metal stream moves from a settling chamber into a mixing chamber through an underflow weir. Each salt stream moves from a settling chamber into a mixing chamber through an overflow weir. Mixed metal and salt streams are pumped out of the mixing chamber(s) and into settling chambers, where the metal and salt are separated before being gravity-fed into the appropriate mixing chambers.

*[Figure 19, STEINDLER-1979C] is a flow diagram of the Mixer-Settler Continuous Process.

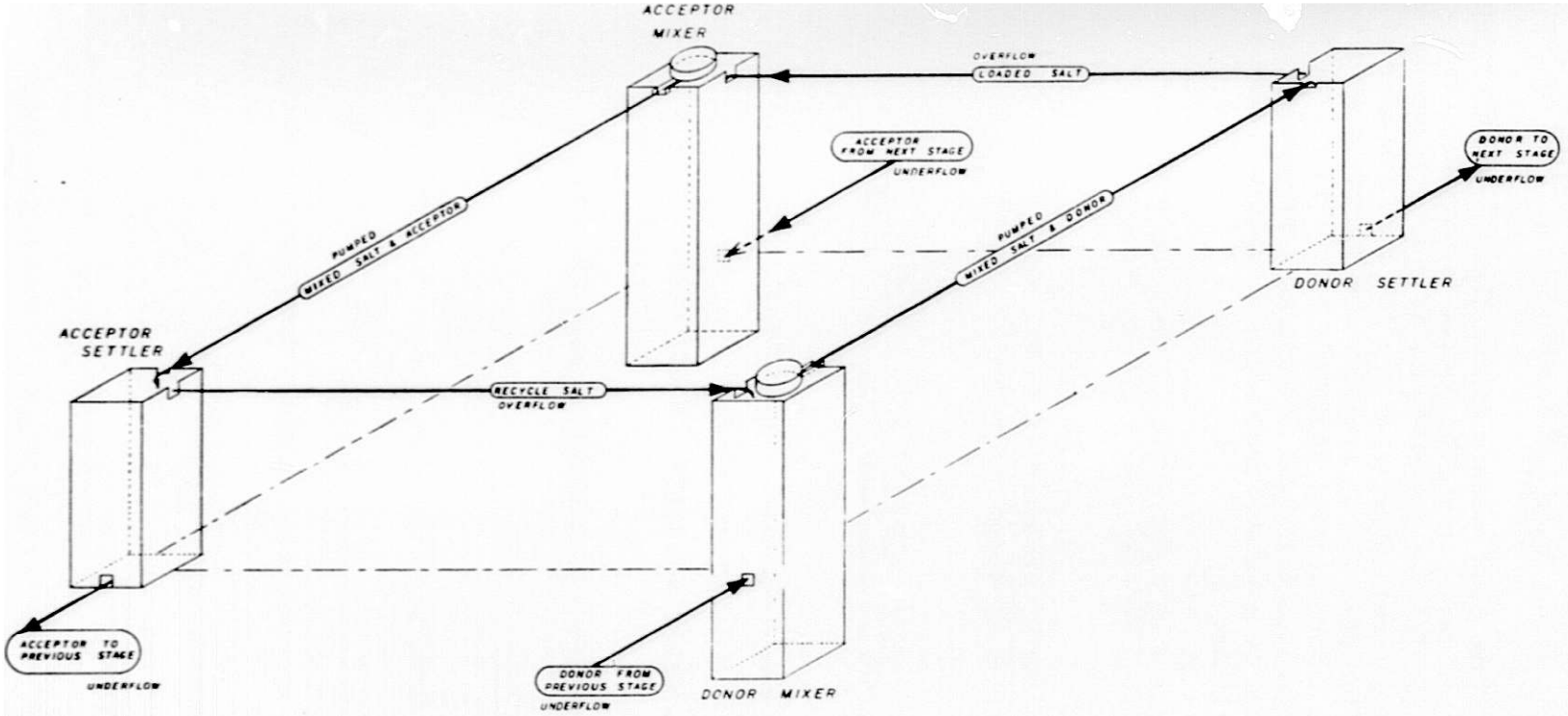

Fig. 11. Flow Pattern in Typical Mixer-Settler Stage--Exploded View

The donor and acceptor metal streams move from stage to stage, countercurrent to each other. The transport salt is captive within each stage and contacts the donor and acceptor in a cross-current fashion.

This flow pattern allows the MSC train to perform as if the donor and acceptor were immiscible phases in countercurrent contact. At steady state, the transferring constituents in the salt streams will reach an equilibrium value and remain constant. The net mass transfer will be between the donor and acceptor phases. By treating the MSC train as a countercurrent contactor, with the transport salt analogous to the interface between the phases, the equilibrium coefficients for transfer between the donor and acceptor can be calculated from known donor-salt and salt-acceptor equilibrium coefficients, as follows:

$$\text{Let } K_{o_i} = \frac{\text{Mass fraction of component i in the acceptor}}{\text{Mass fraction of component i in the donor}} \tag{1}$$

$$k_{d_i} = \frac{\text{Mass fraction of component i in the salt}}{\text{Mass fraction of component i in the donor}} \tag{2}$$

$$k_{a_i} = \frac{\text{Mass fraction of component i in the salt}}{\text{Mass fraction of component i in the acceptor}} \tag{3}$$

K_{o_i} is the overall equilibrium coefficient;

k_{d_i} is the donor-salt equilibrium coefficient;

k_{a_i} is the acceptor-salt equilibrium coefficient

Further, let

Y_i = the mass fraction of component i in the salt

X_i = the mass fraction of component i in the donor

t_i = the mass fraction of component i in the acceptor

then

$$k_{d_i} = \frac{Y_i}{X_i}, \qquad k_{a_i} = \frac{Y_i}{t_i} \tag{4}$$

$$\text{and } K_{o_i} = \frac{k_{d_i}}{k_{a_i}}$$

$$= \frac{Y_i}{X_i} \cdot \frac{t_i}{Y_i}$$

$$= \frac{t_i}{X_i} \qquad (5)$$

The donor-acceptor equilibrium coefficient, K_{o_i}, allows the number of ideal stages for the desired plutonium recovery to be calculated. This number of ideal stages can be compared with the number of transfer units in a countercurrent tower. This calculation has been done for the reference fuel and a representative donor alloy, transport salt, and acceptor alloy at an operating temperature of 800°C, which was arbitrarily chosen. This calculation yields two equilibrium (ideal) stages. A similar calculation done for a donor-crossflow salt system showed that nine stages were required. However, this latter calculation would have yielded a different result if a different salt flow rate had been used.

It is apparent from this that the number of ideal stages, analogous to the number of transfer units, is fixed by the equilibria of the uranium, plutonium, and fission products. These equilibria are affected by alloy and salt compositions and temperature.

The number of real stages required for each ideal stage can be compared to the height of a transfer unit (HTU). In the MSC process, the stage efficiency, or HTU, can be changed by adjusting the salt flow rate. Changing the salt flow has the same effect as changing the diffusivity in an extraction tower.

In the MSC train, the mixture of metal and salt is pumped out of the mixing chamber into the settling chamber by a centraxial pump. This type of pump was developed at Argonne National Laboratory in the early 1970's by J. B. Knighton et al. for use in salt transport systems [KNIGHTON-1971].

The pump itself consists of a truncated cone with the ends closed, forming a hollow chamber (see Fig. 12). In operation, the cone spins about its axis, creating a centrifugal force on the fluid inside the pumping chamber. The centrifugal (radial) force is converted to axial force by the tapered walls of the pumping chamber. Fluid enters the pumping chamber through an inlet orifice in the small end of the truncated cone, exits through slots in the large end, and is carried away by an outflow weir. Flow can be limited by downsizing the inlet orifice.

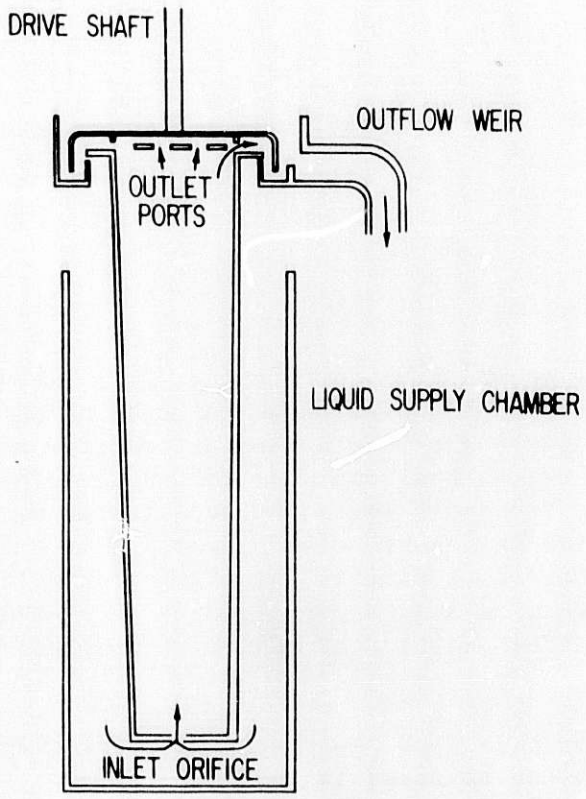

Fig. 12.

Cross-sectional View of Centraxial Pump

(5) Proliferation Study
(J. L. Zoellner*)

One of the criteria in this proliferation study [STEINDLER-1979C] is that the fissile material produced should be sufficiently radioactive and diluted with fertile material so that diversion is difficult, detection of the material is easy, and conversion into weapons-usable material is difficult. Sufficient radioactive contamination will be defined as 500 rads/h at 1 m from a mass of material containing 8 kg of plutonium. The fissile material should be diluted with fertile material so that the fissile content is less than 20%.

The effects of recycle of the core/axial blanket and radial blanket fuel by the U-Pu Salt Transport Process (Fig. 13) were analyzed.

Recycling the radial blanket fuel material, a possible method of increasing its enrichment, was examined. As stated in the preceding report [STEINDLER-1979C], the enrichment of the radial blanket fuel material after one pass through the process is estimated to be 12.4%. Plutonium recovery is 59.9%. If this processed material is returned to the beginning of the process and recycled, an increase in the enrichment of the processed material is obtained. If we assume that the FP-3 transport and uranium-plutonium transport salts are saturated [Table 25, STEINDLER-1979C], the resulting enrichment is 27.2% with 99% recovery after two passes. These values are 17.5% and 99.2%, respectively, after three passes. The gamma radiation associated with the uranium-plutonium acceptor alloy is 782 rads/h at three feet (2.0 kg Pu), which meets the proliferation criteria.

---

*Rockwell International, Rocky Flats.

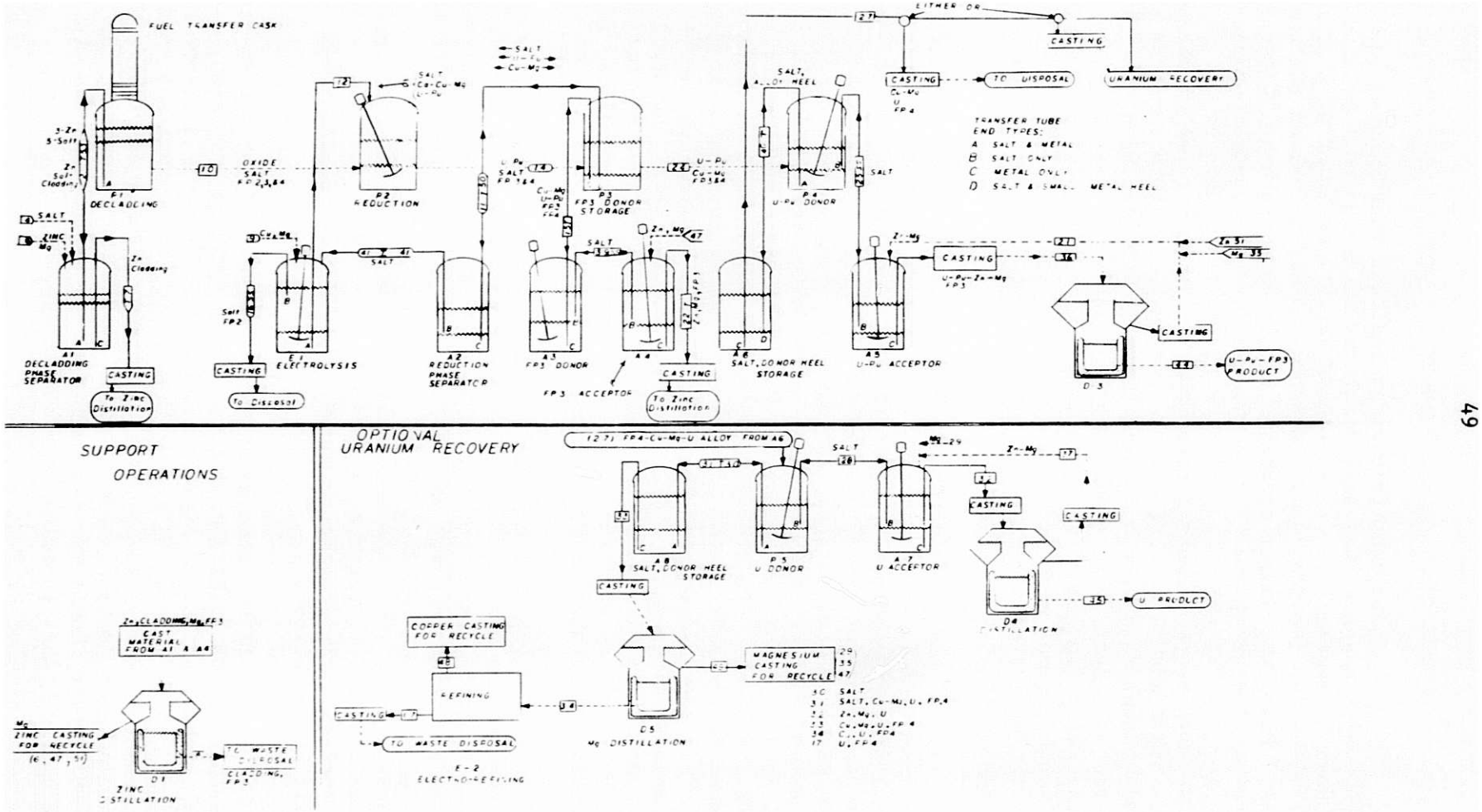

Fig. 13. Salt Transport Process Flow Diagram

These results clearly indicate that recycle is definitely a method by which blanket fuel enrichment may be increased. However, several points should be mentioned: (1) To obtain an enrichment of approximately 20%, the material in the acceptor vessel must be removed either on the second or third pass. Since the number of passes required to reach a 20% enrichment for a core/axial blanket assembly is five, a different set of process controls would be required for the radial blanket assemblies. However, it is desirable to have the same process control requirements for both types of assemblies since this would enable a single plant line to handle both types of assemblies without adjustment to operation sequence. (2) Although 99% of the plutonium is recovered on recycle, the amount sent to recycle is only 59.9% of the amount originally contained in the radial blanket assembly; this would result in significant plutonium losses in the waste streams. (3) Finally, most of the alloy contents are solids, requiring additional activities to remove the solids (uranium and copper) from the vessel.

As yet, a suitable method for obtaining 20% enrichment and 99% recovery of fissile material from radial blanket assemblies has not been established, if the same reagents as are used for core/axial blanket assemblies are used for radial blanket assemblies. As stated above, present enrichment of the radial blanket fuel material after a one-pass recycle process is estimated to be 12.4%, with a plutonium recovery of 59.9%. Conditions are 850°C for the U-Pu donor alloy and 700°C for the U-Pu acceptor alloy. If instead of the single U-Pu transport pass, the number of U-Pu transport passes is continued until 97.7% of the plutonium is recovered, the enrichment drops to 3.1%. This represents virtually no increase in enrichment over the process input material enrichment of 3.05%; moreover, it requires 21 steps to reach 97.7% recovery. The effects of increasing the magnesium content of the U-Pu donor alloy on the reprocessing of radial blanket fuel assemblies, currently under investigation, are discussed below.

When the core/axial blanket acceptor alloy product is recycled through the process (under base-case conditions), the processed material is slightly more enriched. After five passes, this enrichment is 21% and the plutonium recovery is 99.3%. This can be compared with the previously reported values of 18.9 and 99.3%, respectively, obtained after the first process cycle. This indicates that the core/axial blanket process product can be slightly enriched by product recycling. Possibly, enrichment could be significantly increased upon repeated recycle of the product. This effect will be investigated.

It has been noted during recycle of the various types of materials that if the initial conditions assumed the use of fresh, uncontaminated salt, the quantity of fission products in the various alloys was insufficient in all cases. To ensure that sufficient quantities of fission products accompany the plutonium, all recycling, as well as regular processing, should be done with contaminated or spiked salts as mentioned in [STEINDLER-1979C]. Provisions should be made in the design to increase the difficulty of replacing the transport salts in the system during operation.

One method whereby the uranium-plutonium product might be decontaminated for diversionary purposes involves the transfer of contaminated uranium-plutonium transfer salt into the salt and donor heel storage

vessel (A6) (Fig. 13) after transfer of the product to the acceptor vessel (A5). The turntable is then rotated in readiness for the next transport operation and a fresh batch of core/axial blanket material is put into place (P4). Uncontaminated salt is then introduced into the acceptor vessel (A5). From here, it is transferred to the uranium-plutonium donor vessel, where it is contacted with the fresh batch of uranium-plutonium alloy. The salt is then transferred back to the acceptor vessel (A5) where the uranium, plutonium, and FP-3's are reduced by and retained in the acceptor alloy. The acceptor alloy is then transferred to distillation for zinc-magnesium removal. The result is an alloy that has a low FP-3 concentration. This is due to the action of the clean salt which contains a smaller amount of FP-3's than does a salt laden with FP-3's and hence transfers a smaller amount of FP-3 to the acceptor alloy than does the FP-3 laden salt (see Tables 14 and 15). The material is approximately 56.3% enriched and contains 8.9 kg or 89.1% of the plutonium from the donor. The FP-3's associated with this material (0.4 kg) emit 328 gamma rad/h; this is below the level set in the proliferation criteria. The defense against proliferation of this type is to ensure that no introduction of uncontaminated salts into the donor-acceptor vessels at the uranium-plutonium transfer point is possible. This may be accomplished by direct piping of the zinc-magnesium transfer lines from the distillation units. The necessary make-up salts could be added to the salt and donor heel storage vessel.

Another option for producing a highly decontaminated uranium-plutonium product could be initiated in the same manner as discussed above. However, instead of merely adding decontaminated salt to the acceptor vessel, a batch of decontaminated FP-3 transport salt is added. Contacting a sufficient quantity of this salt with the uranium-plutonium alloy in P4 removes the FP-3's almost entirely. This salt is then transferred to the acceptor vessel A5, where the FP-3's are reduced into the acceptor alloy. This alloy is removed and sent to distillation unit D3. Meanwhile, fresh acceptor alloy is placed in A5. After one pass of salt between P4 and A5, the new acceptor alloy now contains 8.9 kg plutonium, 6.9 kg uranium and essentially no FP-3's; this is a very desirable product. Again, for proliferation resistance, there must be no capability for adding salt to the acceptor vessel.

One method of preventing such action that has been considered would be to feed the molten Zn-Mg alloy from the distillation vessel (D3) directly through a transfer line (rather than as solids) into the U-Pu acceptor vessel. Then, salts could not be transferred to the A5 vessel. If the salts mixture were placed in distillation vessel D3, it could not be heated to a sufficiently high enough temperature to evaporate or sublime the salts. Such action requires temperatures in excess of 1600°C; the distillation vessels, however, will be designed to operate at temperatures no higher than 1000°C.

Although direct transfer of the Zn-Mg alloy through a transfer line would be a way of preventing such action, it would not be desirable owing to the difficulty in operating the required valves or freeze seals. Another way to prevent diversion by the above method is by appropriate sizing of the vessel heels. The heel remaining at the bottom of the acceptor

Table 14. Salt Transport with Uncontaminated (Clean) Salt; One-Pass Example--Core/Axial Blanket Fuel Material

	Initial	
	U-Pu Donor, kg	U-Pu Salt, kg
U	22.390	0
Pu	10.074	0
FP-3	1.019	0
Gamma rad/h[a]	836	0
	After Donor-Salt Contact	
	U-Pu Donor, kg	U-Pu Salt, kg
U	15.476	6.914
Pu	1.052	9.022
FP-3	4×10^{-4}	1.0188
Gamma rad/h[a]	0.33	836
	Before Salt-Acceptor Contact	
	U-Pu Salt, kg	U-Pu Acceptor, kg
U	6.914	0
Pu	9.022	0
FP-3	1.0188	0
Gamma rad/h	836	0
	After Salt-Acceptor Contact	
	U-Pu Salt, kg	U-Pu Acceptor, kg
U	0.030	6.884
Pu	0.138	8.884
FP-3	0.6188	0.4
Gamma rad/h	507	328

[a]The radiation noted here is from the FP-3 group only. The FP-4's remain with the donor as a defense, and contribute 13,950 gamma rad/h at 3 ft.

Table 15. Salt Transport with Contaminated Salt; One-Pass Example--Core/Axial Blanket Fuel Material

	Initial	
	U-Pu Donor, kg	U-Pu Salt, kg
U	22.390	0
Pu	10.074	0
FP-3	1.019	1.3
Gamma rad/h[a]	836	1066
	After Donor-Salt Contact	
	U-Pu Donor, kg	U-Pu Salt, kg
U	15.476	6.914
Pu	1.052	9.022
FP-3	9×10^{-4}	2.318
Gamma rad/h[a]	0.73	1900
	Before Salt-Acceptor Contact	
	U-Pu Salt, kg	U-Pu Acceptor, kg
U	6.914	0
Pu	9.022	0
FP-3	2.318	0
Gamma rad/h	1900	0
	After Salt-Acceptor Contact	
	U-Pu Salt, kg	U-Pu Acceptor, kg
U	0.030	6.884
Pu	0.138	8.884
FP-3	1.45	0.868
Gamma rad/h	1189	712

[a]The radiation noted here is from the FP-3 group only. The FP-4's remain with the donor as a defense, and contribute 13,950 gamma rad/h at 3 ft.

vessel will be sized to contain sufficient fission products so that even if a decontaminated salt were introduced into the vessel, the resulting radiation level would meet the proliferation criteria requirements. The Salt II computer model will be used to evaluate the effect of these heels.

Study of the effects of varying the magnesium content of the U-Pu donor alloy has begun, using core/axial blanket fuel assemblies. Table 16 shows the results to date. This table shows data for 800°C (U-PU donor) and 700°C (U-Pu acceptor), since no data exist for higher temperatures. (These results, however, should show trends that can be expected at higher temperatures.) Note that as the magnesium content is increased, the enrichment increases, but the corresponding plutonium recovery decreases. In all cases, sufficient fission products are transferred with the alloy to keep the radiation level well above 500 gamma rad/h, which is the minimum desired level. However, the total mass of material required to keep the magnesium in solution results in volumes that are too large for the 10-ft^3 volume of the design vessel. Therefore, increasing the magnesium content of the donor alloys is not practical as a method of discouraging diversion.

Table 16. Effects of Increasing the Magnesium Content of U-Pu Donor Alloy in Salt Transport Process

Eight U-Pu Transport Passes
U-Pu Donor: 800°C
U-Pu Acceptor: 700°C

Mg Content, wt %	6.5	8.0	13.5	20.0
Enrichment, %	19.9	25.1	50.5	67.9
Pu Recovery, %	98.9	98.7	96.2	76.6
FP-3 Gamma rad/h at 3 ft	803	764	716	690
Alloy Volume, ft^3	2.9	3.4	8.0	14.5
Salt Volume, ft^3	7.8	7.8	7.8	7.8

The effect upon uranium-plutonium transport of using either clean or contaminated transport salt is shown in Tables 14 and 15. The steady-state fission-product buildup in the process transport salts results from the continuous processing of core/axial blanket fuel assemblies. Because radial blanket fuel assemblies have a low content of fission products in comparison to core/axial blanket assemblies, it may be possible to lower the steady-state fission-product content of these process transport salts by running several radial blanket assemblies through the process. It has been found that after five radial blanket fuel assemblies have been processed,

starting with steady-state fission-product salt loadings, the fission-product salt loadings are reduced to approximately one-half the steady-state values for core/axial blanket. Introduction of a core/axial blanket fuel assembly at this point results in a fission-product loading of 554 gamma rad/h for 9.9 kg of plutonium. At steady-state conditions, the same mass of plutonium is associated with enough fission products to produce 821 gamma rad/h at 3 ft. It is predicted that approximately ten radial blanket fuel assemblies would lower the transfer salt fission-product content sufficiently to reduce the radioactivity of the product below the proliferation criteria level. However, recycle of ten radial blanket assemblies has not yet been simulated.

As discussed in the salt transport computer model portion of this report, the Salt-II computer model is operable and is being used to perform the proliferation analyses. Due to algorithmic differences, the results of salt transport processing, using the Salt-II model differ somewhat from those obtained using the first model Salt-I.

Four cases have been run, using the Salt-II model, in which the uranium-plutonium donor and acceptor operating temperatures were varied. Table 17 shows the results for these cases in which 270 kg of transport salt was used. The best combination of recovery and enrichment occurred at donor and acceptor temperatures of 850°C and 700°C, respectively. These results are similar to the results obtained when the same cases were examined using Salt-I. The most significant findings with Salt-II are that only 270 kg of U-Pu transport salt are needed for U-Pu transport and that the FP-3 concentration in the acceptor alloy is high enough to meet proliferation criteria even when the transport salt is initially free of FP-3 fission products (see Table 18).

The Salt-II model is currently being used to generate data for continuation of the proliferation analysis. The main areas of examination will include the fects of recycle and of varying the magnesium content.

Table 17. Effect of Temperature Variation on Salt Transport Process: Initial Case Study for Salt-II Computer Model

Case	U-Pu Donor Temp, °C	U-Pu Acceptor Temp, °C	Weight of U-Pu Trans. Salt, kg	No. of Passes	Pu Enrichment, %	Pu Recovery, %
1	850	750	270	5	19.2	99.07
2	850	700	270	5	19.2	99.17
3	800	750	270	5	38.1	99.23
				10	24.2	99.80
4	800	700	270	5	38.1	99.32
				10	24.2	99.90

Table 18. Uranium-Plutonium Transport Steps with Core/Axial Blanket Reference Fuel (Case 2, Table 17)

Donor Alloy Temp: 850°C
Acceptor Alloy Temp: 700°C
Weight of Transport Salt:[a] 270 kg

Pass	Donor, kg			Salt, kg			Acceptor, kg			Total Enrichment, Pu/Pu + U	Pu Recovery, kg	FP-3 Gamma rad/h at 3 ft from:	
	U[b]	Pu	FP-3	U	Pu	FP-3	U	Pu	FP-3			U-Pu Acceptor	Mass Containing 8 kg Pu
Start	10.824	9.874	0.999	0	0	0	0	0	0	---	---	---	---
1	25.669	3.616	0.002	0.048	0.042	0.149	8.625	6.216	0.848	0.419	0.632	695.3	894.9
2	25.618	1.347	0.0003	0.049	0.025	0.143	15.068	8.470	0.850	0.332	0.863	697.0	658.3
3	25.664	0.511	0.0003	0.049	0.019	0.141	15.057	9.300	0.850	0.269	0.948	697.0	599.6
4	25.744	0.199	0.0003	0.048	0.017	0.140	15.038	9.609	0.850	0.223	0.979	697.0	580.3
5	23.189	0.082	0.0003	0.044	0.016	0.139	15.018	9.726	0.850	0.192	0.992	697.0	573.3

[a] Transport salt is initially free of FP-3 fission products.

[b] All values shown are the amounts of material in solution only.

(6) U-Cu-Mg Ternary Studies

(M. Bracco,* W. A. Averill,* D. L. Olson,* and T. Whipple*)

Uranium and plutonium are separated from FP-4 fission products by the use of a Cu-16 at. % Mg donor alloy. The operation of the alloy is complex, and the ternary phase diagram (U-Cu-Mg) was constructed from available binaries. These measurements will confirm the constructed phase diagram.

The furnace for melting the alloys and the furnace for alloy analysis were built. The furnace used to prepare alloys consists of two semicylindrical heating elements, surrounded by a fibrous, insulating material and enclosed within a thin steel sheath. The heating elements and insulation are sandwiched between two refractory plates.

The furance built for differential analysis measurements is a clam-shell furnace. This design allows the furnace to be removed from around the steel crucible. The sample holder can then cool at a rate that allows thermal measurements to be made.

A thermocouple guide was built to keep the thermocouples positioned in the crucibles and to allow consistent positioning for each measurement. The thermocouple leads are wired into a recorder, and an electronic ice point device was installed to correct for any potentials generated by changes in room temperature. The controller thermocouple used to monitor the furnace temperature was wired into the controller.

Alloy preparation was initiated by subdividing the magnesium and uranium into more workable forms. The magnesium rod was cut into thin disks, then broken into finer pieces. The uranium plates were also cut into small pieces. The initial alloys prepared for analysis were: 95 wt % copper-5 wt % magnesium, 90 wt % copper-10 wt % magnesium, and 85 wt % magnesium-15 wt % copper. The glove box was sealed and purged with argon gas. The oxygen concentration in the glove box atmosphere was found to be below 6% and the Dri-Train was activated. After three days of operation, the glove-box atmosphere was found to be an acceptable 75 ppm oxygen.

The first trial run was made with a binary alloy consisting of 2 wt % magnesium and 98 wt % copper, using pure copper as a reference. Differential thermal analysis (DTA) information, as well as physical observation, indicated that the alloy did not melt completely.

A second trial run was made using a 5 wt % magnesium-95 wt % copper alloy, with pure copper as a reference. A eutectic mixture of calcium chloride and calcium fluoride (20 mol % CaF_2, mp 650°C) was placed on top of the alloy to prevent the escape of excessive amounts of magnesium vapor from the crucible. These data on the liquidus line were compared to the phase diagrams reported in the literature, and some disagreement was noted.

---

* Rockwell International, Rocky Flats.

The composition of the prepared alloy changed during meltdown. A shift of 2% toward the copper-rich side was indicated and later confirmed by atomic absorption analysis.

Differential thermal analysis (DTA) tests to check out equipment have been completed, and data runs are in progress. There was a slight delay in which a stray voltage source was located. This source was significant enough to cause complete masking of the differential signal from the thermocouples. The problem has been solved by grounding one of the legs of the DTA input.

A copper-uranium master alloy was developed for mixing with the copper-magnesium alloy in preparing the ternary alloys. To make the copper-uranium alloy, the uranium was first "pickled" in a dilute nitric acid solution. The "pickled" uranium and the copper were placed in an alumina crucible. This crucible was placed inside a glass assembly, which was purged with argon and then evacuated. The alloy was prepared in an induction furnace. The alloy was then broken into pieces; chemical analysis indicated its composition to be 74 wt % copper and 26 wt % uranium.

Because of the corrosiveness of the ternary copper-magnesium-uranium alloy, a new type of thermocouple was used--tungsten-5% rhenium and tungsten-26% rhenium. The bare thermocouple wires were inserted into a two-hole alumina insulator, and the ends were bent to keep the wires in the insulator. The "bent" ends were placed in the melt; the free ends were connected to a terminal block, which was connected to the recorder.

The first data point taken with the new assembly was obtained using the copper-magnesium master alloy developed earlier. A ternary data point was taken using an alloy composed of 17.5 wt % magnesium, 12.5 wt % uranium, and 70 wt % copper.

Next, the development of an isopleth for 5 wt % uranium was begun. Data points for the following magnesium compositions were taken: 2.5 wt %, 5 wt %, 7.5 wt % 10 wt %, 12.5 wt %, 15 wt %, and 20 wt %. (The remainder of the alloy was copper.) They were based upon the compositions of the copper-uranium master alloy and the copper-magnesium master alloy. After the differential measurements had been made, each alloy was broken up. A small portion of each will be mounted and prepared for micrography. Another portion will be taken for chemical analysis. The amounts of copper and magnesium are determined by atomic absorption; the uranium is determined by X-ray fluorescence. The actual compositions of the alloys are then plotted on graph paper.

Currently, work is being done on the 10 wt % uranium isopleth. This work, along with work on the 5 wt % uranium isopleth, the photomicrographs, and the upcoming analyses of the phases present in the various alloys using energy-dispersive X-ray analysis will continue.

c. Separation Processes

(1) Proof-of-Principle Studies
(M. F. Boyle,* R. F. Fitzpatrick,* and R. O. Wing*)

The experimental runs for the Proof-of-Principle studies are identified by the letters PRO followed by a three digit number (e.g., PRO-001). Nine experimental runs have been completed to date. These runs and the data generated are discussed.

The initial experiments were of little value in obtaining useful analytical data, but were extremely useful in establishing technical expertise and developing consistent sampling methods. We feel that later experimental runs provided practical data. This confidence stems from the use of an improved sampling technique in the later experiments. The improved sampling technique involves drawing a vacuum inside the sample tube while simultaneously pressurizing the furnace cell. The pressure differential across the tantalum frit is sufficient to force either the molten salt or the molten alloy into the tantalum sampling tube (Fig. 14). The new sampling arrangement was necessary because of pressure limitations imposed on furnace cell operations (a pressure vessel) by the Health and Safety Department of Rockwell International, Rocky Flats.

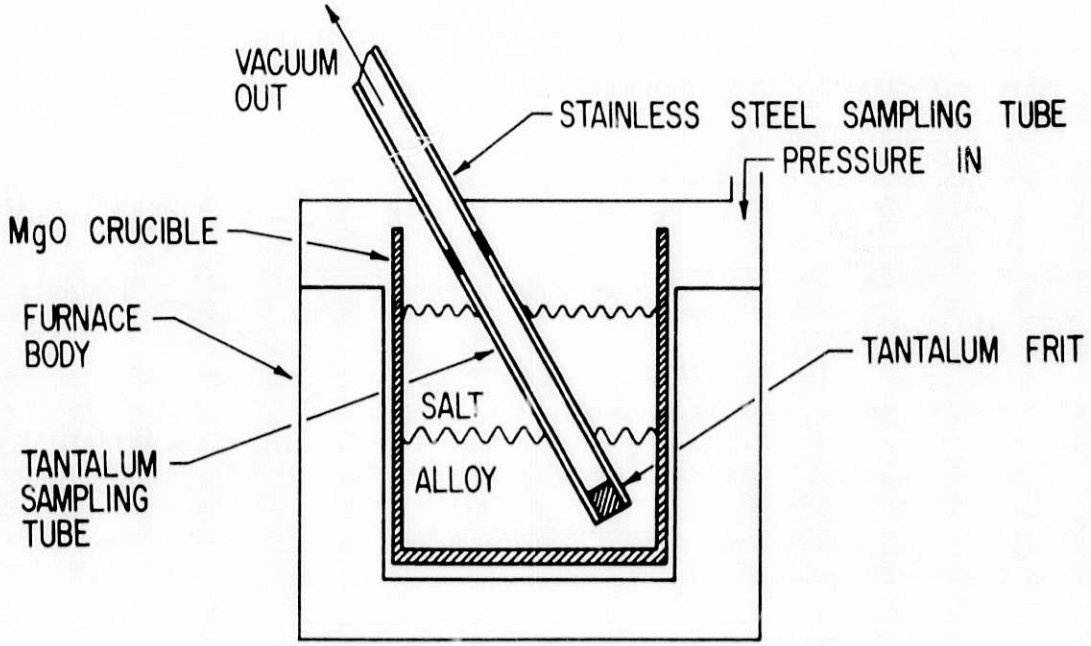

Fig. 14. Schematic of Furnace Cell and Sampling Assembly

*Rockwell International, Rocky Flats.

The first equilibrium experiment, PRO-001, was to determine the partitioning between molten salt and liquid alloy phases of plutonium, uranium, FP-3's (with americium as a stand-in), and FP-4's (with zirconium as a stand-in). This experiment corresponds to the FP-3/Donor Alloy segment of the Salt Transport Process. In the FP-3/Donor Alloy experiments, a molten salt phase consisting of 6.4 wt % $MgCl_2$-17.8 wt % KCl-75.8 wt % $CaCl_2$ is equilibrated with a liquid alloy phase of 79.1 wt % copper-4.6 wt % magnesium-7.2 wt % plutonium and americium (combined)-7.9 wt % uranium-1.2 wt % zirconium. The salt and alloy samples from this system were taken at three temperatures (800, 850, and 890°C). The $MgCl_2$ concentration was then increased to 8 wt %. Again, salt and alloy samples were taken at the three temperatures. The $MgCl_2$ concentration was increased, to 9 wt %, and salt and alloy samples were taken at the three temperatures.

The results from the sample data of experiment PRO-001 were of little practical value owing to the inability to obtain consistent alloy samples. This inability is attributed to the initial sampling technique in which only the cell was pressurized (Δp = 15 psig).

A qualitative analysis of the information from PRO-001 indicates that on the basis of americium behavior, the FP-3's were transferred into the salt phase. The uranium and plutonium were not as readily transferred. This is the only observation of any certainty yielded by the data.

Experiment PRO-002 was another run corresponding to the FP-3/Donor Alloy segment of the process. It was aborted due to mechanical difficulties with furnace thermocouple placement. No sampling was attempted.

In Experiment PRO-003, another FP-3/Donor Alloy run, an objective was to obtain samples large enough for analysis. The sampling method was the same as that used in PRO-001 except that the furnace cell was pressurized to 20 psig. Also, a different, more porous tantalum frit (Type: KL-308-30, Tantalum Pellet Co.) was used as the filtering medium on the sample tubes. Even with these modifications, we were unsuccessful in obtaining alloy samples.

The aforementioned improvement, incorporated into the existing sample tubes, was used in experiment PRO-004. This was also an FP-3/Donor Alloy run, and a sampling apparatus was used that allowed the sample tube to be evacuated simultaneously with pressurization of the furnace cell (Fig. 14). This method provided the pressure differential needed to force liquid alloy into the sample tube. This run was to verify that the improved sampling technique gave consistent samples, and no samples were saved.

Using the new sampling technique, FP-3/Donor Alloy experiment PRO-005 was conducted at temperatures from 810 to 930°C. Salt and alloy samples were obtained, prepared, and sent to the Analytical Laboratory for analysis. The results are tabulated in Table 19.

The distribution coefficients, K_d, for plutonium, americium, and uranium were calculated from the sample results. The distribution coefficient is defined as the ratio of the concentration of a species in the salt phase to the concentration of the same species in the alloy phase:

$$K_d = \frac{\text{Amount in salt phase}}{\text{Amount in alloy phase}}$$

Table 19. Summary of Results from Run PRO-005

Initial Alloy Comp., 79.1 wt % Cu, 4.6 wt % Mg, 7.2 wt % Pu, Am, 7.9 wt % U, 1.2 wt % Zr

Initial Salt Comp., 6.4 wt % $MgCl_2$, 17.8 wt % KCl, 75.8 wt % $CaCl_2$

Sample No.	Sample Type	Temperature, °C	Final Mg, wt %	Final Am, ppm	Final U, wt %	Final Pu, ppm	Final Zr, wt %
16699	alloy	855	4.63	2130	1.59	98800	-
16700	salt	855	1.19	981	0.0103	4450	<0.001
16701	alloy	810	5.16	1990	0.63	88300	-
16702	salt	810	1.11	883	<0.0048	2150	<0.001
16703	alloy	830	4.37	1840	2.36	85500	0.05
16704	salt	830	2.06	1060	<0.0048	1390	<0.001
16705	alloy	850	5.01	2090	2.16	104500	-
16706	salt	850	2.01	1540	<0.0048	2970	<0.001
16707	alloy	930	3.81	1890	4.45	95600	0.05
16708	salt	930	1.94	1780	<0.0048	2830	<0.001

These values are tabulated in Table 20. The distribution coefficients at 810°C can be compared with the estimated distribution coefficients [KNIGHTON-1979] used in the computer modeling of the salt transport process. The FP-3 distribution coefficient, assumed from the americium measurements, is approximately one order of magnitude lower than the cerium value used in modeling the process. This difference is due to the use of americium rather than cerium as the FP-3 stand-in.

Table 20. Comparison of K_d Values from Experiment PRO-005 with Estimated K_d Values

Temperature, °C	Exp. Dist. Coef., K_d			Est. Dist. Coef., K_d, at 800°C[a]		
	Am	U	Pu	Ce	U	Pu
855	0.46	0.0065	0.045			
810	0.44	0.0076	0.024	10.7	0.0015	0.0317
830	0.58	0.0020	0.016			
850	0.74	0.0022	0.028			
930	0.94	0.0011	0.029			

[a] J. B. Knighton, Rockwell International, Rocky Flats Plant, personal communication (1979).

The experimental distribution coefficients for uranium and plutonium, K_d(U) and K_d(Pu), respectively, are close to the estimated values. Also, the data (Table 20) indicate an increase in K_d(Am) as the temperature is increased. This anomaly will have to be verified in future experiments, along with the temperature effects on the uranium and plutonium K_d values. The data did show little tendency for the transfer of the FP-4 stand-in, Zr, from the alloy to the salt phase. These data and trends are preliminary; more testing is planned.

The next proof-of-principle study, PRO-006, was to determine the distribution coefficients of americium, plutonium, and uranium for the U-Pu Donor Alloy system. The alloy phase was 6 wt % Mg-Cu, and the salt phase was 16 wt % MgF_2-$MgCl_2$. Uranium was added to the alloy to make it 10 wt % in uranium. The alloy and salt were heated to 870°C, and samples were taken to provide a background level for the experiment. Plutonium metal containing americium as an impurity was added to the molten salt and liquid alloy and mixed for 1/2 h at 870°C, and additional samples were obtained from this mixture.

The analytical results from these samples indicated that the americium was transferred from the alloy phase to the salt phase (K_d(Am) ≈ 9) and that the distribution coefficient was independent of temperature in the range, 800 to 870°C. The data also indicated that the plutonium was transferred from the alloy phase to the salt phase (K_d(Pu) ≈ 1) and that the transfer was temperature-independent in the same temperature range as americium was. The uranium showed no inclination to transfer (K_d(U) ≈ 0.03). The estimated distribution coefficients are compared with those found experimentally in Table 21. Again, the experimental distribution coefficients for Am are approximately a factor of 10 lower than the estimate for cerium, as in experiment PRO-005. This difference may be due to the differences in reaction of Am and Ce. These are preliminary results, and definitive statements must await additional results.

Experiment PRO-007 was an FP-3/Donor Alloy run. This was part of the verification of the K_d values obtained from PRO-005. The analytical results have not yet been received from the Analytical Laboratory and will be reported when they are obtained.

Table 21. Comparison of K_d Values from Experiment PRO-006 with Estimated K_d Values

Exp. Dist. Coef., K_d			Est. Dist. Coef., K_d[a]		
Am	Pu	U	Ce	Pu	U
≈9	≈1	≈0.03	600	2.1	0.41

[a] J. B. Knighton, Rockwell International, Rocky Flats Plant, personal communication (1979).

Experiment PRO-008 was a U-Pu Donor Alloy run. In this case the alloy was saturated with uranium, and the plutonium distribution coefficient was determined at various temperatures. Again, analytical results have not yet been received.

Experiment PRO-009 was similar to PRO-008, except that the alloy was less concentrated in uranium. Results are awaited. Additional experiments are planned.

(2) Molten Salt Purification Laboratory
(T. D. Santa Cruz)*

The laboratory is now producing salts of prescribed composition for the Proof-of-Principle and Fabrication studies. The salt systems presently under study are the 80.9 wt % $CaCl_2$-19.1 wt % KCl system and the 75.8 wt % $CaCl_2$-17.8 wt % KCl-6.4 wt % $MgCl_2$ system. Different sources of salt constituents are being evaluated. Chemical and instrumental techniques for the analyses of calcium, magnesium, potassium, and chloride are being used to determine the true salt constituent composition.

Black salt studies are focused on (1) the metal (or alloy) contained by the salts and (2) the black salts reported in the electrorefining literature of plutonium. In the electrorefining literature for plutonium, such terms as "black solid," "black material," and "black salt" are used. The modes of containment include simple entrainment, the formation of colloidal metallic fogs ("metallnebels"), and the formation of sub-halide compounds. This problem has been recognized for some time [DROSSBACH, EASTMAN, EITEL, HEYMANN, LORENZ], but little effort was directed towards its solution. The diverse modes or mechanisms for alloy containment find support but are not proven by the physical properties of the salts. These reports come from several laboratories, including Hanford [BECKER], Savannah River [PORTER], and Rocky Flats [AUGE]. The survey has revealed that by increasing the average charge density on the salt cations in the salt, greater solvation of solutes can be accomplished and more complete consolidation of metals in the salt can be made.

Calcium chloride is a major ingredient in many of the salt systems used in the Salt Transport Studies portion of the PDPM program. It is the major constituent of salts for decladding, oxide reduction, and FP-3 transport. The capability of calcium chloride and its salt systems to dissolve calcium oxide has made its use an important part of the Salt Transport Studies.

Reagent anhydrous calcium chloride is said to assay at not less than 96% $CaCl_2$, not more than 2.0% magnesium and alkali salts (as sulfates), and not more than 0.02% $Ca(OH)_2$. The remaining impurity is water, present due to the deliquescence of calcium chloride. This water affects the calcium oxide content upon fusion since at the temperatures needed to make the salts molten, the water reacts with the calcium chloride to produce calcium oxide and hydrogen chloride. Samples of a reagent-grade batch of anhydrous calcium chloride taken before and after fusion had calcium oxide contents of 170 and 6400 ppm, respectively.

---

* Rockwell International, Rocky Flats.

The increase in calcium oxide content of the calcium chloride salts can be corrected either by reducing the content chemically or by preventing its formation. The calcium oxide content can be reduced by sparging the molten salt with anhydrous hydrogen chloride [BAILEY] or by contacting the molten salt with a reductive liquid alloy such as Cd-Mg [JOHNSON-1969].

Buildup of calcium oxide can be prevented by removing the water prior to fusion of the salt [BAILEY]. Los Alamos Laboratories has a program which does just that [MULLINS]. Batches of about 22 kg of calcium chloride are stored in a vacuum oven at 20 in. of mercury and 200°C for one week and then used in their processes. After vacuum drying, about 300 ppm CaO is found in the salt upon fusing.

Sparging was found to reduce the CaO content from 6400 ppm to 320 ppm. Contacting the salt with a liquid alloy appears to lower CaO content to the 2,000 ppm level. Further testing and verification of these techniques is continuing, as well as testing of methods for preserving the salt once it is purified.

The Raman spectrometer has arrived. Plans for coupling it to the laser are under way. The furnace for the UV-Vis-NIR spectrophotometer is being manufactured. A vacuum oven has been set up and is being used to prepare dry salts for fusion.

4. Fabrication of Process-Size Refractory Metal Vessels
(C. M. Edstrom,* C. E. Baldwin,* R. R. Corle,* L. D. Johnson,* and A. G. Phillips*)

a. Introduction

Pyrochemical processing of nuclear fuels requires crucibles, stirrers, and transfer tubing that will withstand the high process temperatures and chemical attack by the molten salts and metals used in the process. The capability of fabricating the necessary hardware is critical to the pyrochemical process. For economics and safety, a crucible is needed that is large enough to contain the entire fuel rod. Tungsten, the material known to withstand process temperatures and chemical attack, is presently not available in sheet size large enough to provide the surface area of a large crucible. This dictates the development of joining, coating, and/or forming processes to achieve crucibles of the desired shape and size.

b. Engineering Analysis

Because this program may not be funded in FY 1980, emphasis has switched from vessel fabrication† to completing the service-life testing of three fabricated crucibles. These crucibles include: a spun molybdenum

---

*Rockwell International, Rocky Flats.

†The development of a brazed tungsten crucible and a riveted tungsten crucible has been stopped because there is insufficient time to test the service life of these crucibles.

crucible, a spun molybdenum crucible CVD coated with tungsten, and a free-standing tungsten plasma-sprayed graphite crucible which has been impregnated with nickel and sintered to improve density.

When the results of the service life test for the three crucibles are complete, R. M. Arons of Argonne National Laboratory and C. M. Edstrom will write a report summarizing material development during the two years of PDPM involvement.

The topical report on the literature search pertaining to tungsten fabrication has been distributed. This report summarizes most of the methods for fabricating tungsten such as sintering, rolling, extruding, spinning, joining, chemical vapor deposition, and plasma spraying. The intent is to provide information for a better understanding of tungsten fabrication, as well as to highlight specific methods for manufacturing PDPM hardware.

A 14-ft-long transfer line of 1-in.-ID tube made from molybdenum-30% tungsten, designed and manufactured by Metallwerke Plansee, would cost approximately $12,000. The tube is made by drilling 24-in. lengths of 1.57-in.-dia rod and threading and joining the lengths with a threaded pipe coupling. Thermo Electron, another supplier of refractory metal tubes, can gun-drill molybdenum - 30% tungsten in 10-ft lengths, which may reduce the manufacturing costs by eliminating some joints. Gun drilling would permit the use of rod having a smaller outside diameter.

c. Separation Processes

The tilt-pour furnace for evaluating the service life of crucibles containing zinc is operating. It was planned to evaluate a drawn and spun molybdenum crucible, a plasma-sprayed tungsten crucible impregnated with nickel and sintered at 1300°C in hydrogen, and a molybdenum crucible chemical vapor deposited (CVD) with tungsten.

To date, the furnace has been operated only during the day shift when it can be observed. It is heated by induction coils; before unattended operations were begun (as described below), a flow switch was installed on the coil cooling water to ensure power shutoff in the event that the water stops flowing.

In the on-and-off mode of operation, the spun molybdenum crucible showed no signs of corrosion after 24 h of exposure to 820°C zinc. However, reaction with zinc was revealed by the steel shaft of the stirrer. After a maximum of 4-min exposure to the zinc, more than 50% of the steel shaft was gone.

The 24 h/day operation of the tilt-pour furnace was delayed. Before a flow switch to turn off the power when the water flow stopped could be installed, an induction coil burst because of a lack of coolant flow. Replacement of this coil and proper joint seals caused a three-week delay in operating the tilt-pour furnace. A flow switch is now installed and the furnace has been operating continuously for 100 h while testing the drawn and spun molybdenum crucible. The zinc and molten salt will be poured after 144 h of continuous operation and the crucible examined for chemical attack.

The molybdenum crucible that is CVD-coated with tungsten appears to be very promising. One crucible has been subjected to thermal cycling at 100°C per hour heatup and cooldown. No visible signs of coating separation were observed. Sections cut from the lip of each crucible have been given thermal cycles of 16 h at 1000°C and 1200°C in a vacuum furnace. The objective of this thermal cycle is to initiate a metallurgical bond between the tungsten coating and the molybdenum. Argonne National Laboratory has examined the microstructure of these samples and has concluded that 16 h at 1000°C is a desirable thermal treatment. This treatment relieves signs of stress in the surface grains of the molybdenum, yet does not cause grain growth. There was no evidence, however, that the thermal treatments created a metallurgical bond. The CVD tungsten coating appears to be mechanically bonded to the molybdenum. Therefore, a rough surface on the molybdenum appears to be advantageous for increasing the bond strength during coating.

As indicated above, it was planned that the plasma-sprayed tungsten crucible to be tested for service life would be impregnated with nickel nitrate and sintered at 1300°C in a 100% hydrogen atmosphere. However, a 100% hydrogen atmosphere furnace large enough to sinter the full-size crucible may not be available. Examination at Argonne indicated no difference in consolidation or porosity in samples sintered in hydrogen atmospheres of different concentrations (25% and 100%); both samples appear to be fully dense. Therefore, crucibles may be sintered in 25% hydrogen-75% nitrogen.

Electrochemical grinding of the sintered tungsten crucibles fabricated by G.T.E. Sylvania has been halted. The intent of this experiment was to reduce the weight of a thick-walled, sintered tungsten crucible by a rapid, low-force electrochemical machining process. A low-force machining process is necessary to avoid breaking the brittle, sintered tungsten. J. Hensley of Oak Ridge National Laboratory, Y-12, found that electrochemical grinding of the sintered tungsten crucible is very slow and costly. A minimum of 2 h was required to machine a 2-in.-long, 0.025-in.-deep cut, on the 5-in.-dia crucible. Most of the tungsten was removed mechanically, as evidensed by the high amperage load on the grinding motor and the loss of 0.012 in. from the radius of the diamond wheel during each cut. The electrolyte used was sodium carbonate plus sodium chloride, heated to 55°C, which should be an aggressive electrolyte. Most of the metal removed, however, came from mechanical grinding. Electrochemical machining does not, at this time, appear to be an acceptable method for reducing the weight of sintered tungsten crucibles. Further development is required before this method can be considered acceptable. Figure 15 shows the result of the electrochemical grinding of the crucible.

As discussed in [STEINDLER-1979C], the fixture for brazing tungsten crucibles presents a problem in that a constant gap in the hooped tungsten is difficult to maintain during brazing. Originally gap movement was thought to be caused by a difference in the thermal expansion of the

Fig. 15. Electrochemically Ground Sintered Tungsten Crucible. The machining feed lines are an indication of mechanical rather than electrochemical machining.

fixture material and the tungsten. However, the use of mullite* as the core for the fixture also proved to be unsatisfactory even though mullite has the same thermal expansion as tungsten. Therefore, the gap movement cannot be attributed to a difference in thermal expansion of the two materials.

*Prior to the mullite core experiment, graphite, which also has the same thermal expansion rate as tungsten, was examined. Graphite unfortunately reacts with tungsten at the 1150°C brazing temperature. To prevent this reaction, two pieces of graphite were coated, one with chrome oxide and the other with chrome and cerium oxides. These pieces were heated to 1150°C in a vacuum. The piece coated with chrome oxide apparently lost all of the coating owing to carbon reduction in the furnace. The piece coated with a combination of chrome oxide and cerium oxide retained some coating after thermal treatment. Neither coating would have prevented tungsten-carbon reaction.

In an attempt to eliminate all movement in the joint area, a stainless steel brazing fixture was made having springs on the outside and inside supports. At the 1150°C brazing temperature, this fixture maintains the joint gap in the rolled tungsten to within 0.090 in., which is considered acceptable.

Rockwell International is presently conducting a one-man, full-time effort to develop a new proprietary ceramic process with the long-range aim of producing and shaping materials capable of withstanding strongly reducing environments. This program is being conducted independently of the PDPM Program at Rocky Flats. If research advancement continues at the present rate, expansion of this program is possible. Because of the vital role of the Rocky Flats facility in the nation's defense system, detailed research exploration and full development of concepts must occur before technical information on this ceramic process is released.

Materials and ceramic process equipment have been secured over the past ten months, and research is now being conducted at an accelerated pace. A test environment will be developed in order to subject systems to severe reducing conditions. Research will also be done to investigate the chemical properties of thermodynamically stable materials. One of the aspects of this product-oriented program is achieving a gradient-density ceramic capable of withstanding thermal shock, a characteristic important in pyrochemical applications.

An impregnation application is being encouraged by the Rocky Flats PDPM team because of its apparently attractive application to materials of construction. Also, Argonne National Laboratory expressed the desire in October 1978 to have Rocky Flats examine materials other than tungsten. Results of the experiments with impregnated ceramics have been encouraging. Static tests to determine their corrosion resistance in either molten zinc or molten copper-magnesium at 800°C showed no corrosive attack during 10- to 15-day exposure. Uncoated 85% alumina-15% silica samples also show no evidence of corrosion. However, they do show absorption of the salts throughout because of the high porosity of the initial samples (60% dense).

The absence of chemical attack by the molten zinc and molten copper-magnesium on impregnated 85% alumina-15% silica discs suggests the need for a more aggressive corrosion test. To achieve more definitive results, egg cups were formed from cold rolled steel. These cups will each be coated with a thin layer of the ceramic to be corrosion-tested. If the thin ceramic coating is attacked by molten zinc, this will be very evident because of vigorous attack of zinc on the steel cups.

Brazed samples of tungsten sheet coated with plasma-sprayed tungsten to protect the PALNISIL (palladium, nickel, silver) braze from attack by molten zinc failed upon exposure for 10 days in molten zinc at 800°C. The plasma-sprayed coating had been applied by Metallwerke Plansee because their fast arc, Swiss gun, and its associated automated equipment, was to provide a dense even-thickness coating. However, a photograph of the as-received plasma-sprayed brazed sample (Fig. 16) makes it obvious that the plasma-sprayed tungsten did not fill in the joint area and that there was no protection for

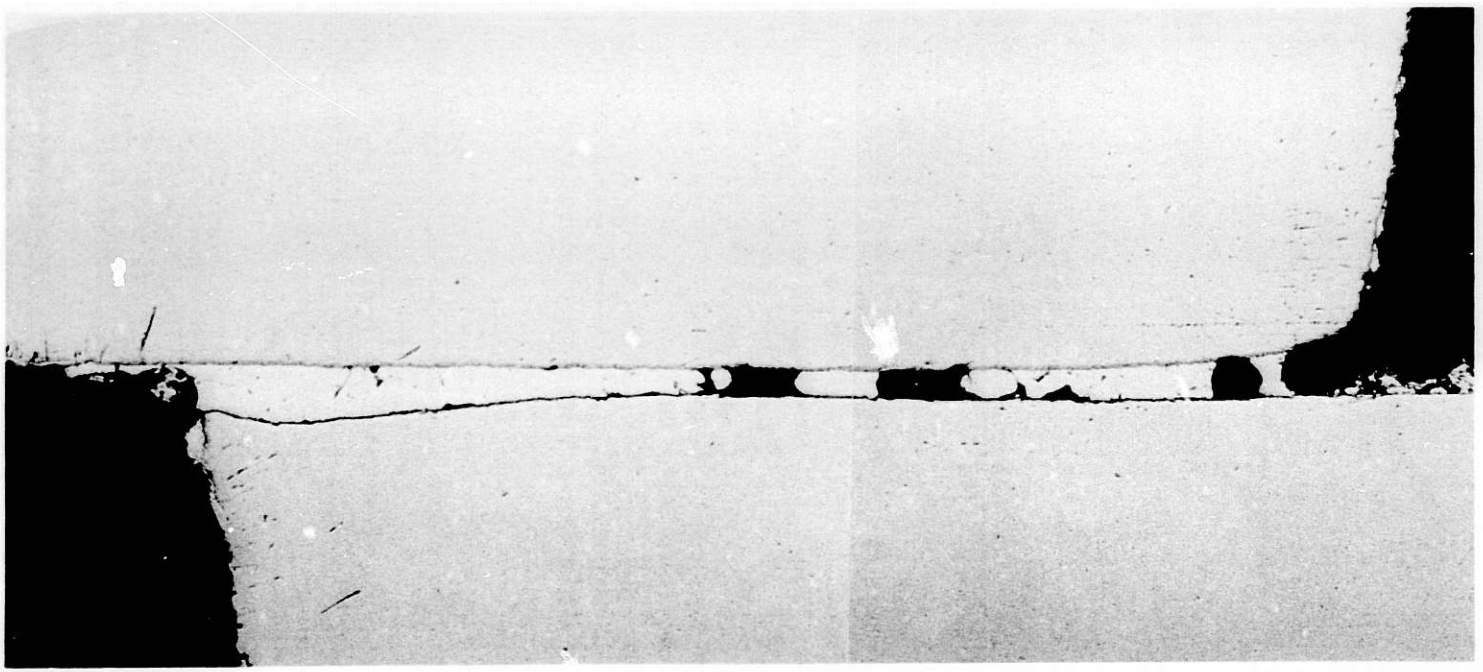

Fig. 16. Brazed Tungsten with Plasma-sprayed Tungsten Coating. 100 X

the PALNISIL braze. The lack of coating was discussed with F. Bydash, the Metallwerke Plansee representative, who explained that plasma spraying is a line-of-sight process and that the operator obviously did not tilt the gun to fill the seam area.

An earlier attempt to protect a brazed joint with plasma-sprayed tungsten also failed because of operator practices. In this case, the coating was nonuniform in thickness. No additional work on plasma-spraying tungsten to protect brazed joints will be performed during this fiscal year because of a lack of funds. If the project receives funding in FY 1980, the recommended trials on coating of brazed joints with plasma-sprayed tungsten will include:

1. Complete operator instructions on where to plasma-spray-coat the joint, and

2. Impregnation with nickel nitrate to improve the density of the coating.

5. Chloride Volatility Processing of Thorium-Based Fuels
(R. L. Bennett*)

a. Introduction

The objective of this research and development is to determine the feasibility and proliferation resistance of (a) a chloride volatility coprocess for the recovery of irradiated thorium-based fuels and (b) a zinc distillation coprocess for the recovery of irradiated uranium-based fuels. Prior work was evaluated to obtain data and information about current technology for the chloride volatility coprocess. A report was prepared that describes the existing data and information and presents a conceptual block diagram. The report is organized to allow evaluation of the technical feasibility, safety, and proliferation-resistance attributes of the chloride volatility coprocess.

Tests were conducted with simulated fuel and fission products to establish bases for technical feasibility and proliferation resistance. Additional tests will be conducted to determine the phase relationships in the zinc-uranium-plutonium ternary alloy system at 1000°C and to determine the coprecipitation coefficients for zirconium, niobium, molybdenum, ruthenium, rhodium, and palladium with $(U, Pu)_2Zn_{17}$ from liquid zinc solutions at 470°C.

b. Engineering Analysis
(L. A Smith* and T. A. Thornton*)

Evaluation was completed of the block flow diagram for the chloride volatility coprocess [Fig. 23, STEINDLER-1979C] to determine its proliferation resistance. It was found that altering either the volatilization temperature or the condensation temperature during volatilization would affect fissile-fertile separation. However, some highly radioactive fission products

*Babcock and Wilcox.

would be associated with the fissile material. This would make initial misappropriation of fissile material more difficult and would add to the difficulty of converting the chloride to the metal. These factors would increase the time and level of sophistication required for proliferation. If process modifications did not occur, radioisotopes would remain with the fuel throughout the process. This would cause the finished fuel element to be radioactive, offering diversion resistance.

Thermodynamic analysis of the phase relationships in the U-Pu-Zn system is continuing. A meeting was held with R. H. Lamoreaux of University of California, Berkeley, to review the use of the HP-67 calculator programs for thermodynamic data and phase-diagram calculations described in [BREWER]. The objective was to establish an understanding of the assumptions upon which the programs are based and of the methods for their use. This objective was accomplished. The programs are described below.

Phase boundaries are calculated by using the programs to calculate constants which characterize the excess partial molal Gibbs energy, $\overline{\Delta G}^{xs}$, of each binary phase. Constants for the binary pairs can then be averaged to allow calculation of the excess free energy of the ternary mixtures.

The HP-67 programs assume that $\overline{\Delta G}^{xs}$ can be represented by a truncated power series. Only the cubic and quadratic terms are used. The coefficients of the quadratic term b_g and the cubic term c_g are the constants required to characterize the phases. These constants can be divided into an enthalpy contribution b_h and c_h and an entropy contribution b_s and c_s where

$$b_g = (b_h/T - b_s)$$

and

$$c_g = (c_h/T - c_s).$$

The enthalpy and entropy terms are calculated by fitting the above equations to a set of $b_g(T)$ or $c_g(T)$ data. It is important to point out that the representation of $\overline{\Delta G}^{xs}$ as a two-term power series has been found to work well empirically but does not have a strong theoretical basis. With much experience, it is possible to develop a "feel" for whether the values of b and c are reasonable; however, the constants have little physical significance.

The programs Ω xb, yx-bc, and Ω yx-bc each allow the calculation of b and, in some cases, c from binary phase diagrams. Each program uses different starting data and different assumptions to calculate the constants which characterize the phases. Therefore, some care is required in selecting the proper program.

The general characteristics of the three programs are described below. Program Ω xb calculates the quadratic and cubic terms for the liquid phase, assuming that the solid solubility is small but finite. Program yx-bc

calculates the quadratic term for two phases of known compositions in equilibrium. There is no assumption of low concentration as there is in Ω xb; however, there is no allowance for a change of state so that the phase boundary must be between two phases of the same state. Program yx-bc is easily modified to allow changes of state. Dr. Lamoreaux has sent us a copy of this more general version of yx-bc. Program Ω yx-bc calculates the b and c constants for a liquid phase in equilibrium with a solid phase when the b and c constants and the heat and entropy of melting of the solid phase are known.

These programs can be used to analyze the existing binary phase diagrams. This will allow constants to be determined which characterize all of the phases on the three binaries. These constants can then be averaged to allow the $\overline{\Delta G}$ of the components in the ternary mixtures to be estimated. From this information, phase boundaries can be calculated.

The method given above has three basic limitations. First, it does not account for any ternary compounds. Secondly, the use of a two-term power series to fit $\overline{\Delta G}^{xs}$ gives limited accuracy. Thirdly, averaging of the binary data to calculate $\overline{\Delta G}^{xs}$ for ternary mixtures is an approximation.

A ternary phase diagram for the Zn-U-Pu system was developed by ManLabs, Inc., of Cambridge, Massachusetts. A copy of this diagram is attached as Fig. 17. In the ManLabs system, the $\overline{\Delta G}^{xs}$ is calculated by [KAUFMAN].

$$\overline{\Delta G}^{xs} = x(1 - x)\ \{(1 - x)\ g[T] + xh[T]\}$$

where x is the atom fraction and g[T] and h[T] are temperature-dependent functions. This formulation results in representing $\overline{\Delta G}^{xs}$ as a truncated power series in x^2 and x^3. The g and h can be directly related to the b and c used by [BREWER].

The exact method by which the phase boundaries are calculated by ManLabs is proprietary. It is limited, like the Brewer method, to using only a quadratic and cubic term and in averaging binaries to calculate $\overline{\Delta G}^{xs}$ for ternary mixtures. Ternary compounds (when they are known to exist) can be included in the calculation, but the program will not predict such compounds.

The calculated phase diagram (Fig. 17) is therefore not expected to be accurate in detail. It will be valuable in early process feasibility studies and will aid in the selection of compositions for experimental melts.

Checking of the ManLabs diagram by analysis of binary diagrams with the Brewer method has been started for the U-Zn system. Values for b and c have been calculated and converted to g and h. The results have thus far confirmed ManLabs work.

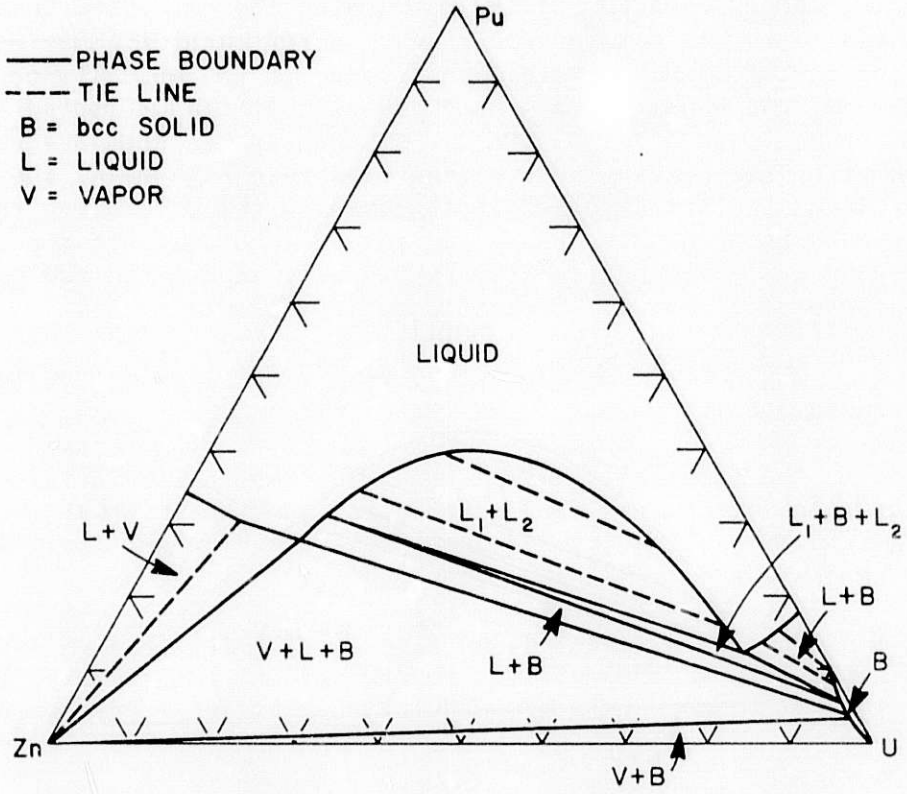

Fig. 17. Ternary Phase Diagram for the Zn-U-Pu System (ManLabs, Inc., of Cambridge,Massachusetts)

The evaluation of the proliferation resistance of the chloride volatility process was completed, and a report describing this work will be completed soon. Checking and refinement of the ManLabs ternary diagram with data generated by further analysis of binary diagrams by the Brewer method will continue.

c. Separation Processes
(C. F. Stafford*)

Glovebox procedures were written and submitted to the Lynchburg Research Center Safety Review Committee (SRC) for approval. At the June SRC meeting, it was decided that the approval of these handling procedures would be deferred until uranium-zinc shakedown runs are performed. The procedures will then be modified as necessary and resubmitted for approval.

Tantalum crucibles like that shown in [Fig. 27, STEINDLER-1979C] were fabricated from tantalum round stock. The only problem that occurred was the tendency of tantalum to gall when the tantalum plug is screwed into the crucible. When the tantalum plug is not tightly inserted, galling does not cause severe problems.

*Babcock and Wilcox.

Using a water-cooled TIG welding system, three tantalum crucibles were sealed by TIG welding the plugs. After careful cleaning with an abrasive and acetone, each crucible was placed in the weld chamber with the cap unscrewed. One crucible was empty and each of the other two contained approximately one gram of zinc metal. The chamber was then evacuated and backfilled with inert gas. The crucible caps were tightened, the electrode aligned, and the arc struck directly cent red on the protruding tantalum cap. Within seconds, the crucible cap melted into a dome over the top of the crucible. In each case, it was necessary to manually adjust the arc gap during welding because of recession of the cap as it melted.

The empty crucible welded easily and formed a uniform dome over the crucible surface.

The first zinc-filled crucible erupted like a volcano during the welding operation owing to zinc vaporization and resultant pressurization within the crucible. Zinc vapor contaminated the weld chamber, and it was necessary to clean the weld chamber thoroughly.

The second zinc-filled crucible was placed in a copper chill block such that only the cap and one-fourth inch of the crucible protruded from it. The chill block maintained the zinc-containing portion of the crucible at a lower temperature to prevent zinc vaporization. This, however, limited the weld penetration. By use of the copper chill, the second zinc-filled crucible was welded without mishap.

To test whether weld penetration was sufficient to seal the crucibles, the second zinc-filled crucible was heated to 1075°C and quenched in water. Fissures appeared in the weld, indicating the escape of zinc vapor. After sectioning of the crucible, it was found that zinc had crept into lower threads of the crucible which had not been reached by the weld. However, it appeared that very little zinc had actually escaped through the weld fissures.

The uranium-zinc shakedown runs, scheduled to begin in May, are being delayed. The uranium metal has been ordered but has not been received. Delivery is expected in late July. Also, the problem of obtaining sufficient weld penetration without volatilizing zinc must be solved; this should be possible by allowing more of the crucible to protrude from the chill block during welding.

Methods of satisfactorily sealing the crucibles will be developed. Following this, uranium-zinc shakedown runs will be completed. It is expected that by September 30, the U-Pu-Zn studies will be initiated.

6. Material Characterization and Process Analysis

(L. J. Jones,* L. F. Grantham,* and R. C. Hoyt*)

a. Introduction

This program is directed toward the Exportable Pyrochemical Process (EPP) or Pyro-Civex Process material characterization and process

* Rockwell International, Atomics International.

analysis for FY 1979. The primary objectives are: (1) to perform an engineering and cost analysis of the FBR fuel cycle utilizing zinc-distillation pyrochemical reprocessing; (2) to perform a literature search of nonaqueous methods for converting the metal product from the EPP to sinterable oxide powder, and to recommend a reference process; and (3) to prepare facilities to support the characterization of product material and to obtain data needed for fuel refabrication of product material obtained from the candidate PDPM processes. Also included in the FY 1979 contract are several minor tasks closing out AIROX, CARBOX, and RAHYD reprocessing, decommissioning of the processing facilities, and the preparation of topical reports.

b. Engineering Analysis of EPP Fuel Cycle

(1) Fuel Cycle Cost Analysis of Exportable Pyrochemical Process

Engineering analysis of the overall Exportable Pyrochemical Process (EPP) is continuing. A literature review of fuel cycle costs is being conducted, and assumptions are being established for the Exportable Pyrochemical Process fuel cost analysis. Literature is being obtained and reviewed on fuel cycle costs associated with: (1) waste treatment, transportation, and storage; (2) spent LWR and FBR fuel transportation; (3) LWR and FBR fuel element fabrication; (4) refabricated LWR and FBR fuel element transportation; and (5) facility decommissioning. Most of these costs are being obtained from fuel cycle costs being established for the Nonproliferation Alternate Systems Assessment Program (NASAP) and the International Nuclear Fuel Cycle Evaluation Program (INFCE). These fuel cycle costs are being reviewed, and EPP fuel cycle costs will be estimated by making necessary cost modifications and adjustments for the EPP fuel cycle.

Fuel cycle costs of the EPP fuel cycle are being examined for alloy-to-oxide conversion, refabrication, waste management, and facility decommissioning. As with any economic evaluation, the result depends to a large extent on the basic assumptions used in the analysis. A meeting was held in June with ANL and Rocky Flats personnel to clarify certain aspects of the EPP and to establish basic assumptions for the cost analysis. At this meeting, it was decided that the reference EPP will be based upon the zinc-distillation process [BEAN] as generally described in the draft report provided by another contractor. Spent fuel will be assumed to have the composition given in ORNL-4436 [ORNL-1970] for the Atomics International Reference FBR [BUTTREY]. This fuel will be assumed to be cooled 90 days, shipped in sodium, and stored in water at the reprocessing facility. The reprocessing and refabrication facilities are assumed to be located on the same site; spent fuel assemblies for reprocessing and refabrication fuel assemblies for recycle to the reactor are assumed to be stored in the same storage area. This storage area will have a 1-y product storage capacity (3.5 cores).

A 60-day surge capacity will be assumed between reprocessing and refabrication, with the stored product being the nonflammable $(U,Pu)_2Zn_{17}$ compound produced prior to uranium-plutonium alloy production by zinc distillation. Only conversion of the (U, Pu) alloy to oxide and refabrication of the resulting mixed oxide is to be considered. The uranium metal precipitate removed from the zinc distillation process is to be treated as a

waste stream. Thus, all blanket fuel is assumed to be fabricated offsite, with axial blanket fuel pellets being shipped to the site for core-axial blanket fuel element assembly. A 1-day surge capacity of the (U, Pu) alloy is to be provided at the head end of the alloy-to-oxide conversion plant. Also, a 1-day surge capacity of the UO_2-PuO_2 mixed oxide will be provided for at the head end of the refabrication plant.

The reprocessing facility will operate for 300 day/y and have a capacity of 300 Mg/y, or a 1 Mg/day capacity. The composition of process and waste streams will be based on coprocessing a core fuel assembly (drive fuel plus axial blanket) with a radial blanket fuel assembly. The composition, gamma activity, and decay heat of these streams are to be taken from the draft report on pyrochemical reprocessing prepared by another contractor. It will be assumed that 10% of the reduction salt stream will be removed as a waste stream during each pass and that all of the zinc will be recovered from the FP-4 separation and recycled. The waste salt will be fixed in a glass matrix and will be packaged as per Waste Isolation Pilot Plant (WIPP) criteria. Waste gases will be stored as compressed gas.

Decontamination and decommissioning (D&D) cost estimates on the EPP facility are to be based on the facility drawings provided in the draft pyrochemical reprocessing report. The analysis assumes that there will be complete unrestricted site use after D&D--even though the site will probably be used as a nuclear park. The D&D is to be based on current regulations, and cost estimating is to be based on previously used techniques [BPNL].

(2) Conversion of EPP Metal Product to Oxide

Review of literature data on the oxidation of fissile metals to oxides has been completed. This information is being used to develop a reference process for the conversion of the EPP mixed alloy to oxides. Although a considerable amount of information is available on the oxidation of fissile metals, very few studies have been made in which the oxide is subsequently fabricated into fuel pellets. Most of the oxidation studies reported in the literature were designed to obtain kinetic and mechanism data, from which it is impossible to predict the sinterability of the oxide produced. A summary of the information on the oxidation of uranium, plutonium, and their alloys is given below.

Most of the oxidation data in the literature are results of studies that were carried out to investigate the corrosion of uranium and plutonium with respect to safety during their handling and storage. Thus, predominantly low-temperature (<300°C) oxidations were studied. Additional investigations have been reported on high-temperature oxidation (>300°C) of these metals; studies were directed at possible metal-water (steam) reactions that might be encountered under accident conditions in a metal-fueled reactor. Since most of these low- and high-temperature investigations were concerned with corrosion and reaction kinetics, reactions were usually terminated after only partial oxidation of the metal samples had occurred, and the oxide product was not fabricated into fuel pellets. In a few studies during development of the EBR-II skull reclamation process, oxidation of uranium metal and

uranium/noble metal/rare earth oxide mixtures was completed. However, the oxide product was recycled for additional liquid-metal processing, not refabricated into oxide fuel pellets.

Data in the literature show considerable discrepancies among different investigators, indicating possible interdependencies among various parameters that affect metal oxidation. In general, it appears that the oxidation behavior of uranium is similar to that of plutonium. Metal oxidation rates are significantly higher in moist air than in dry air, particularly at temperatures below 200°C. At temperatures below 100°C, oxidation by water vapor is actually inhibited by the presence of oxygen in the oxidation atmosphere.

For plutonium, there appears to be no significant difference between oxidation rates in dry air and moist air at temperatures above 300°C. A transition from a low-temperature regime to a high-temperature regime occurs during the oxidation of plutonium at temperatures above 300°C. This transition is such that the oxidation rate drops drastically (about one order of magnitude) as the temperature is increased from 300 to 400°C. If temperature is further increased, the oxidation rate increases such that the maximum oxidation rate in the high-temperature regime at 450 to 500°C exceeds that achieved in the low-temperature regime (at 300 to 350°C). This transition is believed to be the result of the oxide film becoming more protective. No information has been found on oxidation of plutonium by high-temperature steam.

Uranium oxidation does not show the transition from a high-temperature regime to a low-temperature regime that plutonium shows. For the oxidation of uranium with steam, peak oxidation rates are in the temperature range from 250 to 400°C; however, these rates are lower than those achieved with air oxidation at temperatures above 500°C.

For both uranium and plutonium, there is a definite trend of increased oxidation rate with increased temperature and, if the oxidation rate is high enough, the exothermic reaction can be self-heating to the extent that the metal burns in the oxidizing atmosphere. This phenomenon is less pronounced when oxidations are done with steam than with oxygen; however, when it occurs, temperatures may exceed 800°C. Thus, it is easier to control oxidation temperatures (and oxidation rates) when oxidations are carried out at high temperatures than when they are carried out at low temperatures.

Significantly less information is available on the oxidation of alloys of uranium and alloys of plutonium. Oxidation tests have been reported on: binary uranium alloys of silicon, titanium, vanadium, zirconium, molybdenum, niobium, copper, aluminum, and plutonium; binary plutonium alloys of aluminum, iron, thorium, zirconium, gallium, and molybdenum; and ternary uranium-plutonium alloys of copper, aluminum, carbon, zirconium, iron, and molybdenum. In addition to these investigations, some ignition studies have been performed on binary plutonium alloys of manganese, nickel, zinc, chromium, cerium, iron, carbon, silicon, and cobalt. Oxidation of these alloys depends upon both oxidation conditions and alloy compositions. Some alloys of uranium and some alloys of plutonium exhibit lower oxidation rates than either unalloyed uranium or plutonium. However, in general, alloys containing both

uranium and plutonium have significantly higher oxidation rates than either unalloyed uranium or unalloyed plutonium. This has been attributed to the presence of zeta phase, which has notoriously little resistance to cracking and oxidation. Although these binary alloys are very susceptible to oxidation, the presence of another element can increase resistance to oxidation considerably. Such ternary alloys, though more resistant to oxidation than binary uranium-plutonium alloys, are usually less resistant to oxidation than pure uranium. Of these alloys, ternary uranium-plutonium alloys of molybdenum and ruthenium are the most resistant to oxidation. This has been attributed to the suppression of the zeta phase.

The possibility exists that the oxidation rate of EPP alloy may be low because both ruthenium and molybdenum will be present. It is believed, however, that the molybdenum and ruthenium concentrations in the alloy will be low enough that some zeta phase will be present to promote rapid alloy oxidation; data in the literature on the oxidation of uranium-fissium alloys for the EBR-II skull reclamation process indicated rapid alloy oxidation at temperatures of 700°C and above. These uranium alloys, which had molybdenum and ruthenium contents similar to those expected for the EPP alloy, are expected to be more difficult to oxidize than the EPP alloys since they do not contain significant quantities of plutonium. Therefore, it is felt that EPP alloys will be readily oxidized at temperatures near 700°C and above.

The only data found that involve oxidation of a metal to an oxide powder with subsequent fabrication of this powder into fuel pellets are for steam oxidation of uranium. These data were briefly discussed in [STEINDLER-1979C] wherein it was stated that these oxide powders had poor sintering characteristics. It was also suggested that an AIROX oxidation-reduction cycle might improve the sinterability of these powders. Additional information that supports this hypothesis is discussed below.

The densities and surface areas of various UO_2 powders that have been produced from uranium metal are given in Table 22, which adds data for Method 7 to Table 32 of [STEINDLER-1979C]. It can be seen by examination of the data in Table 22 that steam oxidation of uranium produces powder particles having near-theoretical density and that air oxidation yields particles that are less dense. [CLAYTON] reported that the powders produced by steam oxidation have a much higher density and lower surface area than do UO_2 powders produced by other methods. [BELLE] reported that these same powders had poor sintering characteristics since it was difficult to produce high-density pellets with them.

Examination of various reports on the characteristics of UO_2 powders [BELLE, GARDNER, DOI] has indicated that in order to produce a high-density sintered pellet, powders must be compacted to achieve significant particle-to-particle contact. This tends to crush agglomerates, reduce void volume, and force particles into close contact with one another. Then, as sintering takes place, densification is achieved by the reduction of void volume and by grain growth--first within particles and then between particles. Powders having poor sintering characteristics cannot be compacted sufficiently to reduce void volume or to place particles into intimate enough contact to facilitate sintering to a high pellet density. Although the poorly compacted powder particles may sinter to high densities, extensive intergranular porosity will still remain in the fuel pellets.

Table 22. Properties of UO_2 Prepared from Uranium Metal[a]

Method	Method of Preparation	Reaction Conditions	O/U	Powder Density,[b] g/cm^3	Surface Area, BET, m^2/cm^3
1	High-pressure steam oxidation of uranium	72-h oxidation at 343°C and 2200 psig	1.97	10.92 ± 0.1	12.9
2	Controlled low-pressure steam oxidation of uranium	24-h oxidation at 150°C and 5 psig; dried 8 h in vacuo at 700°C	2.02	10.85 ± 0.1	2.4
3	Uncontrolled low-pressure steam oxidation of uranium	5-h oxidation at 350°C and 5 psig; heated in hydrogen 5 h at 900°C	2.03	10.92 ± 0.05	9.0
4	Steam oxidation of uranium from uranium hydride	4-h oxidation at 400°C and 5 psig; heated in hydrogen 15 h at 700°C	2.03	10.98 ± 0.1	22.6
5	Air pyrolysis of uranium metal to U_3O_8; hydrogen reduction to UO_2	15-h oxidation at 800°C; 16-h reduction at 800°C	2.01	10.02 ± 0.1	5.8
6	Hydrided-air oxidized uranium; hydrogen reduction of U_3O_8 to UO_2	24-h oxidation at 740°C; 16-h reduction at 800°C	2.02	10.32 ± 0.15	9.4
7	Air ignition of high-pressure steam-oxidized UO_2 to U_3O_8; hydrogen reduction to UO_2	24-h oxidation at 800°C; 15-h reduction at 780°C	2.01	10.69 ± 0.10	4.3

[a]Data taken from [CLAYTON] and [BELLE].

[b]Theoretical density = 10.96 g/cm^3.

Powders produced by steam oxidation of uranium have poor compacting and sintering characteristics because: (1) the particles are dense and resist crushing during pressing operations, and (2) the particles are too large for efficient compacting to low void volumes. Such compacting and sintering difficulties have been observed in UO_2 powders prepared by methods other than steam sintering of uranium. Various studies have been done to develop techniques for increasing UO_2 powder sinterability. Processing the powder through an oxidation-reduction cycle has proved to be an effective way of improving the sinterability of UO_2 powders [ARENBERG, BARD, BARR, FUHRMAN]. One of the most thorough investigations of the effects of an oxidation-reduction cycle on the chemical reactivity, and hence sinterability, of UO_2 powder was done by Bard et al. Their work involved oxidation of UO_2 (produced by a precipitation technique) to U_3O_8, followed by reduction to UO_2. They found that the oxidation-reduction treatment substantially increased the surface area, reduced the particle size, and increased the particle microporosity of UO_2 powders. They also reported that these effects were at a maximum when oxidation was done in air at 400°C and that at oxidation temperatures near 900°C, the oxidation-reduction cycle had very little effect on the chemical reactivity of the powder. This information suggests that if oxide powders produced from metal oxidation have poor sintering characteristics, treatment with an oxidation-reduction cycle can readily convert the powder into one having good sintering characteristics.

Although the use of an oxidation-reduction cycle to improve sinterability has not been demonstrated with powders produced by metal oxidation, some of the data given in Table 22 support this idea. Uranium dioxide powder produced by high-pressure steam oxidation (Method 1 in Table 22) has been treated with an oxidation-reduction cycle (Method 7 in Table 22). Note that this treatment decreased the particle density and decreased the powder surface area. The latter effect was probably the result of oxidation being done at 800°C rather than at the optimum temperature of 400°C.

One important consideration in choosing oxidation conditions for the EPP alloy is the volatilization of ruthenium, which is one of the major fission products contributing to the radioactivity of the fuel. It is desired that volatilization of ruthenium be low to ensure adequate proliferation resistance. The behavior of ruthenium under oxidizing conditions at various temperatures is not yet understood, and the literature contains a lot of conflicting data. Ruthenium volatility has been shown to differ for wastes of different compositions [CHRISTIAN], and this probably accounts for some of the discrepancies in the literature.

Significant quantities of ruthenium have been reported to be volatilized during spray calcination at temperatures of 350 to 500°C, but not at temperatures near 700°C [NEWBY]. In other work, ruthenium has been significantly volatilized during spray calcination at temperatures of 400 to 800°C [CHRISTIAN] and during voloxidation tests at 450 to 750°C [ORNL-1973]. Data on ruthenium volatilization during air oxidation of uranium-fissium metal and oxide skulls, however, showed no significant volatilization in the temperture range from 700 to 900°C [JOHNSON-1964]. Many of the tests also involved successive oxidation-reduction cycles without loss of ruthenium. Ruthenium was not even volatilized from oxidized skulls heated in oxygen at the lower

temperatures of 100, 200, 300, and 400°C. Therefore, ruthenium volatilization during the oxidation of uranium-fissium metals and fission-product skulls was not expected to be a problem.

It is not possible to predict the behavior of ruthenium during the EPP alloy-to-oxide conversion process because of conflicting data in the literature summarized above. Only an experimental test program involving the oxidation of EPP alloys can accurately establish ruthenium behavior. However, since ruthenium volatility depends upon the chemical composition of the material from which it is volatilizing, ruthenium behavior during the EPP alloy oxidation can be expected to be similar to that occurring during uranium-fissium metal and skull oxidation. If this is true and if the data on ruthenium volatilization during oxidation of uranium-fissium metal and skulls are correct, there will be insignificant volatilization of ruthenium during EPP alloy oxidation in air at temperatures of 700 to 900°C.

Work is continuing on the development of a reference EPP alloy-to-oxide conversion process. Process oxidation conditions are being evaluated with respect to their effects on reaction rates, product powder sinterability, and volatilization of ruthenium.

(3) Waste Management

Waste management flow schemes have been developed for both solid and gaseous waste produced in Exportable Pyrochemical Process reprocessing and fuel refabrication. Waste produced during reprocessing is much more radioactive and, therefore, much more costly to manage than waste produced during refabrication. In the waste treatment cost evaluation, emphasis will be placed on the waste form (salt, alloy, gas), composition, gamma activity, heating rate, and volume. How much of the waste produced during reprocessing must subsequently be transferred to a government waste isolation facility depends to a great extent on whether proposed waste recovery schemes are successful. For example, the major waste stream produced during EPP reprocessing is the CaO salt waste produced during the reduction step. It will be assumed that electrolytic recovery of calcium from this waste salt will be successful, as early experiments indicate. Thus, the major waste stream will be reduced to a small fraction of its original value, significantly reducing waste management costs. It will also be assumed that 90% of the reduction salt will be recycled in each pass and that all of the zinc from the FP-4 separation will be recycled.

Waste management volume and costs will also be significantly influenced by whether the waste product is in a form which will be acceptable for disposal. Much of the waste from the EPP reprocessing fuel cycle will be salt ($NaCl$-KCl-$CaCl_2$). It will be assumed that these wastes are not acceptable for disposal at the government isolation facility without additional insolubilization processing. This will substantially increase waste volume and waste management costs. These salts will be fixed by vitrification or other appropriate means after sufficient delay (about 90 days) to

let the iodine-131 decay to manageable levels. Vitrification of such chloride-containing wastes is much more difficult than vitrification of oxide wastes but, contrary to some reports, these wastes can be insolubilized.*

It was decided during the June meeting with ANL and RF personnel that uranium precipitate removed during the zinc-distillation process is to be treated as a waste stream. Storage of this material onsite is under consideration.

(4) Decontamination and Decommissioning of the Reprocessing Plant

An engineering analysis and cost evaluation for decontamination and decommissioning (D&D) an EPP reprocessing plant has been started. The major emphasis of this subtask will be on cost-effective D&D by (1) minimization of radiation exposure to personnel; (2) optimization of schedule and manpower requirements; (3) minimization of radiation levels and waste volumes generated; and (4) optimizing plant design criteria. Numerous assumptions must be made early in the evaluation. It was decided that to obtain comparable costs, this analysis and study should use assumptions similar to those used in a recent Battelle Northwest [BPNL] evaluation of the cost to D&D the aqueous Barnwell reprocessing plant. Unfortunately, the size of the Barnwell reprocessing plant (1,500 MTHM/y) does not correspond to the size of the EPP reprocessing plant (300 MTHM/y); scale factors must be used to compare the cost directly. It will be assumed that current regulations will be in effect when D&D takes place. It will also be assumed that all spills during the 30-y plant life will be cleaned up when they occur.

Many plant design features will also markedly affect the D&D cost. Some of these considerations are listed below.

1. The plant should be designed for accessibility for operational maintenance. As a general approach, any modifications that ease maintenance will also aid decommissioning.

2. Concrete surfaces in vaults, on floors, trenches, pits, building columns, and footings need to be protected. Metal liner, plastic cover, paint, or some hard smooth coating could be used as covering. Expansion joints or other crevices should be avoided.

3. The use of massive monolithic concrete for shielding and containment should be reconsidered. Other materials (for example, lead shot, blocks, or water) could be used. Where integrated concrete structures are necessary for containment, means should be provided for easily removing or spalling the concrete. Local heating elements could be embedded in the concrete. The rebar, properly designed, could become a resistance heater

---

*With company funding, Rockwell has verified in a proprietary program that up to 40 wt % salt in an insolubilization matrix can be produced; the leach rate of this insolubilized salt is within a factor of two of that of glassified fission-product oxides.

element. Explosive charge holes or hollow rebar (reinforcing rods) for explosives could be incorporated in the concrete. Modular construction of the shields would facilitate handling. Access in the shielding for instrumentation probes should be included.

4. The locations and the attachments of pipe, grid plates, and other reaction vessel internals should be considered in terms of the limitations of the available cutting equipment. Support structure for cutting-equipment installation should be included. Penetrations into the reaction vessel should not be made through the biological shield, but through the top of the vessel. Cooling coils should be made easily removable and should not be embedded in concrete unless needed for concrete cooling.

5. R/A waste holdup tanks should not be buried in soil, but should be contained in isolated vaults, and there should be provisions for the handling of spills.

6. In the design of process equipment, particularly large components such as heat exchangers, ease of dismantlement should be a consideration. Installation should include adequate access for removal operations.

7. Building construction should assume that an accidental spill or fire might occur; therefore, surfaces or crevices where contamination could collect should be protected.

8. Instrumentation probe holes should be included throughout the plant that will allow assessment of the degree of contamination at the time of decommissioning.

Generally, a preliminary decommissioning plan should be prepared at the time of plant design. Plant maintenance equipment should be designed with added features that will assist decommissioning. A capability for containing airborne contaminants during decommissioning should be provided. The gas and liquid waste systems should be designed with consideration of the decommissioning operations. Adequate space should be provided near the facility for decontamination and packaging.

Several decommissioning problems encountered in the past can provide guidance for D&D of an EPP reprocessing plant. Some of these problems are listed below:

1. A particularly troublesome decommissioning problem is decontamination of concrete surfaces. To solve this problem, many techniques were employed, ranging from washing down with solvents to direct removal of the surfaces. None were wholly satisfactory since they included a high utilization of manpower, and since surface cracks, expansion joints, and porous concrete were not easily cleaned.

2. Radioactive waste holdup tanks buried in soil were easily removed; however, leaky valves, pipes, and fittings caused contamination of the adjacent soil.

3. Access limitations and residual contamination make the removal of process system equipment (heat exchangers, pumps, purification equipment, and supporting structures) a problem.

4. Disposal of the 50- to 60-Mg massive components can be accomplished easily. The high-volume, high-weight components can be shipped intact or burial.

5. In building construction incorporating open beams, electrical wire trays, conduits, and numerous nooks and crannies, cleaning and surveillance (to ensure that surfaces are clean) are very difficult.

6. The assessment of soil contamination is difficult if access is not provided and instrumentation sensitivity is limited.

c. Characterization of PDPM Product for Recycle

Two remotely operated inert-gas alpha boxes, received at the Rockwell International Energy Systems Group Hot Cell Facility for checkout, are to be used: to convert the Pyro-Civex metal product to sinterable-grade oxide powder, to refabricate the powder into fuel pellets, and to characterize the products of the metal-to-oxide conversion and pellet refabrication process steps. One alpha box has been installed in the mockup area of the Hot Cell Facility, and the checkout task has been initiated. The mockup area duplicates equipment and interfaces of the actual hot cells for which the boxes have been designed. It provides the capability of full-size mockup and checkout with remote manipulators for operations expected to be encountered in hot cell operations. Thus, any modifications or additions to the boxes that might be required during hot processing can be made while the boxes are still uncontaminated.

Tests to be mocked up and checked out include: (1) procedures for installation and removal of the glove boxes in the hot cells, (2) procedures for installation and removal of master-slave manipulators in the glove boxes, (3) layout and installation requirements of process equipment for optimum accessibility to manipulators during operation, and (4) layout and procedures for remote maintainability of process equipment and glove box auxiliaries.

7. Molten Salt Processes Applied to Nuclear Fuels
(D. H. Smith,* and E. C. Douglas*)

The purpose of this program is to establish chemical bases for proliferation-resistant methods utilizing molten salts and/or metals for reprocessing nuclear reactor fuels.

---

* Oak Ridge National Laboratory.

a. Progress

(1) Engineering Analysis

In the PROMEX flowsheet, the purified actinides (both the pure uranium and the coprocessed U-Pu-Am-Cm streams) are recovered by oxidative extraction from molten bismuth into NH_4AlCl_4 and subsequent "distillation" of the NH_4AlCl_4 to leave the concentrated actinide chlorides. The "distillation" at about 380°C (653 K) actually occurs by the reactions

$$NH_4AlCl_4(l) = NH_3AlCl_3(l) + HCl(g) \quad (1)$$

$$NH_3AlCl_3(l) = NH_3AlCl_3(g). \quad (2)$$

During the course of the process, all of the HCl is eventually driven off and, for the uranium stream, the solubility of the uranium chloride in NH_3AlCl_3 is exceeded, leaving a saturated solution of uranium chloride at unit activity over the solid salt. The possible carryover of uranium during the distillation due to formation of the volatile compound, $UCl_4 \cdot 2AlCl_3$ [probably $UCl_2(AlCl_4)_2$], has previously been noted [SMITH-1979]. The postulated formation of $UCl_2(AlCl_4)_2$ occurs via displacement of NH_3 from NH_3AlCl_3 by UCl_4:

$$UCl_4 + 2NH_3AlCl_3 = 2NH_3(g) + UCl_2(AlCl_4)_2(g) \quad (3)$$

The Gibbs free energy of reaction 3 has now been calculated from data in the literature [GRUEN, LAUGHLIN, STULL], and the equilibrium is found to be strongly to the left. In particular, at 653 K, $\Delta G = +31.39$ kcal/mol UCl_4.

This calculation confirms that in the reaction with the Lewis acid $AlCl_3$, NH_3 is a much stronger base than is UCl_4. Hence the carryover of uranium as $UCl_2(AlCl_4)_2$ during the distillation is strongly inhibited by the weak basicity of UCl_4. Although plutonium presumably forms the analogous compound $PuCl_2(AlCl_4)_2$, the relatively weak basicity of $PuCl_4$ should similarly prevent process difficulties from $PuCl_2(AlCl_4)_2$.

The first step in the PROMEX flowsheet for oxide fuels is the dissolution of the fuel into a molten mixture of $LiCl/AlCl_3$. It might be desirable to keep the volume of Al_2O_3 formed in this step to a minimum. According to [MOORE], who studied the dissolution of uranium oxide in $KAlCl_4$, sparging of the melt with carbon chlorides reduced the amount of Al_2O_3 formed to 1/3 to 1/25 the amount of Al_2O_3 produced without sparging.

Accordingly, sparging of the $LiCl/AlCl_3$ melt with a carbon chloride gas has been proposed as a possible modification of the PROMEX flowsheet.

(2) Separation Processes

Study of the dissolution of ThO_2 and UO_2 in molten $LiCl/AlCl_3$ mixtures by the reaction

$$3AnO_2 + 4AlCl_3(salt) = 3AnCl_4(salt) + 2Al_2O_3 \quad (4)$$

where An is an actinide has now been extended to the reaction temperature, 610°C. The initial molar ratios were $N_{AlCl_3}/N_{LiCl} = 1.50$ and $N_{AnO_2}/N_{AlCl_3} = 0.75$. These ratios correspond to stoichiometric equivalents of AnO_2 and $AlCl_3$ and, if complete dissolution were obtained, would give final concentrations of 53 mol % $AnCl_4$ in 47 mol % LiCl.

The equilibrium constant for this reaction may be written as

$$K = \frac{(a_{AnCl_4})^3(a_{Al_2O_3})^2}{(a_{AlCl_3})^4(a_{AnO_2})^3}, \tag{5a}$$

where a_i is the activity of compound i. Since Al_2O_3 and AnO_2 are insoluble solids whose activities equal one, Eq. 5a may be rewritten as

$$K = \frac{(a_{AnCl_4})^3}{(a_{AlCl_3})^4}$$

$$= \frac{(\gamma_{AnCl_4})^3(C_{AnCl_4})^3}{(\gamma_{AlCl_3})^4(C_{AlCl_3})^4}. \tag{5b}$$

where C is concentration.

Because of the chemistry of the next step in the process, a small value of C_{AlCl_3} (i.e., $N_{AlCl_3}/N_{LiCl} \leq 0.1$) at the end of the dissolution step is desired.

Hence, the experiment was designed to reach the minimum obtainable (i.e., equilibrium) concentration of $AlCl_3$, and the (presumably) very long reaction times of 48, 88, and 120 h were used. The temperature 610°C was chosen because it is the lowest possible temperature to which the system would be exposed in the next process step and because 610°C was expected to exceed the liquidus temperature of any composition that would be reached in either the $ThCl_4/LiCl/AlCl_3$ or the $UCl_4/LiCl/AlCl_3$ phase diagrams [DESYATNIK].

As shown by the data in Table 23 representing dissolution by reaction 4, for both UO_2 and ThO_2, equilibrium was obtained in less than 48 h, and greater than 95% of the UO_2 dissolved. Approximately the same fraction of the ThO_2 dissolved, although the analytical scatter was considerably greater for ThO_2 than for UO_2. At equilibrium, the molten-salt solutions contained approximately equimolar amounts of $AnCl_4$ and LiCl and about 3 mol % $AlCl_3$.

Table 23. Equilibrium Dissolution of UO_2 and ThO_2 into $LiCl/AlCl_3$ at 610°C

Initial weights per sample: $AlCl_3$, 0.8249 g; LiCl, 0.1751 g; UO_2, 1.2556 g; ThO_2, 1.2778 g

W_{insol}, weight of insoluble material after reaction
S_{An}, concentration of soluble actinide
R, percent of actinide which dissolved, calculated from change in weight of the insoluble oxide

Reaction Time, h	W_{insol},[a] g	S_{An},[b] wt %	R, %		
			R_1[c]	R_2[d]	$(R_1 + R_2)/2$
		UO_2			
48	0.3596	55.1	95.4	94.4	94.9
88	0.2603	51.6	105.9	93.0	99.5
120	0.3570	58.1	95.6	99.7	97.6
(found, average)	0.3256	54.9	99.0	95.7	97.3
(theoretical)	≥0.3157[e]	≤56.3[f]	≤100.0[f]	≤100.0[f]	≤100.0[f]
		ThO_2			
48	0.2716[g]	41.8/41.5	104.9	75.5	90.2
88	0.2363[g]	51.9/52.2	108.8	96.1	102.4
120	0.1442[g]	36.2/36.1	118.9	69.8	94.4
(found, average)	0.2174[g]	43.3	110.8	80.5	95.6
(theoretical)	≥0.3157[e]	≤56.3[f]	≤100.0[f]	≤100.0[f]	≤100.0[f]

[a] At the end of the reaction time, each sealed silica tube was opened; the insoluble fraction was filtered, dried, and weighed (W_{insol}), and the soluble contents were dissolved in ethanol/water solution.

[b] The soluble fraction was analyzed for dissolved actinide (S_{An}). In the case of uranium, initial implausible results for S_{An} were traced to slow hydrolysis and precipitation of the dissolved actinide; the analyses were repeated, and only the later, corrected results are shown here. Attempts to trace implausibly low values of S_{An} for thorium to its hydrolysis and precipitation were unsuccessful and so duplicate sets of analyses are reported for dissolved thorium.

[c] Percent dissolution of AnO_2, calculated from W_{insol}, with Al_2O_3 the assumed reaction product.

[d] Percent dissolution of AnO_2 calculated from $R_2 = (W_s - W_{insol})(S_{An}/W_{An})$ where W_{An} is the total weight of actinide in the sample and W_s is the total weight of the sample.

[e] Minimum W_{insol} is for complete reaction to Al_2O_3.

[f] Maximum value is for complete dissolution of AnO_2.

[g] W_{insol} values for thoria samples are seen to be smaller than the theoretical W_{insol} value, indicating that some insoluble material was lost during filtration. This explains the excessively large R_1 values for thoria.

These results show that very high concentrations of UCl_4 and $ThCl_4$ and low concentrations of $AlCl_3$ can be obtained via reaction 4. Similar results can be expected for plutonium. Hence, thermodynamically, the reaction is very favorable for the first process step, the dissolution of the oxide fuel in LiCl.

Studies are planned to determine if the dissolution reaction is rapid enough at 610°C to be of practical interest. A report on the dissolution studies will be written.

8. Molten Tin Process for Reactor Fuels
(O. Krikorian,* J. Grens,* M. Coops,* and W. Parrish*)

The objective of this effort is to identify chemically feasible pyrochemical reprocessing methods within the general framework of non-proliferation. This effort is aimed at the decomposition and dissolution of spent fuel elements and the formation of thorium, uranium, and plutonium nitrides in molten tin solutions. Separation of fission-product elements and other impurities by use of various physical and chemical processes is anticipated.

a. Scope of Work

Lawrence Livermore Laboratory will provide program management, studies and analyses, fuel-reprocessing flowsheet development, and general support for the research and development of molten tin processes for the removal of fission products and other impurities from spent uranium-plutonium and thorium-uranium (plutonium) fuels in oxide, metal, or carbide form. Initial effort should be on oxide fuel, followed by metal and then carbide fuel.

More specifically, effort will be directed in FY 1979 to determining the technical feasibility of a selected process flowsheet. Laboratory experiments will be performed with small-scale simulated fuel specimens to refine process parameters and to test process performance. A topical report will be prepared on a review of thermodynamic and kinetic data relevant to the process, and a proliferation analysis will be made for the process according to the guidelines established by Argonne National Laboratory.

b. Process Description

Molten tin is used as a solvent and reaction medium in the molten tin process to separate actinide fuels from fission products and other materials by precipitating out the actinide nitrides (which are insoluble in molten tin). The process is applicable to uranium-plutonium and thorium-uranium (plutonium) breeder fuels in oxide, carbide, or metallic form. If the fuel is an oxide, the cladding is first removed and then the fuel is introduced directly into molten tin at about 1900 K, contained in a graphite crucible. Carbon will dissolve in the molten tin and react with the actinide and fission product oxides under these conditions, converting them to a metallic solution in tin and releasing CO gas. Carbide or metallic fuels are

*Lawrence Livermore Laboratory.

dissolved directly in molten tin. After dissolution of the fuel, gaseous nitrogen is introduced and a nitriding reaction is carried out at about 1900 K to form an actinide nitride precipitate. We also expect that under these conditions, some of the fission products, such as the lanthanides, will form mixed crystals with the actinide nitrides and precipitate out with them. A significant amount of the fission products should remain in the molten tin. The actual partitioning behavior of the fission products between the actinide nitride and the molten tin phases needs to be experimentally established. Retention of a certain amount of highly radioactive fission products within the actinide fuel is consistent with the nonproliferation goal, since a highly radioactive fuel material is a deterrent to theft. After nitriding, the molten tin is filtered from the fuel nitride, and the fuel nitride is further processed to convert it to the appropriate chemical form required for a new fuel element.

c. Engineering Analysis

We are developing new flowsheets for the molten tin process to analyze $^{238}U/^{239}Pu$ and $^{232}Th/^{233}U$ breeder fuels. Initially, we are looking at oxide systems, but expect to follow up with carbide and metallic fuel options. About 1 to 2% ^{239}Pu of ^{233}U is assumed to be in the blanket region for this initial analysis, and we expect to attain an enrichment of about 20% for the core fuel.

Nitriding experiments to date on Th/U and U/Pu mixtures in molten tin indicate that uranium can be enriched relative to either thorium or plutonium (see experimental results below) in the nitride phase. Thus, although considerable work yet needs to be done to establish optimum operating conditions for a process, these results indicate that it should be possible to produce fuel-enriched and fuel-depleted product streams from breeder reactor fuels.

It has recently become clear to us that the molten tin process can produce separate product streams that present important advantages in terms of nuclear waste disposal. The process produces essentially five streams (see Figs. 18 and 19): (1) gaseous fission products, (2) fission products that are the major decay-heat producers, (3) fissile-rich actinides, (4) fissile-depleted actinides, and (5) fission products that are low decay-heat producers.

The gaseous fission products (I_2, Kr, Xe, hydrogen plus tritium) are in relatively concentrated form, being accompanied primarily by CO produced during the carbothermic reduction of oxide fuels. This provides for relatively simple processing to concentrate the gaseous fission products prior to storage (if required). The fission-product elements that are the main decay-heat producers for the period of 10-1000 y are Cs, Sr, and Sm. We anticipate that virtually all of the Cs and Sr and a large portion of the Sm can be removed in a metal-volatization (evaporation) step in this process (see Fig. 19), substantially reducing heat generation in the remaining fission products. The high-decay-heat and low-decay-heat fission products can then be stored separately, utilizing different storage design concepts to accommodate the differences in heat-generation rates. If storage of the actinide streams is required, yet different storage design concepts would be utilized since they contain alpha-emitters that can cause severe radiation damage in solid container or matrix materials.

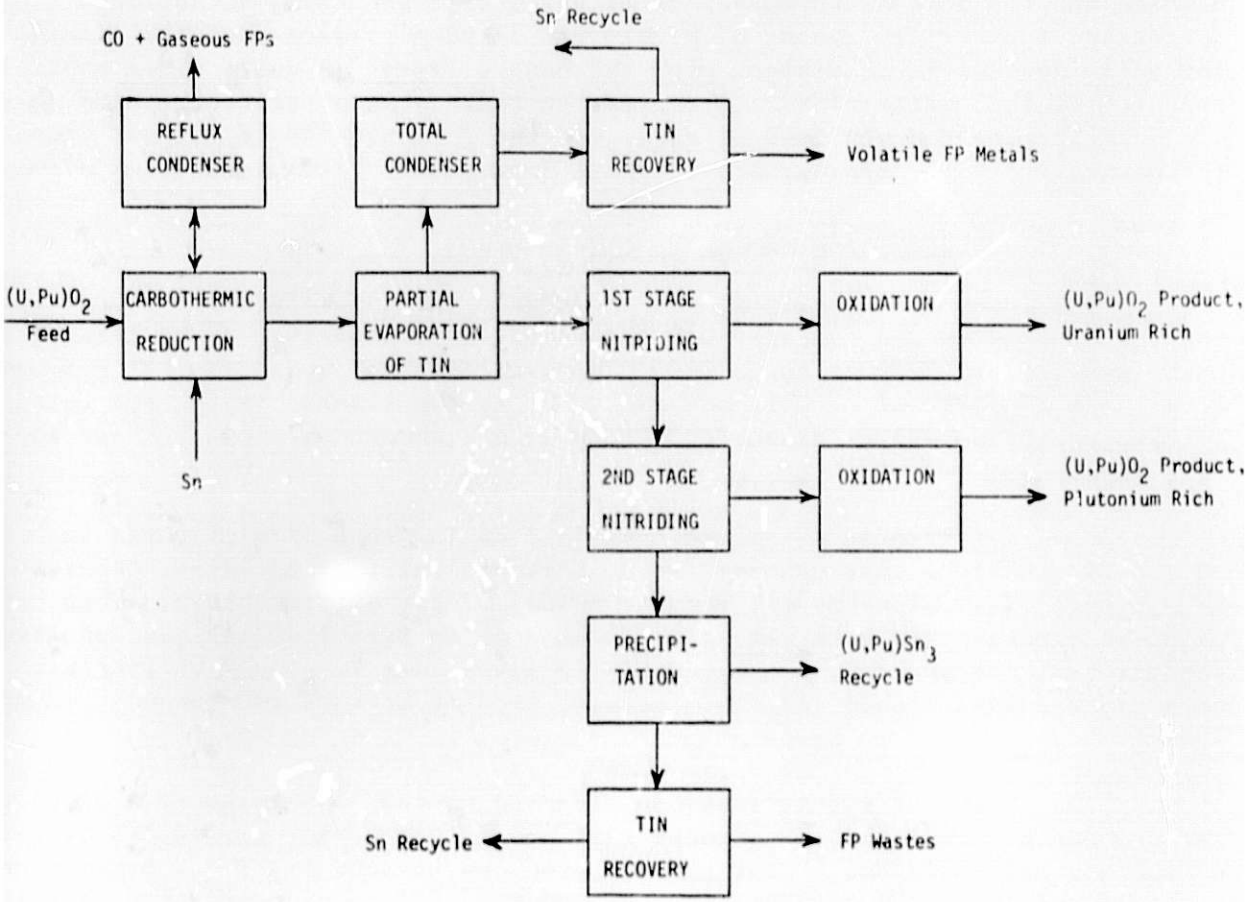

Fig. 18. Molten Tin Process Flowsheet

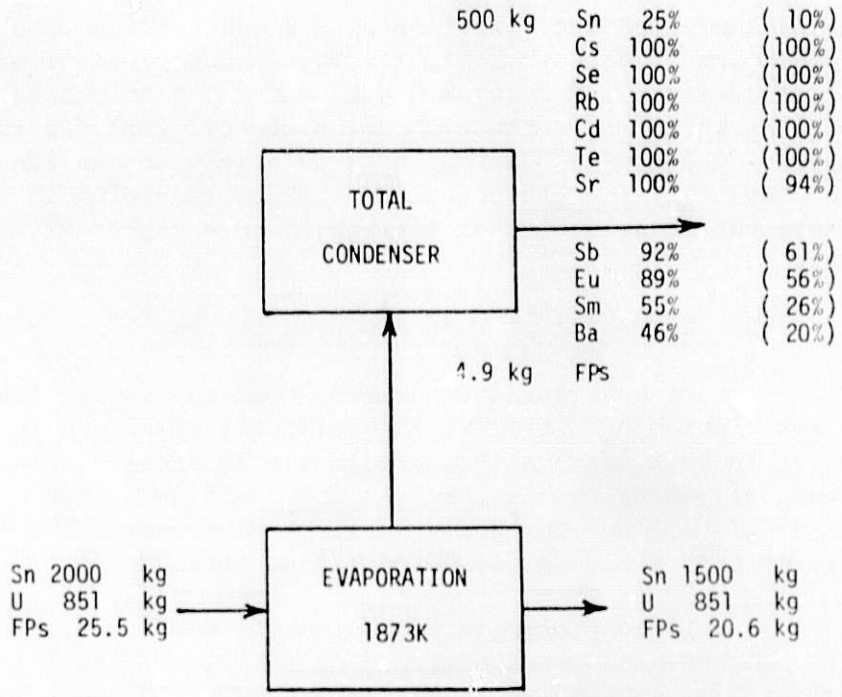

Fig. 19. Fission-Product Distribution during Evaporation Step of Molten Tin Process. Estimated percentages of fission products are given for distillation of 25% and 10% of the tin solvent, respectively.

d. Separations Processes

(1) Nitriding of U/Pu Mixtures in Tin

Additional work has been done to complete a nitriding run on a $^{238}U/^{239}Pu$ mixture in molten tin previously reported in [STEINDLER-1979C]. The reaction mix had the composition:

50.2 g tin
1.5 g calcium metal shot
8.0 g uranium, 3.2-mm-dia. rod
1.74 g plutonium, WR grade

All metals were well cleaned and shiny. Nitriding was done in a graphite reactor at 1900 K under about 680 torr nitrogen pressure for 2 h. The product was a solid brittle metallic ingot that was very adherent to the graphite walls. The product was reheated in a stainless steel vessel and was pressurized with argon to drive out the molten tin through a porous carbon filter, and the remaining nitride phase was analyzed by mass spectrometry. It showed a $^{238}U/^{239}Pu$ ratio of 10.14 compared with a ratio of 4.88 in the initial melt before nitriding. The mass spectrometric analysis was carried out by dissolving the nitride phase in HNO_3, adding known amounts of ^{233}U and ^{242}Pu

as calibration standards, and volatilizing a small portion on a tungsten filament in the mass spectrometer. Thus, for these conditions of nitriding, i.e., for a sample of 50 g Sn, 1.5 g Ca, 8.0 g U, and 1.7 g Pu heated for 2 h under about 700 torr N_2 at 1900 K, uranium tends to become enriched in the nitride phase and consequently the plutonium tends to remain in the liquid-tin phase. We would speculate that the plutonium and uranium remaining in the liquid tin can be nitrided out in a subsequent step by using a higher nitrogen pressure for nitriding.

(2) Nitriding of Th/U Mixtures in Tin

We have begun experimentation to explore the separation of thorium from uranium by nitriding Th/U mixtures dissolved in molten tin. Nitriding seems to be a reasonable approach for separation, considering that ThN is substantially more stable than UN (e.g., $\Delta H^\circ_{f,298}$ = -90.6 kcal/mol for ThN, and -70.7 kcal/mol for UN). We might thus expect thorium to nitride under conditions that would not lead to uranium nitridation.

Three preliminary experiments were carried out and reported last quarter. The results are summarized as follows: With 1 g of U in 50 g Sn and 1 g of Ca, no uranium reacted at 1900 K under 704 torr N_2 pressure, in marked contrast to complete reaction when 10 g U was in solution. When 9 g of Th was added to the above solution, the data at 1880 K indicated that thorium was reacting, but not uranium. Finally when thorium alone was nitrided (9 g Th in 50 g Sn and 1 g Ca), the nitriding was complete in 320 min, compared with 80 min for uranium under identical conditions. Thus, the nitriding rate for uranium was four times that for thorium. A productive approach would be to preferentially nitride uranium relative to thorium.

Next, a nitriding run was made on a mixture of 5.8 g U and 5.8 g Th in 50 g Sn without any calcium catalyst present. The rate of nitrogen uptake for 1 h run at 1900 K and 700 torr initial N_2 pressure was 10.5 torr/h. This compares with 6 torr/h nitrogen uptake for 9 g Th/g Ca in 50 g Sn and 12 torr/h for 9 g U/g Ca in 50 g Sn in earlier experiments. Although these results suggest that uranium is nitriding at a more rapid rate than is thorium, more definitive results should become available when our filtration unit becomes operational for separating the nitride phase and analyzing the U/Th ratios in these nitriding runs. We also need to repeat the experiment with calcium catalyst present to see whether it further accelerates uranium nitriding.

II. METAL ENCAPSULATION OF RADIOACTIVE WASTE IN METAL

(L. J. Jardine, K. F. Flynn, W. J. Mecham, and R. H. Pelto)

The major objective of this program is to idenify the advantages and disadvantages of encapsulating solidified radioactive waste forms in a metal matrix. The net attributes of metal encapsulation, if any, are to be identified by comparisons of waste-form properties and fabrication methods with those of other well-developed solidification alternatives--i.e., calcination and vitrification in the special case of high-level radioactive wastes. Laboratory-scale investigations are in progress specifically aimed at generating data required to further assess likely or unresolved problem areas.

A study aimed at assessing the impact resistance of metal-encapsulated waste forms in comparison to glass waste forms has continued during this period. Experimental studies have continued to focus upon determining (1) leach rates and (2) the impact resistance of simulated waste forms.

A. Determination of the Leach Rates for Nuclear Waste Materials

(K. F. Flynn)

1. Introduction

Leach-rate determinations of potential nuclear waste materials are necessary to evaluate the rate at which specific hazardous radionuclides will migrate from the waste if the waste form comes in contact with an aqueous medium. Waste materials under consideration have been extended to include crystalline waste forms. Studies are in progress to establish the effects of leach-rate variables associated with the leaching medium. Paramount among these variables is temperature. High pressure autoclaves are being used to make masurements in the 250 to 300°C temperature range. These higher temperature experiments will result in more comprehensive temperature correlations of the leach-rate data.

Neutron activation analysis techniques [FLYNN] have been used predominantly in the leach-rate studies reported here.

2. Experimental Results

Classically, leach rates are reported in units of mass of material leached in grams (g), per square centimeter (cm^2) of surface area exposed to the leaching medium per unit time (usually days). This unit is abbreviated $g/cm^2 \cdot d$. Since a very low rate of leaching is most desirable for any radioactive waste form, it is desirable to minimize the surface area available to the leaching medium (i.e., to minimize the ratio of surface area to volume). The surface area of the final waste form is a major concern because the surface is the interface where radioactive species are transported from the solid phase to the aqueous phase.

The surface area-to-volume ratios (S/V) for a series of sizes of spheres and for a specific cylinder are given in Table 24. The cylindrical shape in Table 24 represents an often-proposed canister size (0.3-m ID by 3.0 m) for glass monoliths. Spherical glass beads are an alternative glass waste

Table 24. Surface Area(S) to Volume(V) Ratios

	Diameter, m	S/V, m^{-1}
Spheres	0.005	1200
	0.01	600
	0.02	300
	0.05	120
	0.10	60
Cylinder (0.3 mD x 3.0 m)		14

[a]Proposed reference waste canister size.

form. The data in Table 24 indicate that the surface-to-volume ratio for a sphere of diameter about 0.01 m is only a factor of about 40 greater than that of the proposed reference cylindrical glass monolith. Only for spheres with diameters smaller than 0.005 m is there a two-orders-of-magnitude difference. Measurements of surface areas of actual large cast cylinders of glass [MENDEL, SLATE] indicate that surface areas increase by a factor of 10 or more due to cracking during cooling. The surface area is further increased if internal fins are used to improve heat transfer. Hence, a canister containing a given mass of glass as about 1-cm-dia glass bead spheres may have a surface area available for leaching comparable to that of an actual large cast glass ingot. That is, a canister filled with 1-cm-dia spheres may have approximately a factor of five more initial surface area available for leaching. This discussion suggests that the rate at which radioactive species would be leached from a canister containing spherical glass beads may not be dramatically different (i.e., no more than an order of magnitude) from the rate at which the same species would be leached from a large cast glass ingot of the same mass of glass.

Estimates of the rate of destruction for a solid material of uniform density, ρ, and thickness, X_o, can be made from the total mass leach rate, L, and the density if uniform attack from the outer surface is assumed. The rate of destruction can be expressed in units of thickness attacked, X, per unit time, t, by a penetration rate, P. The basic relationships are

$$L = \frac{X}{t}\rho$$

$$= P \cdot \rho$$

A plot of this relationship is shown in Fig. 20. Curves for three different densities (i.e., 1, 3, and 10 g/cm^3) are represented to allow one to estimate the rate of penetration for any solid material from the total mass leach rate and the density. For example, borosilicate glasses have densities of about 3 g/cm^3 and leach rates of about 10^{-6} $g/cm^2 \cdot d$. Interpolating from

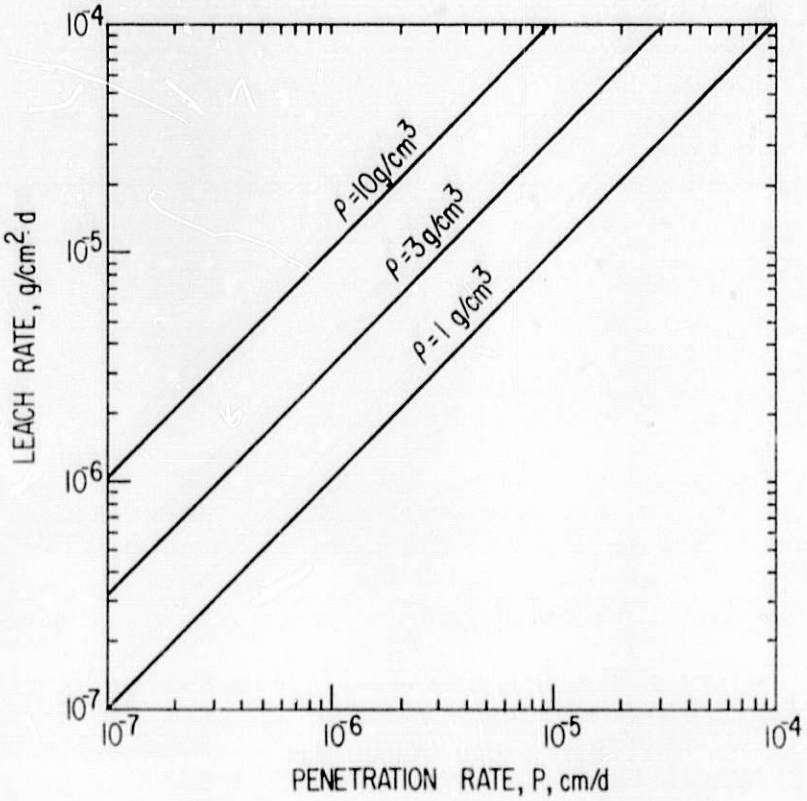

Fig. 20. Leach Rate vs. Penetration Rate.
P = density

Fig. 20, this material will be penetrated at the rate of about 3×10^{-7} cm/d (i.e., about 10^{-4} cm/y). Hence, a 1-cm-dia sphere of borosilicate glass immersed completely in the leaching medium will destruct in 5000 y. A 30-cm-dia solid cylinder of this material would last about 1.5×10^{5} y. The life of the solid cylinder, however, would be reduced significantly (i.e., by one or two orders of magnitude) by an extent related to the increases in the surface area during cooling (see [MENDEL, SLATE]).

Incremental leach rates using 25°C quiescent distilled water for copper, aluminum, and lead have been reported previously [STEINDLER-1979C]. These data are correlated in Table 25, using the relationships in Fig. 20 to calculate the relative thicknesses necessary to prevent penetration by water or to maintain long-term security against water intrusion. Similar data for borosilicate glass [STEINDLER-1979B] and for Zircaloy (reported in [STEINDLER-1979A]) are included to allow comparison. Many metals, of course, exhibit pitting type corrosion, for which these estimates would not apply.

Among the variables associated with the leaching medium, temperature probably has the most significant effect. Hence, studies of leach rates at elevated temperatures using high-pressure autoclaves are in progress. The use of high pressure allows leach rates to be measured conveniently in aqueous media at temperatures up to about 300°C.

Table 25. Material Thickness Required to Resist Penetration

Material	Leach Rate,[a] g/cm^2d	Density, g/cm^3	Penetration,[b] Rate cm/d	Rate cm/y	Thickness To Resist Penetration for 1000 y, cm
Copper	1.2E-6	8.9	1.4E-7	5.1E-5	5.1E-2
Aluminum	1.5E-6	2.7	5.6E-7	2.0E-4	2.0E-1
Lead	2.0E-5	11.3	1.8E-6	6.6E-4	6.6E-1
Zircaloy	2.0E-9	6.4	3.1E-10	1.1E-7	1.1E-4
Glass	1.0E-6	3.9	2.6E-7	9.5E-5	9.5E-2

[a]Data based on quiescent distilled water leachant at 25°C, as measured at ANL.

[b]Assumes the indicated leach rate and density to be constant.

Three autoclaves are currently in operation for these studies. They are (1) a type 304 stainless steel vessel having a volume of two liters, manufactured by Autoclave Engineers, Incorporated, (2) a Hastelloy-C vessel having a volume of one liter, also manufactured by Autoclave Engineers, Incorporated, and (3) a type 316 stainless steel vessel having a volume of about 0.16 L, manufactured by the High Pressure Equipment Company. These autoclaves are being operated at about 4.14 MPa (600 psig), corresponding to an aqueous temperature of about 254°C. At such a pressure, the temperature varies only slowly as a function of the pressure (i.e., 1°C per 70 kPa). Hence, small variations in pressure resulting from feedback mechanisms in the control circuits do not seriously affect the temperature of the experiment.

Secondary containers, consisting of type 304 stainless steel 1/2-in. schedule 40 pipe nipples, are being used to facilitate the use of the autoclaves for several samples simultaneously. The pipe nipples are sealed by wrapping the threads with teflon tape and securing the ends with pipe caps.

In autoclave experiments done to date, quiescent distilled water has been used. However, experiments using alternative leaching media (including saturated brine in the Hastelloy-C autoclave) are planned.

Preliminary results using a simulated high-level-waste glass have been reported previously [STEINDLER-1979C]. The results of studies based on weight loss measurements for several commercial-grade materials are given in Table 26. These results are based on an "initial" leach test of about 20 days.

Sequential testing could produce significantly different results. The titanium, type 304 stainless steel, and aluminum samples all showed weight gains, indicating possible oxidation of the surface. For these materials, sequential testing will be most important if information regarding rates of destruction based on weight loss is required.

Table 26. Leach Rates[a] at 254°C Based on Weight Loss

Material	Surface[b] Area, cm^2	Time Interval, d	Initial Wt, g	Final Wt, g	Weight Change, g	Leach Rate,[c] $g/cm^2 \cdot d$
Copper	28.6	19.8	10.0644	10.0643	-0.0001	--
Titanium	11.1	19.8	2.4193	2.4233	+0.0040	--
304 Stainless Steel	27.7	19.8	10.2740	10.2757	+0.0017	--
Aluminum	19.2	19.8	7.6933	7.7071	+0.0138	--
Lead	40.5	19.8	9.7481	9.4090	-0.3391	4.2E-4
Borosilicate Glass	28.3	19.8	3.4909	3.4505	-0.0404	7.2E-5

[a]Data obtained with distilled water as the leaching medium.

[b]Calculated surface area based on the geometric shape of the material.

[c]Units of grams per square centimeter of surface area per day ($g/cm^2 \cdot d$).

The weight change for copper, although negative, is not outside experimental error. Hence, there is significant uncertainty in this result. The leach rates determined for lead and glass are considered to be meaningful. However, continued testing would be necessary to establish greater credibility. Because of increased sensitivity and reduced ambiguity with the neutron activation analysis (NAA) technique [FLYNN], it is being used as the primary method for determining leach rates. Experiments are in progress using this technique (NAA) to establish, with greater sensitivity, the rate of destruction of a host of proposed radioactive waste materials including the barrier materials given in Table 26, by reaction with aqueous media.

Studies are continuing of the effects on leach rate of changing various parameters associated with the leaching medium [STEINDLER-1979C]. These studies have been expanded to include rock-equilibrated (e.g., climax granite,* basalt, etc.) aqueous solutions. The use of rock-equilibrated leaching media allows closer approximation of the conditions extant in geologic repositories. Initial results from a leach test using PNL-glass (76-68 formulation) [McELROY] and climax-granite-equilibrated water are given in Table 27. These results are for about 20 days of leaching at both 25 and 100°C. The samples used weighed about 1 g and had about 3 cm^2 of surface area based on a geometric calculation.

The leach rates for the thirteen elements studied are remarkably similar at a given temperature, particularly at 100°C where the higher leach

*Climax granite comes from the Nevada Test Site (NTS).

Table 27. Leach Rates (∿20-day Duration) for PNL-Glass,[a] Using Climax Granite-Equilibrated Water (pH, ∿8)

Isotope Analyzed	Leach Rate,[b] g/cm²d	
	25°C	100°C
^{51}Cr	c	1.2E-5
^{59}Fe	c	1.2E-5
^{60}Co	c	1.4E-5
^{65}Zn	9.0E-7	1.3E-5
^{86}Rb	c	1.5E-5
^{95}Zr	3.7E-7	1.1E-5
^{103}Ru	c	1.2E-5
^{110}Ag	c	1.3E-5
^{134}Cs	4.6E-7	1.5E-5
^{140}Ba	4.4E-7	1.7E-5
^{141}Ce	2.2E-7	1.5E-5
^{152}Eu	2.3E-7	1.3E-5
^{181}Hf	c	1.4E-5

[a]PNL-glass formulation 76-68 as defined in [McELROY].

[b]The unit of grams per square centimeter per day ($g/cm^2 \cdot d$) represents the equivalent grams that would have been leached if the entire matrix had leached at the same rate as the specific isotope measured [STEINDLER-1978A].

[c]Because of the very low leach rate for this material at 25°C, more sophisticated analyses of the data are necessary to determine the values.

rates result in more radioactivity in the leachant and hence reduced uncertainty in the results. Under these conditions, the leach rates for all elements studied seem to increase about 50-fold as the temperature is increased from 25°C to 100°C. This behavior seems to differ somewhat from that observed with distilled water [STEINDLER-1979C]. These studies are continuing and are being expanded to include autoclave studies at about 250°C. After additional

studies and more detailed analyses of the data are made, leach rates using this leaching medium will be compared with rates using other potential leaching media (e.g., saturated brine). These results will help to establish the type of behavior that might be expected from solid waste forms in geologic repositories.

The proposed high-level-waste materials being studied have been expanded to include crystalline waste forms. The first sample for this series of experiments was a SYNROC*-type material prepared by the ANL Materials Science Division (MSD). Leach-rate measurements were made on these SYNROC samples, using distilled water at 25 and 100°C. The results of an initial test lasting 20 days are given in Table 28. These results are preliminary and are based on results obtained by the neutron activation technique [FLYNN]. The unit of grams per square centimeter per day ($g/cm^2 \cdot d$) represents the equivalent grams that would have been leached if the entire matrix had leached at the same rate as the specific isotope measured. These units are defined in detail and the rationale for their use is given in previous reports (e.g.,

Table 28. Initial (∿20-Days Duration) Leach Rates ($g/cm^2 \cdot d$)[a] in Distilled Water

Isotope	Leach Rate at 25°C		Leach Rate at 100°C	
	ANL SYNROC[b]	PNL Glass[c]	ANL SYNROC[b]	PNL Glass[c]
^{95}Zr	<3.8E-7	4.4E-7	5.6E-7	2.4E-6
^{131}Ba	2.0E-6	--	1.1E-6	--
^{134}Cs	<2.0E-4[d]	8.4E-7	<7.8E-4[d]	8.9E-5
^{152}Eu	--	3.5E-7	--	1.0E-6
^{181}Hf	1.0E-7	6.6E-7	5.5E-7	--
^{192}Ir	--	--	6.0E-7	--
Wt Loss	--	--	<3.0E-5	1.1E-4

[a]The unit of grams per square centimeter per day ($d/cm^2 \cdot d$) represents the equivalent grams that would have been leached if the entire matrix had leached at the same rate as the specific isotope measured [STEINDLER-1978A].

[b]SYNROC material manufactured according to a formulation suggested by A. E. Ringwood and co-workers [RINGWOOD].

[c]PNL-glass formulation 76-68 as defined in [McELROY].

[d]These data represent limits since insufficient cesium was present to make precise determinations.

*SYNROC material was manufactured according to a formulation suggested by A. E. Ringwood and co-workers [RINGWOOD].

[STEINDLER-1978A]. The data from previously reported leach-rate studies [STEINDLER-1978A] using a simulated high-level-waste glass obtained from Battelle Pacific Northwest Laboratories (PNL) are included in Table 28 to allow comparison. The composition of this waste glass (formulation 76-68) has been defined by PNL [McELROY].

The major radioactive isotopes present in the neutron-activated SYNROC material are ^{95}Zr, ^{131}Ba, ^{181}Hf, and ^{192}Ir. Since no "pseudo waste" elements were added to this initial formulation, the observed radioactivities should be assumed to be part of this matrix material. Hence, the calculated leach rates represent the leach rate for the matrix material. As can be seen from the data in Table 28, the leach rate for this SYNROC material under the stated conditions is at best marginally better than the leach rate for the PNL 76-68 glass.

It was not possible to obtain quantitative leach-rate data for cesium and the rare-earth elements from these samples. New SYNROC samples are being prepared that contain appropriate concentrations of "pseudo waste" elements. These samples will allow quantitative evaluation of the leach rates of the specific hazardous radionuclides present in high-level waste. More detailed comparisons with proposed waste glass formulations will then be made. These samples will be tested at 250°C, a temperature at which most glass formulations have serious stability problems [STEINDLER-1979C].

3. Conclusions

The surface area of the final waste form is a major concern because the surface is the interface where the radioactive species are transported from the solid phase to the aqueous phase. Hence, a minimum surface-to-volume ratio for a solid waste form is most desirable. However, because of problems associated with the cooling of large glass ingots, glass spheres of 1-cm diameter may have less than an order of magnitude (about 5 times) greater surface-to-volume ratio than a large production-size, cylindrical glass casting.

Comparisons of the relative thicknesses estimated to resist penetration by uniform corrosion for 1000 y of several metals indicate that resistances of the metals tested vary by three orders of magnitude. These estimates were based on leach rates for 25°C quiescent distilled water leachants and hence bear little relationship to actuality. Nevertheless, the results indicate the need for detailed studies of proposed canister materials under specific canister environment conditions. Further, these preliminary results indicate that certain materials (e.g., Zircaloy) may have very attractive barrier properties.

Elevated temperatures (e.g., up to 300°C) can have detrimental effects on the leach rates of proposed waste forms. High-pressure autoclaves are being used as apparatus for attaining these high temperatures in aqueous media. Preliminary experiments with this type of equipment have been conducted satisfactorily. These equipments are continuing in order to establish accurate relationships between leach rate and temperature.

Alternative leaching media (e.g., rock-equilibrated aqueous solutions) have been introduced into our leaching studies. Initial results indicate significant, although not dramatic, differences in the leach rates with

those solutions in comparison with similar studies using distilled water. Further studies at higher temperatures and on an expanded time scale are in progress to quantify the differences.

Leach-rate studies of crystalline waste materials have been initiated. Preliminary studies, using a "first-attempt" product of SYNROC-type material, indicated only marginally better leach-rate behavior than has been observed for a PNL glass. It will be necessary to obtain simulated material containing significant concentrations of "pseudo waste" elements (e.g., cesium, strontium, europium, etc.) before definitive conclusions can be drawn regarding the leaching behavior of crystalline waste forms.

B. Comparative Evaluation of Impact Resistance of Metal-Matrix Waste Forms

(W. J. Mecham, R. H. Pelto, and L. J. Jardine)

1. Introduction

The resistance of solid-waste forms to mechanical impacts during in-plant storage and transportation is an important aspect of the evaluation of the risk of potential dispersion of high-level radioactive wastes. A study of the analysis and evaluation of the effects of impacts has been initiated for reference metal-matrix waste forms. The general objective of this study is to develop sufficient information so that decisions can be made (by others) regarding either the need or the effort required for demonstrations of the impact resistance of metal-matrix waste forms in comparison with other waste forms, particularly borosilicate glass. This is the fourth quarterly progress report of this study.

In the three previous quarterly reports, the relevant scientific and engineering literature and the available data on impact effects of simulated waste forms were reviewed. Also, descriptive and calculational models were developed for relating impact energy to deformation effects, for both brittle and ductile materials, and for characterizing the surface area and particle-size distributions resulting from impact fracture of brittle materials. In the present report period, preliminary experimental measurements have been made of simulated waste glass specimens. Results are presented and are compared with data reported by others, by means of a methodology based on the impact-deformation models developed and reported in earlier stages of this study [STEINDLER-1979C].

2. Methodology for Study of Brittle-Ductile Composites

One of the objectives of the present program [STEINDLER-1979A] is to use available data to characterize the impact resistance of solid-waste forms such as metal-ceramic composites.

Impact of a typical ductile metal body results in permanent deformation in the form of a localized "dent" at the zone of applied compressive stress; because the material itself is essentially incompressible, the volume of the inward "dent" is equal to the volume of an outward bulge in a contiguous region of the body. A quantitative measure of the plastic deformation from impact is the configurational change represented by the displacement volume of the "dent." The nature of plastic flow of ductile metals is such that the energy absorbed (W_D) in this deformation is the product of the above displacement

volume (ΔV_D) and a material "property," labeled the dynamic flow stress (σ_D). The property σ_D is nearly constant over a range of typical impact conditions, and approximate values of σ_D for mild steel and lead are, respectively, 3.4 x 10^8 Pa (50,000 psi) and 6.2 x 10^7 Pa (9,000 psi) [SHAPPERT]. Thus, in general, for ductile bodies

$$W_D = \sigma_D \, \Delta V_D \tag{1}$$

Brittle fracture of a typical solid glass or ceramic under an impact results in fragmentation and formation of additional surface area (ΔS_F). As described in previous quarterly reports in this series [STEINDLER-1979A, 1979B, 1979C], the fracture energy (W_F) absorbed is proportional to ΔS_F for a given type of specimen and mode of impact--even for a considerable range of energy inputs. The proportionality constant, termed the fracture surface energy, γ_F, was found to be nearly constant at about 80 J/m^2 for small Pyrex specimens impacted in a dual-pendulum device at input energy densities of up to 17 J per cm^3 of material [PIRET-1962]. Thus, in general, for impact energy absorbed in the brittle material,

$$W_F = \gamma_F \, \Delta S_F \tag{2}$$

In Eq. 2, W_F is smaller than the input or available gross impact energy (W_I), due to deformation in test equipment components; for "bare" glass specimens impacted by hard steel surfaces, W_F is typically in the range of 50% to 90% of the gross impact energy. Also, γ_F can be expected to vary somewhat with type of material, size and shape of the impacted material, and the input energy concentration (density) in the volume (V_o) of the specimen. As will be shown later, γ_F varies systematically with energy densities (concentrations) as represented by (W_I/V_o) or (W_F/V_o) over a wide range of fracture conditions. This applies both to impacts and to slow-compression crushing of brittle specimens.

The particulate solid formed in brittle fracture typically has a particle-size distribution that can be described by the lognormal probability function, with its two parameters, namely, the geometric mean diameter, D_g, and the geometric standard deviation, σ. The ratio of total particulate surface area, S, to solid volume, i.e., S/V_o, can be expressed as a particulate "equation of state" in terms of the lognormal parameters:

$$\frac{S}{V_o} = \frac{\alpha \, \sigma^{0.5 \ln \sigma}}{D_g} \tag{3}$$

where α is a dimensionless shape factor [HERDAN]. The minimum value of α is 6 (for spheres and cubes); for brittle fragments, σ is typically two to three times higher (as discussed later in this report). The above total particulate surface area S is related to the original specimen surface area S_o and to the increased surface area formed in fracture, ΔS_F as

$$\Delta S_F = S - S_o \tag{4}$$

The relations expressed by Eqs. 1 through 4 provide quantitative parameters that can serve as a basis for a systematic test program for characterizing the results of impact on various composite bodies of brittle and ductile material--in particular, solid-waste forms of the metal-matrix type.

One confirmation of the above energy methodology is provided by a reinterpretation of data reported in preliminary impact studies of glass waste that had been cast in stainless steel canisters; in this work, reduced-scale models of reference waste-canister designs were used [SMITH-1975]. Although the scaling factors and impact mechanisms were not established definitively by [SMITH-1975], the principal results of the scale-model tests provided engineering estimates of (1) the total fracture surface area of the glass and (2) the mass fraction of particle fragments of respirable size (i.e., having diameters less than 10 μm). These estimates were reported [SMITH-1975] graphically as nonlinear functions (with indicated margins of uncertainty) of the impact velocity at which the scale models struck an essentially unyielding surface. According to the energy-relation equation presented (Eq. 2), these impact effects should correlate as a linear function of impact energy, i.e., the kinetic energy, which is converted into deformation energy. As shown in the plots of respirable fraction and increased surface area in Figs. 21 and 22, these impact effects appear to be approximately linear when the original data

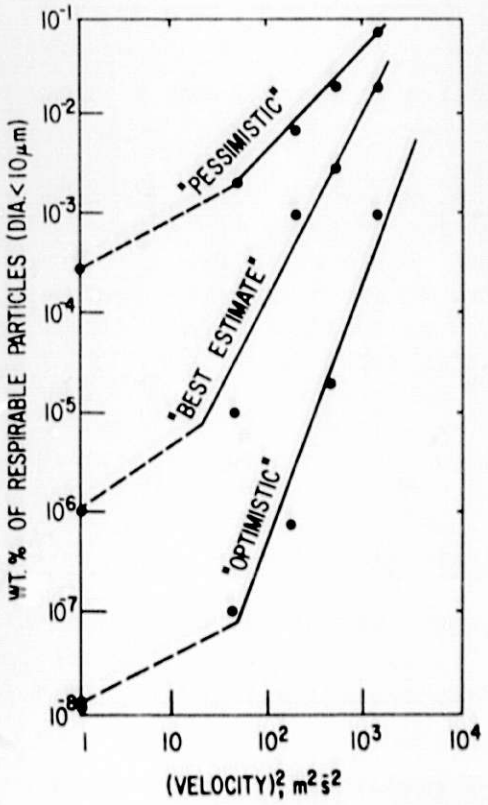

Fig. 21. Respirable Fraction for Canistered Glass Waste Form Originally Reported by [SMITH-1975] but Replotted as a Function of the Relative Kinetic Energy of Impact

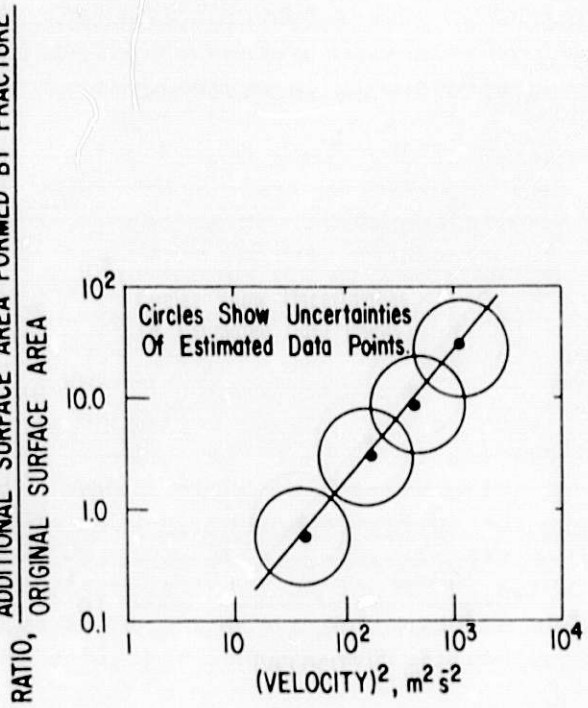

Fig. 22. Increased Surface Area for Canistered Glass Waste Form Originally Reported by [SMITH-1975] but Replotted as a Function of the Relative Kinetic Energy of Impact

are replotted against the square of impact velocity, which represents the relative energy input of the reported scale-model tests of the reference canistered glass waste form. (Both plots use log-log scales because of the wide range of numerical values.) The departures from linearity, indicated as dashed lines in Fig. 21, are due primarily to the thermal-stress fracture of the glass that occurs during specimen fabrication prior to any impaction; this can amount to a 10-fold increase of surface area in full-size canistered glass waste forms [SLATE]. In the following sections of this report, the methodological approach described above is used to interpret experimental data on impact fracture of various experimenters.

3. Relevant Particle-Size Data from Impact Fracture of Brittle Materials

Data from impact tests of brittle material performed at ANL, Savannah River Laboratory, Battelle Pacific Northwest Laboratory, and Monsanto Mound Laboratory are being evaluated and will be reported in the next quarterly report in this series.

4. An Overview of Brittle Fracture in Impacts and in Slow-Compression Tests

In the preceding quarterly report [STEINDLER-1979C], the work on brittle fracture of Edgar L. Piret and associates was reviewed [PIRET-1950, 1961, 1962]. In this work, both single impacts and slow-compression crushing were

applied to small (about 1/2-in.) solid specimens (spheres and cylinders) of Pyrex glass and to similar-sized prisms of natural quartz. Also, multiple impacts and slow-compression crushing were applied to particulate samples (10-14 mesh) of natural quartz. The principal result of this work was measurement of the net energy absorbed in the brittle specimens in producing the fracture surface (the latter was measured by a gas adsorption technique). Calorimetric methods were used to establish the net energy absorbed. We plotted all data on the net fracture-surface energy, γ_F, vs. the net energy density (W_F/V_o) applied to the specimens. A representative selection of the data points is plotted in Fig. 23. Although there is a great deal of scatter in the slow-compression data, e.g., tenfold variations of γ_F for some values of W_F/V_o, the uniformity of γ_F upon impact fracture ($\gamma_F > 70$ J/m^2) is notable. Even the scatter of slow-compression crushing ($\gamma_F > 70$ J/m^2) is much reduced from earlier work because of close controls applied to both the specimen preparation and the crushing methods.

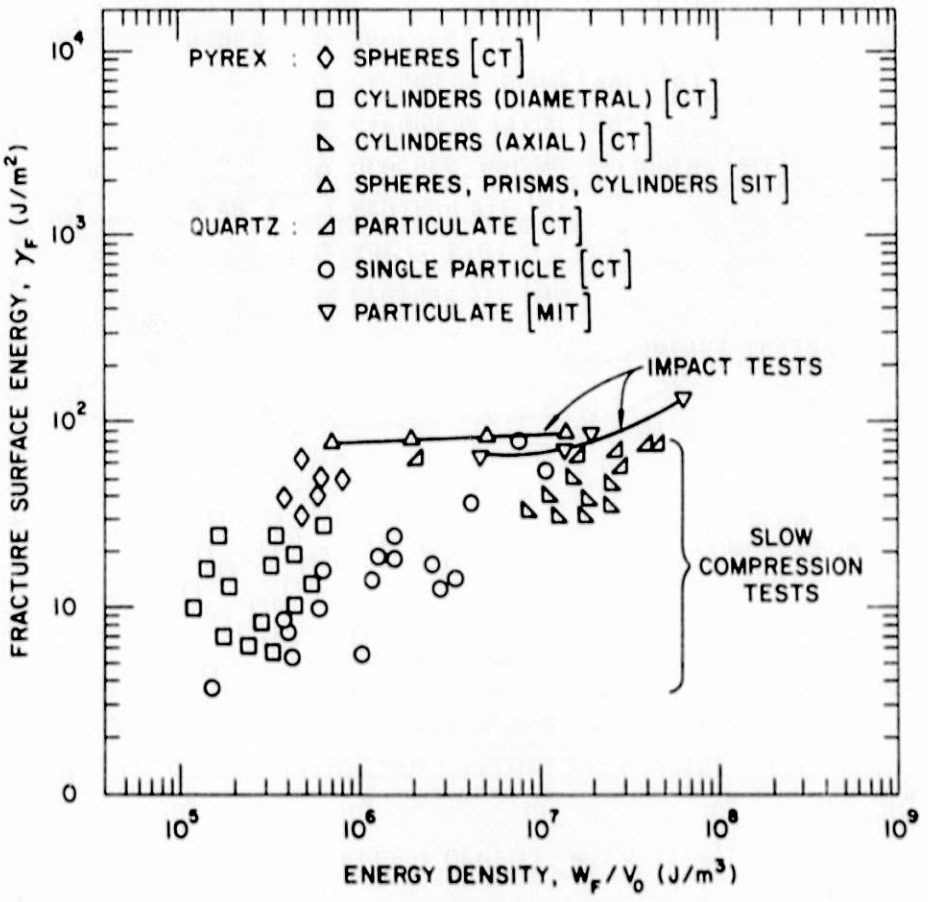

Fig. 23. Summary of Fracture-Surface Energy Data from Impact Tests and Slow-Compression Tests. After [PIRET-1950, 1961, 1962]

The principal impact results are these:

1. For single impact of the Pyrex specimens, the value of γ_F was nearly constant at 77 ± 7 J/m^2 over a 20-fold range of energy densities up to 1.5×10^7 J/m^3; there was no effect of specimen shape.

2. The multiple drop-weight impacting of particulate quartz shows an increase of γ_F with increasing W_F/V_o.

3. These impact results indicate that for sharp impacts (single impacts), γ_F has a value of about 100 J/m^2 over a wide range of energy densities and that γ_F tends to increase at energy densities above about 2×10^7 J/m^3; also, fracture behaviors of relatively flaw-free glasses and crystalline minerals seem to differ little.

The principal results of slow-compression crushing are:

1. In slow-compression crushing, the chief uniformity was a low value of γ_F when fracture occurred at low values of W_F/V_o (i.e., averaged over the specimen volume). This means that for "weaker" specimens, more fracture surface was generated per unit of energy absorbed.

2. There was a shape effect in slow-compression crushing. Cylinders crushed diametrally ("on the round side") fractured at lower energy densities than did cylinders crushed axially ("on the flat side"). An explanation is that stresses in the latter case are more uniform over the volume of the specimen, whereas there are high local concentrations of stresses in the former case. Fracture occurs at the highest stress concentration so that the average energy density is lower for the specimen with widely varying stress concentration, i.e., in the diametral application of force.

3. The general explanation for higher γ_F (lower energy efficiency for fracture of a specimen) is that, when fracture occurs at higher energy densities, the three-dimensional fissures tend to be mutually terminating (short of whole-body cleavage) so that (more and shorter) cracks allow more elastic energy to be converted to heat as a result of interparticle contact.

4. In slow-compression crushing of quartz, the crushing of single particles is more energy-efficient for fracture than the crushing of a large number of particles (about 1000 particles of 10-14 mesh quartz were used). The explanation offered [PIRET-1950] was that multiple-particle crushing to a considerable extent was a shearing action rather than a shattering action. The latter mode occurs when a single particle is subjected to large stored elastic energy, whereupon multiple cleavages of the particle occur.

The brittle fracture process can be considered in terms of well-known tests of brittle strength, namely, (1) the diametral compression test for cylindrical specimens and (2) the 3-point bend test of elongated rods or prisms. The result of such slow-compression tests is that the body breaks in two at the cross section of greatest tensile stress. In practical fracture processes, such breaking-in-two steps occur many times, so that the resulting particle-size distribution can be described in terms of the number of times (N) the basic binary-fracture step has taken place. The variation of particle diameter thus corresponds to the value of N.

If every portion of the specimen volume fractured with the same N, the resulting particle size D would be related to the original size D by $\frac{D}{D_o} = \left(\frac{1}{2}\right)^N$, a binary exponential function. Actual particle population varies in particle size such that if the variation of N in the volume of the fragmented material is distributed normally, then the resulting particle size D is distributed lognormally, i.e., $\ln \frac{D}{D_o} = N \ln \frac{1}{2}$.

The above empirical generalizations, together with the relation of fracture surface to absorbed energy, provide a physical rationale for the use of the lognormal probability function to express accurately the particle-size distribution from brittle fracture. Further evaluations are in progress.

III. TRANSPORT PROPERTIES OF NUCLEAR WASTE IN GEOLOGIC MEDIA

(M. G. Seitz, N. Meldgin,* Jacqueline Williams,†
P. Rickert,‡ S. Fried,‡ A. M. Friedman,‡
and M. J. Steindler)

A. Introduction

A method considered for permanent disposal of radioactive waste from nuclear power generation is to place the waste in geologic formations deep beneath the earth's surface. The safety of such disposal can depend upon the capacity of the rock surrounding the repository to immobilize radionuclides that are carried from the repository by flowing groundwater.

The capacity of a rock material for radionuclide adsorption depends on the amount of surface area available for adsorption and is related to properties of the rock porosity (pore size distribution, pore morphology, open or closed porosity, etc.). To gain some knowledge of rock porosity, an Aminco 30,000-psi porosimeter was employed to examine pore size distributions for pores smaller than 20 μm in diameter for Columbia River basalt, Sentinel Gap basalt, and oolitic limestone. A specific objective of the analyses was to test for porosity that was postulated to account for the penetration of americium into basalt particles to a depth of approximately 500 μm during batch adsorption experiments [SEITZ-1978].

In safety evaluations of a repository, the concept of a partition coefficient, K_d, is widely used to predict the migration velocity of a radionuclide through rock. The partition coefficient expresses the amount of a radionuclide partitioned onto a solid phase per mass of solid to the amount of the radionuclide in solution. Among many possible reasons for the failure of a prediction of migration velocity from a partition coefficient are (1) the radionuclide species investigated in the laboratory may not be the species generated in the radiation field of the repository and (2) the fraction of radionuclide adsorbed by the rock may depend upon the nuclide concentration. To test for radiolysis effects on solution species and to extend the studies of the concentration dependence of adsorption that were performed previously [SEITZ-1979], batch experiments were conducted in which strontium was adsorbed onto limestone by rotating test tubes containing particulate stone and ^{90}Sr-bearing synthetic groundwater.

Although the partition coefficient is expressed explicitly in the solute transport equation, a single value of the coefficient used with specific solutions of the equation may not represent migration because (1) the partition coefficient may not be constant but may vary with solute concentration or with other parameters and (2) the assumptions used to arrive at a solved representation of the equation may not apply to the situation to which the representation is applied.

---

*Consultant from the Mayfield Engineering Co., Chicago Ridge, IL.

†Member of the Analytical Group of the Chemical Engineering Division.

‡Member of the Chemistry Division.

Because there is a wealth of partition coefficient data available and the amount of data continues to grow, we have conducted experiments to establish the relationship between the migration observed experimentally in columns of rock material and the migration predicted by partition coefficients measured for the same material. This work is considered the first of several steps required to successfully predict nuclide migration in a geologic formation from partition coefficients measured in the laboratory.

In this report period, column-infiltration experiments were used to examine the migration properties of cesium in granulated limestone. Results will be compared with the results of batch tests to examine the validity of using a measured K_d value to predict migration.

B. Pore Size Distributions of Pores Smaller than 20 μm in Diameter for Three Rocks

Pore size distributions for pores less than 20 μm in diameter for Columbia River basalt (mesh ranges, 16-20, 30-40, and 50-70), Sentinel Gap basalt (mesh range, 20-50), and oolitic limestone (mesh range, 20-50) were examined with an Aminco 30,000-psi porosimeter. The oolitic limestone and Sentinel Gap basalt samples were supplied as part of the Controlled Sample Study [RELYEA] and were included in this study because they had been previously used in adsorption experiments and no accurate porosity data had been gathered on either. The Columbia River basalt samples had been used in a previous study of americium adsorption on different mesh ranges of basalt [SEITZ-1978].

The porosimeter enables one to quantitatively measure the volume of pores in different sizes by intruding mercury at increasingly higher pressures into pores of progressively smaller diameters. Pores at the surface of rock grains resist penetration by mercury. The amount of pressure required to infiltrate these pores varies inversely with the diameter of the opening and varies directly with the surface tension and the contact angle between the pore and mercury as follows:

$$p = \frac{-4\phi \cos \theta}{d}$$

where p is the mercury pressure at the pore opening,

d is the pore diameter,

ϕ is the mercury surface tension, and

θ is the contact angle.

Surface tension and contact angle are assumed to remain constant during a test and to be equal to 473 dynes/cm (mercury surface tension at 25°C) and 130°, respectively, so that the relationship between pore diameter and mercury pressure is

$$d = 1.216/p$$

where: d is the pore diameter, in micrometers and

p is the mercury pressure, in pascals.

At a pressure of 2.1×10^8 Pa (30,000 psia, the working limit for the porosimeter used), the pore diameter of the smallest pore filled with mercury is calculated by the equation to be 0.006 µm.

In the operation of the porosimeter, a dry solid sample is placed in a penetrometer cell, which is evacuated and then filled with mercury to 31 kPa (4.5 psia). The glass penetrometer stem is removed from the mercury, and the pressure in the cell is increased by admitting air to the bottom of the stem. The mercury pressure is determined by reading a 0 to 15 psi range gauge. The position of the mercury meniscus in the penetrometer stem is determined by eye.

The full penetrometer is then transported to the high-pressure test cell for porosimeter readings from 103 kPa to 2.1×10^5 kPa. Pressure is read from a gauge having a 0-30,000 psi range. The lower pressure readings (below 3 MPa) are adjusted to account for the pressure from the column of mercury in the stem of the porosimeter (approximately 20 Pa). As the pressure rises, the volume of mercury displaced is measured by a thin wire which is moved up the penetrometer stem and acts as an electrical contact ceasing motion each time connection is made with the mercury. The porosity measurements are then blank-corrected to negate the effect of the compressibility of mercury on the final results. The pressures and corresponding stem readings for a test of the 30-40 mesh Columbia River basalt are listed in Table 29 to exemplify the type of data obtained from the porosimeter (penetrometer).

Corrected penetrometer readings were plotted against absolute pressure in Figs. 24, 25, and 26. The initial positive slope of these graphs up to a plateau at approximately 20-µm-diameter pore level is produced by mercury infiltration of the interstitial grain voids. The fraction of pore space equals the difference between the volume for the highest pressure run and the volume at which interstitial grain filling stops, measured in cm^3/g, multiplied by the density of the sample tested. The interstitial void volume is greater for smaller-particle-size samples of the same weight, as is graphically illustrated in Fig. 24.

The oolitic limestone was found by (displacement of water in a graduated cylinder) to have a density of 2.6 g/cm^3. This compact limestone has a measured porosity for pores smaller than 20-µm diameter just below 0.25% of the particle volume.

If a density of 3.1 g/cm^3 is assumed for Sentinel Gap basalt, the porosity of this basalt is 0.03% as determined by the porosimeter method.

The density of the Columbia River basalt (30-40 mesh) was found to be 3.1 g/cm^3. Using this value, the Columbia River basalts have the following measured porosities: 16-20 mesh, 0.04%; 30-40 mesh, 0.03%; and 50-70 mesh, 0.06%.

Table 29. Pressures, Corresponding Stem Readings, and Corrected Volumes of Infiltrated Mercury for a Test with 0.4 g of 30 to 40-mesh Columbia River Basalt

Pressure, psia	Penetrometer Stem Reading, mL	Corrected Penetrometer Reading, mL
1.8	0.0020	0.0020
2.8	0.0070	0.0070
3.8	0.0090	0.0090
4.8	0.0100	0.0100
6.8	0.0110	0.0110
8.8	0.0110	0.0110
11.5	0.0110	0.0110
61.5	0.0116	0.0116
211.5	0.0116	0.0116
311.5	0.0119	0.0118
411.6	0.0125	0.0124
511.6	0.0129	0.0128
765	0.0131	0.0128
1265	0.0133	0.0131
2015	0.0136	0.0132
3015	0.0146	0.0141
5015	0.0148	0.0141
10015	0.0154	0.0142
12515	0.0160	0.0144
15015	0.0165	0.0147
17515	0.0170	0.0149
20015	0.0180	0.0157
22515	0.0190	0.0165
28015	0.0195	0.0167

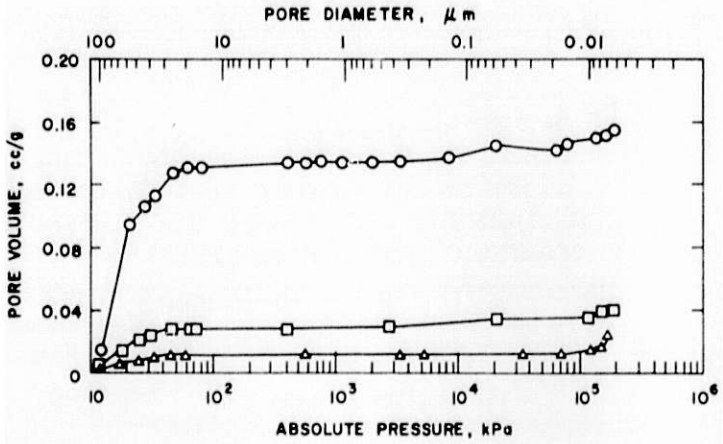

Fig. 24. Integrated Pore Volume vs. Pore Diameter for Three Size Fractions of Columbia River Basalt. Circles are for the 50 to 70 mesh material, squares, for the 30 to 40 mesh material, and triangles for the 16 to 20 mesh material

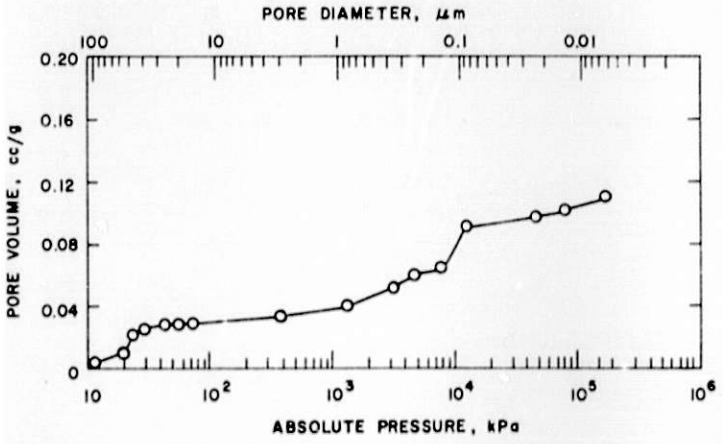

Fig. 25. Integrated Pore Volume vs. Pore Diameter for 20 to 50 Mesh Oolitic Limestone. Porosity due to pores smaller than 20 μm in diameter is 0.25% of the particle volume

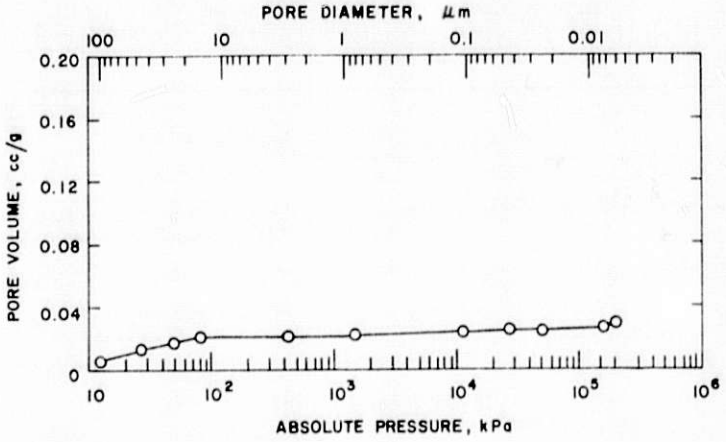

Fig. 26. Integrated Pore Volume vs. Pore Diameter for 20 to 50 Mesh Sentinel Gap Basalt. Porosity due to pores smaller than 20 μm is about 0.3% of the particle volume

For the basalts, the correction due to the compressibility of mercury reduced the porosity indicated by the recorded data by 0.02% of the particle volume. This correction is assumed to be approximately the error associated with the measurements and so the observed difference in porosities for the three size ranges of Columbia River basalt may not be significant.

1. Estimated Pore-Surface Area of Columbia River Basalt

To judge the significance to adsorption phenomena of the porosity determined by the porosimeter measurements, the surface area of the pores was estimated by assuming that the pores are tubes about 500 μm in length (a length suggested by the apparent penetration depth obtained by adsorption of americium [SEITZ-1978] and that pores are about 0.008 μm in diameter (as suggested by the porosimeter results described here).

The ratio of the pore surface area to the particle fracture area (assuming nonporous spheres) is given in Table 30 for the three size fractions of Columbia River basalt. Because the estimated pore surface areas greatly exceed the fracture areas of the rock particles (calculated by assuming nonporous spheres), we conclude that fine-grained pores in the basalt may be important to nuclide adsorption--even though they constitute only a fraction of one percent of the rock volume. This conclusion is not sensitive to the pore morphology used in the calculation. If the pores are assumed to be hemispheres rather than long cylinders, the numbers in the last two columns of Table 30 are reduced by only a factor of 6.

Table 30. Estimated Pore Surface Area of Particles of Various Sizes. Columbia River Basalt. Pore surface area relative to the surface area of the particles

Mesh Size	Opening Width for Screen	Porosity of 0.008-μm-dia. Pores, %	Surface Area of Pores,[a] m^2/g	Ratio of Pore Surface Area to Particle Fracture Area[b]
16-20	850 to 1180	0.04	0.06	34
30-40	425 to 595	0.03	0.05	13
50-70	212 to 300	0.06	0.10	13

[a] Surface areas were calculated by assuming that the pores were tubes 500 μm long and 0.008 μm in diameter.

[b] Each particle fracture area was calculated by assuming particles to be nonporous spheres having a diameter equal to the average mesh size opening.

2. Implications of Porosity in Small Pores to Adsorption

The oolitic limestone exhibits a porosity of about 0.25% due to pores with diameters smaller than 20 μm. In comparison with this porosity, porosities of about 19% were measured by tritium infiltration, suggesting that most of the porosity consists of large voids between oolites.

Neither of the basalts tested has appreciable porosity (less than 0.1%) from pores smaller than 20 μm that intersect the particle surface. Even so, as demonstrated for the various mesh sizes of Columbia River basalt, the pore surface area may greatly exceed the fracture surface area. Therefore, adsorption may occur predominantly on pore surfaces rather than on the fracture surfaces of these rocks. This means that the attainment of equilibrium in batch adsorption experiments could be limited by the rate of diffusion of nuclides along the lengths of the pores. The rate of diffusion of a nuclide along the length of a pore is a multistep process that includes adsorption, desorption, and random motion of the nuclide within the fluid.

Because the extent of adsorption is dependent on surface area, adsorption experiments described previously [SEITZ-1978] that use different mesh sized materials to estimate the extent of penetration of adsorbed nuclides into rock particles may be more sensitive indicators of rock porosity than the porosimeter experiments.

C. Radiation and Concentration Dependence of Strontium Adsorption by Limestone

Batch partitioning experiments were performed with strontium and oolitic limestone, using synthetic groundwater solutions containing four different concentrations of strontium. Fractions of the four solutions were irradiated in the radiation field of a ^{60}Co source before the batch tests to determine whether radiolysis affects the subsequent adsorption of strontium onto the limestone.

1. Experimental Procedures

a. Synthetic Groundwater Solution

A synthetic groundwater used in the experiments was prepared using reagent grade chemicals mixed with distilled water [RELYEA]. The solution contained, per liter of distilled water, 92.3 mg $Ca(OH)_2$, 18.1 mg $MgSO_4$, 7.6 mg NaCl, and 0.9 mg KCl. After two weeks of mixing, the solution was filtered through a 0.45-μm-pore-size pleated-membrane filter (producing no visible particulate). Strontium was added to aliquots of the groundwater solution in quantities to produce solutions containing 1.03×10^{-6}, 0.91×10^{-7}, and 0.9×10^{-8} M strontium. These solutions, together with the original groundwater solution (with no added strontium), were used to wash the oolitic limestone and after the addition of radioactive ^{90}Sr were used in the batch experiments.

The range of strontium concentrations was chosen to be as wide as possible without causing precipitation of a strontium compound. Strontium carbonate has a solubility product of 1.6×10^{-9} M at 25°C. With a bicarbonate concentration in the solution of about 2×10^{-3} M [SEITZ-1979] and an assumed equal concentration of carbonate ion, the solubility limit for Sr^{2+} is about 1×10^{-6} M, and so solutions at or below this concentration were used in the experiments.

b. Rock Material

Oolitic limestone, of 20- to 50-mesh size aggregate, was wet-sieved on a 60-mesh screen and was dried for use in the experiments. The material is described by [AMES].

c. Rock Material Washing Procedure

In each batch experiment, 3.0 g of limestone was placed in a 15-mL polystyrene centrifuge tube and was washed three times with aliquots of one of the four groundwater solutions containing differing concentrations of strontium (but containing no radioactive ^{90}Sr). Each wash used 10 mL of solution in the capped centrifuge tube. To promote the reaction of the solution with the rock material, the tubes were rotated end-over-end at six revolutions/min for one continuous hour out of every six hours. Each wash was continued for about four days, after which the limestone was allowed to settle, and the wash solution was decanted. The centrifuge tubes containing limestone were weighed before and after washing to determine the weight of wash solution remaining with the limestone.

d. Addition of Radioactive Strontium

A trace quantity of radioactive ^{90}Sr was added to each of the four solutions containing different concentrations of strontium. The four solutions were each halved and were placed in borosilicate Erlenmeyer flasks. One set of these solutions was irradiated in a ^{60}Co gamma field of 7.5×10^5 rad/h for 100 h. The radiation field was measured by the change of absorbance

of cobalt glass dosimeters at a light wavelength of 450 nm. Irradiated solutions were used in experiments 72 h after irradiation was terminated. The concentrations of strontium in the solutions and the activities of the solutions (counted with 0.5- and 1.0-mL aliquots of solution in 15 mL of scintillation liquid) are given in Table 31 and show the range of strontium concentrations explored in the experiments.

Table 31. Strontium Concentrations and Activities of Solutions Used in the Batch Adsorption Experiments

Solution	Added Strontium Concentration, M	Solution Irradiated	Solution Activity, c/m-mL	
			1.0-mL Aliquot Counted	0.5-mL Aliquot Counted
1	1.03×10^{-6}	No	199020	195680
2	0.91×10^{-7}	No	203990	185890
3	0.90×10^{-8}	No	196400	202310
4[a]	1.0×10^{-11}	No	199920	205120
5	1.03×10^{-6}	Yes	197740	208030
6	0.91×10^{-7}	Yes	197730	204830
7	0.90×10^{-8}	Yes	198170	203070
8[a]	1.0×10^{-11}	Yes	198170	210490

[a]The concentration of strontium in this solution is that added as radiotracer ^{90}Sr containing 38% stable ^{88}Sr.

e. Batch Experiments--Procedure and Results

Triplicate batch experiments were run with each solution by adding 10 mL of an irradiated or a nonirradiated solution to the appropriately washed limestone. Blank tests to evaluate strontium adsorption on the test tube walls were performed by placing the solutions in centrifuge tubes containing no limestone.

The test tubes were rotated (the same as in washing). Four tubes with solutions having different strontium concentrations were removed from the rotator after 7 days, four after 14 days, and four after 21 days. The solutions were filtered through 0.4-μm-pore membrane filters and counted by scintillation detection after 3, 10, and 17 days after filtering (to establish decay equilibrium between ^{90}Sr and ^{90}Y).

Results of the batch experiments, listed in Table 32, indicate that strontium adsorption is not sensitive to strontium concentration in the concentration range explored nor is it sensitive to irradiation of the solutions by gamma rays at the conditions used to expose the solutions.

D. Relationship of Experimental Radiation Dose to the Possible Dose in a Waste Repository

The batch partitioning experiments were used, in part, to explore the possibility that radiolysis or the concentration of strontium may affect the adsorption of strontium by limestone. The radiation dose of 7.5×10^7 rads to which the solutions were subjected is comparable to doses to which groundwater around a waste repository may be subjected. Groundwater traveling through a breached waste cylinder (having an inside diameter of 15 cm, a length of 244 cm, and steel wall thickness of 0.6 cm and containing 10-y-aged waste initially generating 5000 W) and through the surrounding rock will be subject to a radiation dose of 7.5×10^7 rads if the groundwater moves at a velocity of 12 m/y (The dose, averaged for the initial 10 y of burial, was calculated from the data of [BLOMEKE, Fig. 2]. At greater flow rates, the dose will be lower. Because no effects of radiation were seen in the work reported above, it is likely that the irradiation of the groundwater in a repository by the radioactive waste will not affect subsequent adsorption of strontium from the groundwater by limestone.

E. Batch Partitioning Experiments--Conclusions

From the results of the batch partitioning experiments, we have seen that the adsorption of strontium by limestone, as measured by a partition coefficient, is not dependent on prior irradiation of groundwater solutions or on the concentration of strontium in the groundwater. This behavior may considerably simplify a detailed treatment of strontium migration from a repository allowing effects due to radiation and strontium concentration to be ignored in an accurate treatment of strontium migration.

F. Cesium Migration in Granulated Basalt--Column-Infiltration Experiments

In an experiment, dissolved cesium-137 was injected into a synthetic groundwater solution stream that was passed through a column of granulated basalt. The groundwater solution was formulated to represent groundwater in basalt and is described by [RELYEA]. Concentrations of cesium of 10^{-4} to 10^{-8}M were added to different aliquots of the solution. Each eluate from the column was sampled and was analyzed for cesium-137.

A series of six experiments were performed. The curves of activities in the eluates for the six experiments, using groundwater solutions with six different concentrations of cesium, are illustrated in Figs. 27-32.

Table 32. Results of Batch Partitioning Experiments for Strontium Adsorption on Oolitic Limestone

Strontium Concentration in Solution, M	Batch Experiment Number	Solution Irradiated	Volume of ^{90}Sr-Bearing Solution, mL	Volume of Residual Wash Solution, mL	Activity of Filtrate,[a] c/m·mL	Measured Partition Coefficient, mL/g
First Series (Contact for 7 days)						
1.0×10^{-11}	1	No	9.96	1.20	77740	4.8
0.90×10^{-8}	2	No	9.99	1.19	62440	6.7
0.91×10^{-7}	3	No	10.04	1.21	88870	3.9
1.03×10^{-6}	4	No	9.96	1.19	80520	4.4
1.0×10^{-11}	9	Yes	10.05	1.19	74430	5.2
0.90×10^{-8}	10	Yes	10.00	1.22	79510	4.6
0.91×10^{-7}	11	Yes	9.98	1.25	82550	4.2
1.03×10^{-6}	12	Yes	10.02	1.22	83470	4.2
Second Series (Contact for 14 days)						
1.0×10^{-11}	5	No	10.02	1.18	62380	7.0
0.90×10^{-8}	6	No	10.00	1.21	51650	8.9
0.91×10^{-7}	7	No	10.01	1.23	71960	5.7
1.03×10^{-6}	8	No	10.01	1.28	64420	6.5
1.0×10^{-11}	13	Yes	10.06	1.19	58100	7.7
0.90×10^{-8}	14	Yes	10.00	1.19	64660	6.5
0.91×10^{-7}	15	Yes	9.98	1.21	71010	5.5
1.03×10^{-6}	16	Yes	9.98	1.16	64360	6.5
Third Series (Contact for 21 days)						
1.0×10^{-11}	17	No	10.04	1.21	59940	7.4
0.90×10^{-8}	18	No	9.99	1.19	55160	8.1
0.91×10^{-7}	19	No	9.98	1.19	67360	6.4
1.03×10^{-6}	20	No	9.98	1.20	65130	6.4

(contd)

Table 32. (contd)

Strontium Concentration in Solution, M	Batch Experiment Number	Solution Irradiated	Volume of ^{90}Sr-Bearing Solution, mL	Volume of Residual Wash Solution, mL	Activity of Filtrate,[a] c/m·mL	Measured Partition Coefficient, mL/g
1.0×10^{-11}	29	Yes	10.00	1.19	65020	6.4
0.90×10^{-8}	30	Yes	9.99	1.23	71480	5.5
0.91×10^{-7}	31	Yes	10.00	1.19	71340	5.5
1.03×10^{-6}	32	Yes	9.99	1.29	71810	5.4
Fourth Series, Blank Tests[b] (Contact for 21 days)						
1.0×10^{-11}	21	No	10.03	0.0	195520	--
0.90×10^{-8}	22	No	10.04	0.0	184360	--
0.91×10^{-7}	23	No	9.98	0.0	199080	--
1.03×10^{-6}	24	No	10.00	0.0	189820	--
1.0×10^{-11}	25	Yes	10.01	0.0	193200	--
0.90×10^{-8}	26	Yes	10.01	0.0	194450	--
0.91×10^{-7}	27	Yes	9.99	0.0	197100	--
1.03×10^{-6}	28	Yes	10.00	0.0	196170	--

[a] Solutions were filtered through 0.4-μm-pore membrane filters. Solutions in Series 1 were counted in vials containing 1 mL of solution and 15 mL of scintillation liquid. Solutions in Series 2, 3, and 4 were counted in vials containing 0.5 mL of solution and 15 mL of scintillation liquid.

[b] No limestone present.

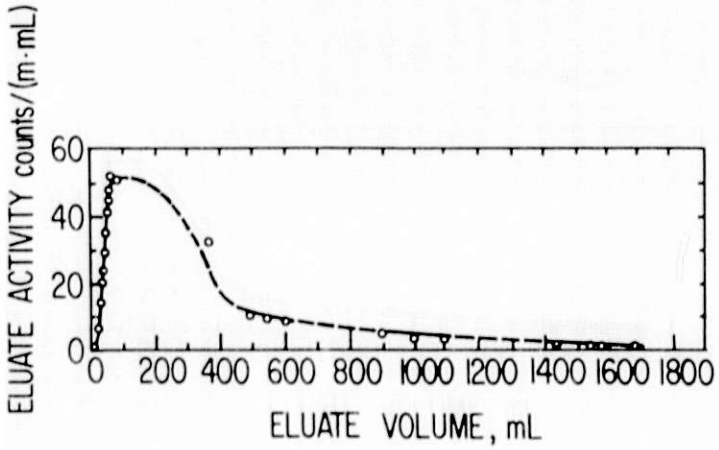

Fig. 27. Elution of ^{137}Cs (0.1 μCi) through a Column of Granulated Basalt. The solution contained 1×10^{-4} M Cs and flowed at a velocity of 4.9 km/y. Experiment 148-126

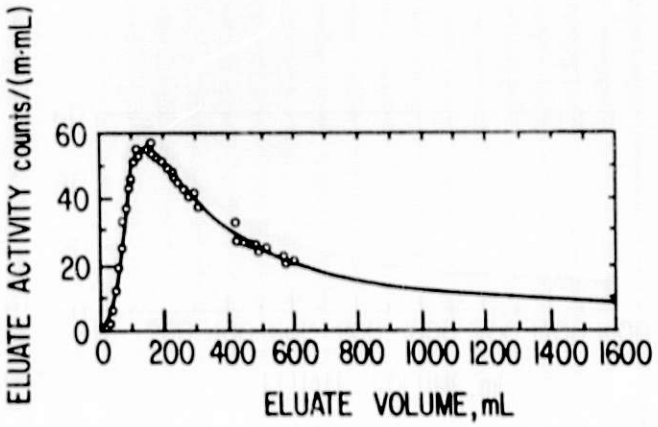

Fig. 28. Elution of ^{137}Cs (0.2 μCi) through a Column of Granulated Basalt. The solution contained 1×10^{-5} M Cs and flowed at a velocity of 5.0 km/y. Experiment 148-133

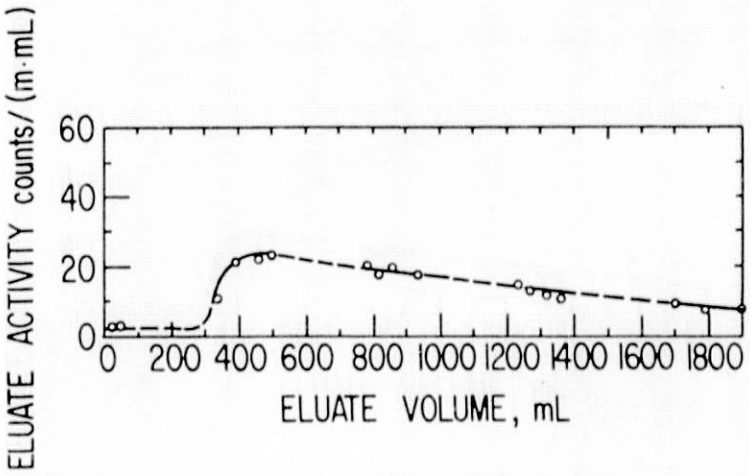

Fig. 29. Elution of ^{137}Cs (0.2 μCi) through a Column of Granulated Basalt. The solution contained 1×10^{-6} M Cs and flowed at a velocity of 5.3 km/y. Experiment 148-138

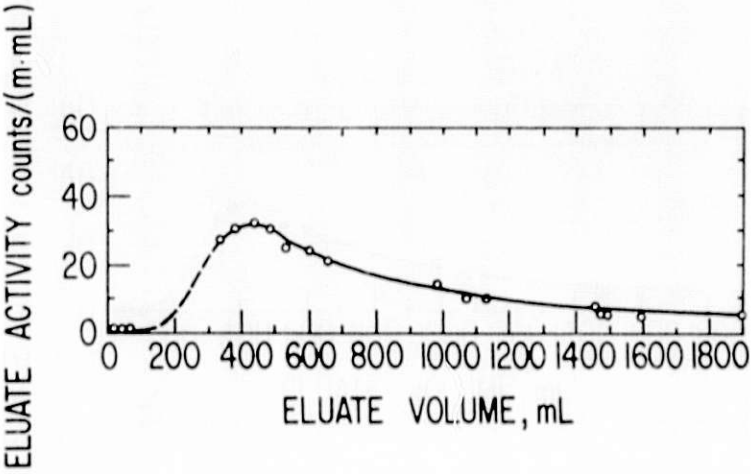

Fig. 30. Elution of ^{137}Cs (0.2 μCi) through a Column of Granulated Basalt. The solution contained 1×10^{-7} M added Cs and flowed at a velocity of 5.0 km/y. Experiment 148-141

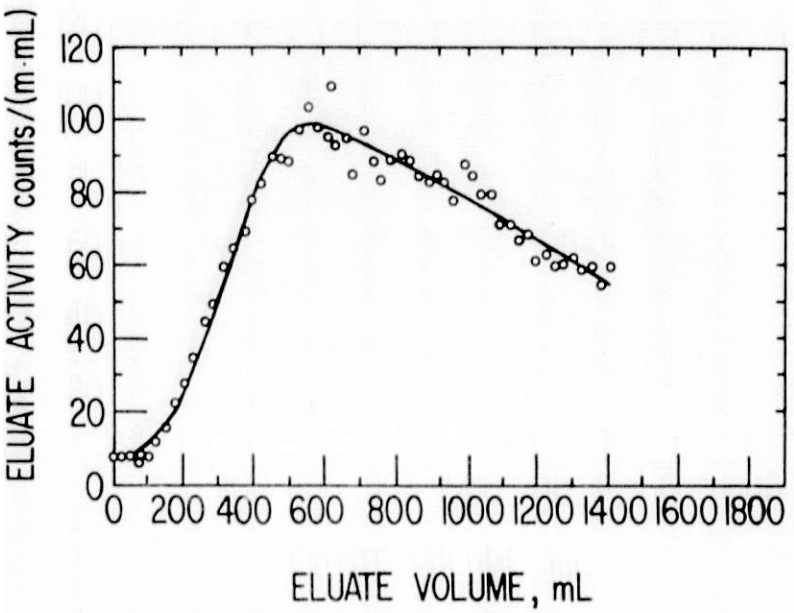

Fig. 31. Elution of ^{137}Cs (1.0 µCi) through a Column of Granulated Basalt. The solution contained 1×10^{-8} M added Cs and flowed at a velocity of 5.2 km/y. Experiment 148-147

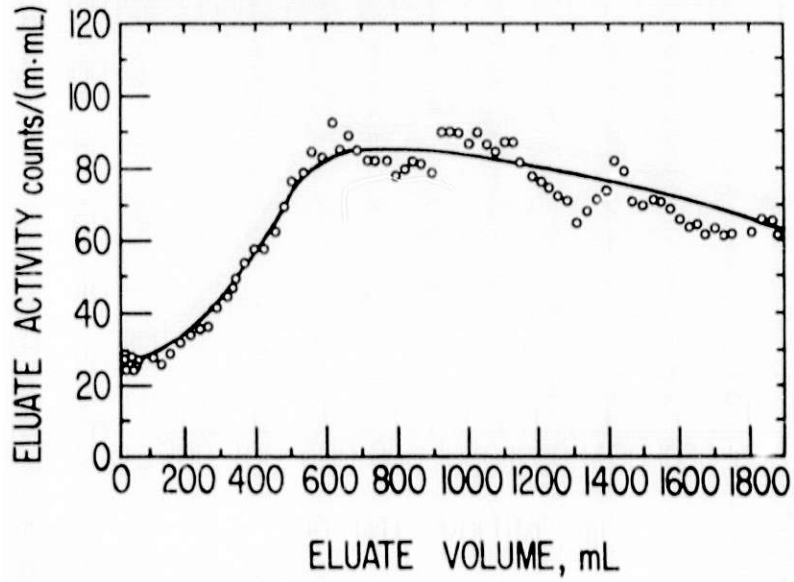

Fig. 32. Elution of ^{137}Cs (1.0 µCi) through a Column of Granulated Basalt. The solution contained only the radioactive cesium spike and flowed at a velocity of 5.2 km/y. Experiment 164-2. No CsCl added

G. Discussion of the Results of the Cesium Migration Experiments

The results of the infiltration experiments indicate that cesium migrates more slowly through basalt in solutions containing lower concentrations of cesium. This is probably a saturation effect caused by a significant loading of cesium adsorption sites by solutions containing concentrations of 1×10^{-4} M cesium and less. This behavior parallels the behavior seen for cesium adsorption on basalt in batch experiments [RICKERT], in which partition coefficients were seen to increase with decreasing cesium concentrations (and hence cesium would be predicted to move more slowly through basalt in solutions containing lower concentrations of cesium).

H. Future Direction

The infiltration experiments with cesium and basalt columns will be continued in order to compare observed migration with that predicted from the results of batch experiments (reported in RICKERT).

A rock column holder which uses a pressurized jacket to confine a 6.8-cm-diameter by 15-cm-long rock core for infiltration has been designed and built. Tests are being performed on the holder, which is part of the apparatus being assembled for leach-migration experiments.

IV. TRACE-ELEMENT TRANSPORT IN LITHIC MATERIAL BY FLUID FLOW AT HIGH TEMPERATURE

(M. G. Seitz and R. A. Couture)

A. Introduction

In the proceding quarterly report [STEINDLER-1979C], the isotherm for adsorption of iodate by hematite was reported at three pH values. Adsorption of iodate was found to depend on iodate concentration in the range, 10^{-6} to 10^{-2}M, and to increase with decreasing pH. This quarter, an attempt was made to fit these data to a mathematical model.

[HINGSTON] found that the adsorption of selenite by geothite (FeOOH) follows a Langmuir isotherm, which assumes an ideal solid solution; [WHITEHEAD] found that the sorption of iodide by soils approximately follows a Langmuir isotherm; and [NEAL] found that sorption of iodate by ferric hydroxide follows the empirical Freundlich isotherm. Thus, it seemed reasonable and desirable to attempt to fit the data to these models.

B. The Langmuir Isotherm

If C_A = amount of species A adsorbed or exchanged, C = exchange capacity, [A] = concentration of sorbate, and K = a constant, and if the competing ion concentration is held constant and ideal solid solution is assumed, one can derive one form of the Langmuir equation:

$$C_A = \frac{C[A]}{K + [A]}$$

This can be rewritten as

$$\frac{[A]}{C_A} = \frac{[A]}{C} + \frac{K}{C}$$

A plot of $\frac{[A]}{C_A}$ against [A] should give a straight line if the data follow a Langmuir isotherm. However, this is not the case for our data on the adsorption of iodate by iron oxide, and so the Langmuir isotherm clearly does not apply.

C. Regular Solution Model

Many solid solutions approximate the behavior of regular solutions, which are one step more complicated than ideal solutions. According to regular solution theory, the activity coefficients of components A and B in a two-component system are given by

$$\lambda_A = \exp\ (D\ X_B^2)$$

$$\lambda_B = \exp\ (D\ X_A^2),$$

where D is a constant, and X_A and X_B are mole fractions. The equilibrium condition is given by

$$\frac{\lambda_A\ X_A}{\lambda_B\ X_B} = K\ \frac{[A]}{[B]},$$

where [A] and [B] are activities in solution. From these equations, it follows that

$$\ln\ [A] = \ln\ K[B] + \ln\ \frac{X_A}{X_B} - D(X_A - X_B).$$

This can be transformed into a function of the exchange or sorption capacity $C = C_A + C_B$, and the concentration of A (i.e., C_A). The result is

$$\ln\ [A] = \ln\ K[B] + \ln\ \frac{C_A}{C - C_A} + D\left(\frac{C - 2C_A}{C}\right),$$

which can be rewritten as

$$\ln\ [A] - \ln\ \frac{C - C_A}{C_A} = D\left(\frac{C - 2C_A}{C}\right) + \ln\ K[B]. \qquad (1)$$

This is a linear function of the variables, $\ln\ [A] - \ln\ \frac{C - C_A}{C_A}$ and $\frac{C - 2C_A}{C}$.

Values of D and ln K[B] were determined by choosing a value of C, and doing a linear least squares fit to determine the values of D and ln K[B] in Eq. 1. The value of C was adjusted by iteration to minimize the function, $\sum \left(\ln \frac{[A]_{obs}}{[A]_{calc}}\right)^2$, which is a measure of the closeness of fit. A fit was also attempted by minimizing the function $\sum \left(\frac{[A]_{obs}}{[A]_{calc}}\right)^2$, but this did not improve the fit.

The fit obtained at pH 5.77 is shown in Fig. 33. Unfortunately, no completely satisfactory fit was obtained for any value of C. Values of C up to an unreasonably high value of 10 mmol/g were tried. The fit obtained is virtually independent of values of C from 200 μmol/g to 3000 μmol/g. Thus,

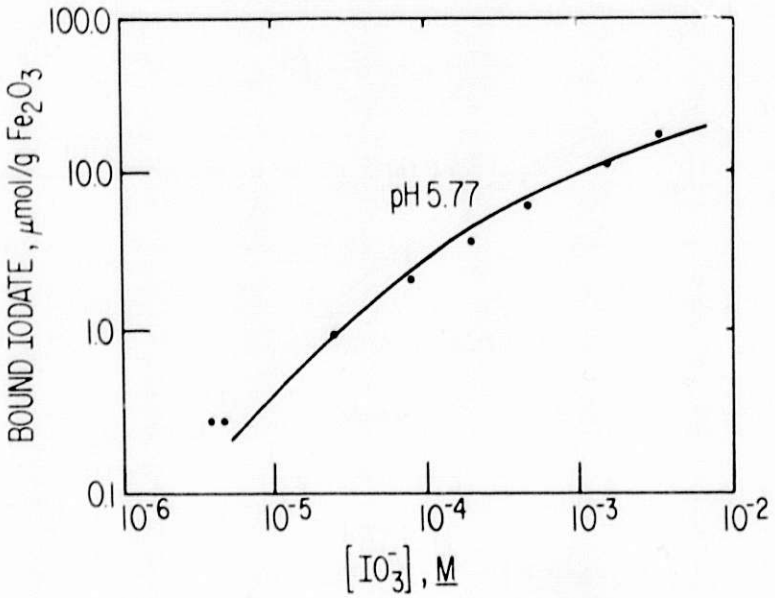

Fig. 33. Adsorption of Iodate by Hematite--Experimental Data Compared with Regular Solution Model

the data do not appear to correspond well enough to the model of a regular solution for the model to have much predictive value. An ideal solution, with the resulting Langmuir isotherm, is a special case of regular solution, and so an ideal solution model would give a worse fit.

D. Discussion

The calculations suggest to the author that the sorption capacity of hematite for iodate may be higher than previously suspected--hundreds of μmol/g rather than tens of μmol/g.

[NEAL]'s data on sorption of iodate by ferric hydroxide in 0.27M NaCl was observed to fit the equation

$$C_B = 0.7[I]^{2.16}$$

at iodine concentrations less than 0.31μM. C_B is given in μg I/g sorbent, and [I] is in μg I/L. The parabolic curve shape is odd. Inasmuch as [NEAL] did not publish his data and since [NEAL]'s curve contrasts markedly with our results (which seem more reasonable), [NEAL] might have arrived at an erroneous formula that does not describe his data.

APPENDIX

SCOPE OF WORK FOR HOT CELL EXPERIMENTS

(S. P. Sontag*)

*Rockwell International, Rocky Flats

A. Introduction

This R&D task pertains to the construction and operation of experimental equipment in a hot cell. Verification of transplutonium and fission product behavior during Salt Transport Fuel Reprocessing steps will be obtained.

The R&D effort will include acquisition of suitable irradiated fuel, construction of the laboratory equipment and its subsequent installation in the hot cell, direct and remote operation of the equipment through all phases of the salt transport process, detection of individual elements in each chemical phase produced by the salt transport process, and ultimate disposal of the equipment and process waste.

It is extremely important to determine the partitioning of the fission products and transplutonium elements between the salt and metal phases. Accurate analyses of many samples are required. Experience is also needed in remote operation of the high-temperature equipment.

The entire effort will necessitate thorough and accurate record keeping. Records will include drawings of all equipment, detailed experimental procedures, all analytical results, photographs when possible, and descriptions of all equipment and procedure fixes.

B. Salt Transport Process Outline

What follows is only a basic outline of the experimental work to be performed in the hot cell. The precise operating temperatures, contacting time periods, and number of extraction cycles will be based on the results of ongoing laboratory work at Rock Flats. A complete description of the salt transport process is given in [STEINDLER-1979B]. The values listed are as exact as the theoretical calculations and basic experimental data allow. Tables A-1 and A-2 list the initial salt/alloy compositions and the weight ratios of metal to salt used in steps of the process.

The fission product elements in each of four groups are classified in Table A-3. Elements with a group behave similarly during fuel reprocessing.

I. Fuel Preparation

a. Mechanically remove any excess stainless steel hardware from the bottom of the fuel pin(s), but don't pierce the annular gas space.

b. Load the fuel pin(s) into an air lock fixture.

c. Place the correct amount of zinc and cover salt in the process crucible.

d. Seal the fixture to the crucible/furnace shroud.

e. Fill the interiors of both the air lock fixture and the shroud with inert gas.

Table A-1. Initial Salt and Alloy Compositions

Operation	Alloy Composition	wt %	mol %	Salt Composition	wt %	mol %
Decladding	Zn	100	100	$CaCl_2$	80.9	74.0
				KCl	19.1	26.0
Reduction	Cu	88.0	80.6	$CaCl_2$	80.2	74.0
	Mg	2.1	5.0	CaF_2	18.8	24.6
	Ca	9.9	14.3	KCl	1.0	1.4
FP-3 Donor	Complex, fixed by reactions during reduction			$MgCl_2$	6.4	6.8
				$CaCl_2$	75.8	69.1
				KCl	17.8	24.1
FP-3 Acceptor	Zn	88.0	73.2	$MgCl_2$	6.4	6.8
	Mg	12.0	26.8	$CaCl_2$	75.8	69.1
				KCl	17.8	24.1
U-Pu Donor	Complex, changed by FP-3 transport			$MgCl_2$	84.4	78.0
				MgF_2	15.6	22.0
U-Pu Acceptor	Zn	88.0	73.2	$MgCl_2$	84.4	78.0
	Mg	12.0	26.8	MgF_2	15.6	22.0
U Donor	Complex, changed by U-Pu transport			$MgCl_2$	84.4	78.0
				MgF_2	15.6	22.0
U Acceptor	Zn	88.0	73.2	$MgCl_2$	84.4	78.0
	Mg	12.0	26.8	MgF_2	15.6	22.0

Table A-2. Weight Ratios in Salt Transport

Type of Ratio	Weight Ratio[a]
Decladding zinc: SS cladding	4.00
Reduction alloy: oxide fuel[b]	3.52
FP-3 donor alloy: total alloy	0.10
FP-3 transport salt: FP-3 donor alloy	1.00
U-Pu transport salt: U-Pu donor alloy	1.42
U-Pu transport salt: U-Pu acceptor alloy	3.42
U-transport salt: U donor alloy	0.84
U transport salt: U acceptor alloy	0.79

[a]Weights are for alloy/salts prior to a step.

[b]"Oxide fuel" includes UO_2, PuO_2, fission products, and the oxygen combined with the fission products.

Table A-3. Fission Product Groups

Group	Type	Elements
FP-1	Gases	^3H (tritium), Xe, Kr
FP-2	Alkali & alkaline earth metals + chalcogens and halogens	Rb, Sr, Cs, Ba, O, Se, Te, Sm, Eu, Br, I
FP-3	Rare earths	Y, La, Ce, Pr, Nd, Pm, Gd, Tb
FP-4	Noble and refractory metals	Zr, Nb, Mo, Tc, Ru, Rh, Pd, Ag, Cd, In, Sn, Sb

II. Decladding

a. Heat the zinc and cover salt to the operating temperature of 800°C.

b. Lower the fuel pin(s) slowly into the molten zinc until the stainless steel cladding dissolves. This releases most of the FP-1 group elements and leaves the fuel pellets in the bottom of the process crucible.

The upper atmosphere in the furnace now contains inert gas contaminated with FP-1, which is now ready for off-gas treatment. (See VIII. Facility Requirements, Part C.)

Some volatile fission products are also released from the fuel pellets but either react with the molten zinc, i.e., iodine forms ZnI_2, or displace an anion in the cover salt, i.e., cesium displaces potassium in the KCl to form CsCl.

c. Tilt the crucible and decant the zinc-stainless steel solution and the cover salt into a mold. Allow the furnace to cool, and then remove the air lock fixture.

d. Weigh the zinc-stainless steel-salt mass after cooling to determine transfer efficiency. Observe and note the condition of the fuel pellets.

e. Separate the salt from the metal. Sample and analyze both the salt and the metal.

f. Save the salt for use during reduction, and save the metal for recovery of the zinc by distillation.

III. Reduction

a. Add the recovered decladding cover salt, the copper-magnesium reduction alloy, the metallic calcium, and the new cover salt to the crucible containing the MOX pellets. Seal the furnace with a top equipped with a stirrer motor and stirring shaft. Provide an inert furnace atmosphere.

b. Bring the temperature of the crucible and contents to 800°C.

c. The calcium reduces the uranium, plutonium, and fission product oxides, forming CaO; the uranium, plutonium, FP-3 elements, and FP-4 elements then dissolve in the donor alloy.

Either by exchange reactions or inertness to the reducing agent, the FP-2 elements should now be in the salt phase.

d. Stirring during reduction is necessary, but to prevent the stirring rod from jamming on contact with the pellets, it must be lowered incrementally.

e. After reduction is complete (approximately 30 min), pour the donor alloy and salt into a mold and allow them to cool.

f. Separate the metal from the salt. Save the salt for reuse. Analyze and weigh both phases.

IV. FP-3 Transport

a. Cut off 10 wt % of the cleaned metal ingot. Swing aside the "stirrer" top of the furnace. Place the cleaned metal and the FP-3 transport slat in a process crucible. Reseal the furnace.

b. Fill the furnace shroud with inert gas, and bring the furnace temperature to 800°C.

c. Stir the two phases for approximately 30 min. This mixing would allow the FP-3 elements to oxidize into the salt phase.

d. Cease stirring to allow phase disengagement.

e. Pour the crucible contents into a mold.

f. When cool, completely separate the phases and analyze both phases for FP-3 removal efficiency.

g. Return the FP-3-depleted alloy to the remaining donor alloy.

V. Uranium-Plutonium Transport

a. Place the U-Pu donor alloy and the U-Pu transport salt in the process crucible, and place the U-Pu acceptor alloy in the neighboring process crucible.

b. Fill the furnace shroud with inert gas.

c. Bring both crucibles to their operating temperatures--850°C for the donor alloy and 700°C for the acceptor alloy.

d. Stir the U-Pu donor alloy with the transport salt for the time interval specified.

e. Cease stirring, and allow phase disengagement.

f. Sample the salt and the donor alloy. Transfer the transport salt (now containing U and Pu) into the acceptor alloy crucible by decanting.

g. Stir the acceptor alloy and the transport salt for the time interval specified.

h. Cease stirring, and allow phase disengagement. Sample both the salt and the acceptor alloy.

i. Return the transport salt (now actinide-exhausted) to the donor alloy crucible.

j. Continue repeating V.d. to V.i. for enough cycles to remove 99% of the plutonium from the donor alloy. (Computer simulations show that five cycles should be sufficient.)

k. At the end of this step, the transport salt is on top of the plutonium donor alloy.

l. Pour (1) the donor alloy plus transport salt and (2) the acceptor alloy into separate molds. After the U-Pu acceptor alloy cools, store it for later distillation. Separate the donor alloy from the transport salt.

VI. Uranium Transport

a. Place the uranium acceptor alloy in one empty process crucible, and the uranium donor alloy and transport salt in the neighboring crucible. Seal the furnace shroud and fill with inert gas.

b. Bring the two crucibles to operating temperatures--850°C for the uranium donor alloy and 700°C for the uranium acceptor alloy.

c. Perform the uranium salt transport by following the same steps as for uranium-plutonium transport given in V.d. to V.i.

d. Continue repeating V.d. to V.i. for a sufficient number of cycles to remove 99% of the uranium from the donor alloy. (Computer simulations show that twelve passes should be sufficient.)

e. End cycling with the transport salt on top of the uranium-exhausted donor alloy.

f. Pour the donor alloy and salt into one mold and the uranium acceptor alloy into another mold. Allow the furnaces to cool.

g. Sample and analyze both of the alloys and the salt.

VII. Distillation

a. Place a charge of volatile plus nonvolatile metals (i.e., zinc from decladding or U-Pu acceptor alloy) in the still. The zinc will distill, separating it from the stainless steel, or the zinc-magnesium will distill from the U-Pu alloy.

b. Seal the still for operation. Provide an inert still atmosphere.

c. Obtain a still vacuum of approximately 1 mm Hg, and start heating slowly. Heating is slow to prevent violent bumping of the alloy.

d. Control the still pot temperature to prevent overloading of the condenser. Maintain the vacuum at the set value.

e. Continue distillation at higher and higher temperatures until the maximum recommended temperature, 1000°C, is reached.

f. After distillation is complete, cool the still while maintaining the vacuum.

g. Weigh and analyze both the distillate and the still bottoms.

VIII. Facility Requirements

a. Fuel Acquisition and Licensing

The required irradiated fuel will be mixed oxide with an initial plutonium content of approximately 20%. It will be stainless steel clad and have between 5 and 10% core burnup. A short-cooled fuel is preferred. Since only a small amount of encapsulated fuel, 500 ± 100 g, is required for a single experiment, the proposed fuel source is a single, short-length fuel assembly which has been separated into individual fuel pins. The fuel assembly could be dismantled at another hot cell. Experimental irradiated fuel assemblies meeting the above requirements, including the 500 g actinide limit, could also be used.

License type depends on the total quantity of MOX fuel to be handled and the location of the hot cell facility. Many states have more severe licensing requirements than NRC (Nuclear Regulatory Commission). Approximately one year lead time is needed for licensing.

NRC requires that an alpha box be used inside a conventional hot cell to handle plutonium. A hot cell could be modified to meet plutonium regulations--primarily by installing four-stage HEPA filtration and triple containment. If more than 2.5 kg of plutonium or enriched uranium will be used, special security measures such as full-time guards, fences, controlled access points, etc. will be required [McCURNIN].

b. Fuel Handling

Fuel handling requirements will be complex due to the nature of the fuel and the process. The high burnup means that the hot cell curie limit must be large. The short cooling time necessitates cooling capabilities for both the cask and fuel pin(s) at the subcontractor facility. Shipping cask handling and unloading capabilities are required. The hot cell must have interior dimensions and weight-handling capabilities great enough to allow manipulation of the fuel pin(s). Clearances must be great enough that the fuel pin(s) can be inserted vertically downward into the process furnace. The gas inside the fuel pin(s) must not be released prior to the decladding operation.

c. Process Equipment Construction

The major equipment required will be a two-crucible, dual-axis, tilt-pour furnace with separate temperature controls for each crucible, a two-stirrer motor top for the tilt-pour, a distillation furnace with crucible and condenser, an air lock fixture for use during decladding of the fuel pins, and an alpha box system (if the hot cell is not plutonium-approved).

Rocky Flats will supply the process crucibles and stirrers. The process crucibles will most likely be spun-form tungsten, 3 in. ID by 6 in. long. Stirrers will be sized to the crucible and most likely will be fabricated of tantalum.

Construction of the two-chamber, tilt-pour furnace system can probably be most easily accomplished by adapting a commercial unit for this application. An atmosphere box or furnace shroud to enclose the tilt-pour mechanism will be needed. Provisions must be made for molds inside the furnace shroud. Two different tops will be needed for the furnace shroud. One will consist of an air lock capable of (1) holding the correct number of fuel pins, (2) maintaining an inert-atmosphere seal during experimentation, and (3) slowly lowering the fuel pins into a process crucible during decladding. The other top will incorporate two stirring motors and shafts; one of the shafts will be capable of being raised and lowered to avoid jamming on fuel pellets during reduction. Thermal baffles and off-gas lines will also be needed in the system.

The distillation furnace will consist of a vacuum furnace capable of reaching 1000°C, a still pot, metal vapor tubing, and a condenser. A commercial vacuum furnace could be adapted for this use. For the still pot, the suggested material is silicon carbide-coated graphite, and tantalum is suggested for the tubing and condenser.

The alpha box or hot cell off-gas system must be capable of handling the FP-1 elements and any volatiles. The FP-1 elements will be contained within the furnace shroud after decladding and can be handled (1) by compression and storage or (2) by controlled discharge through the vent system. Either the NRC's or state's regulations on allowable radioactive emission levels must be followed, whichever are stricter. A condenser for volatile species such as cesium should be an integral part of the system. The salt transport process is designed to minimize the release of volatiles but should be coupled with baffled condenser plates inside the furnace shroud to lessen the condenser burden. Sampling access to the off-gas stream at two or more points will be necessary.

All equipment must be designed to allow proper operation and repair remotely with the existing manipulators and/or cranes.

d. Process Equipment Installation

To ensure maximum value from hot cell operation, all equipment should first be set up and operated using "cold" material. A hot cell mockup area in which the equipment could be operated would be ideal for checking the feasibility of remote operation.

Modularization of the equpment would be helpful in the installation of units in the hot cell. It also promotes compact designs, which will be necessary if an alpha box is used.

e. Process Operation

Many utilities are required during process operation. An inert gas such as helium or argon will be necessary as the atmosphere in the furnace shrouds. (Nitrogen is a totally unacceptable gas due to nitride formation.) Many instrument feed-throughs in the hot cell walls will be needed for oxygen analyzer probes, pressure transducers, and thermocouples. Recorders for all of these are also needed. A refrigeration unit with a fairly high capacity will be required for cooling the alpha box or hot cell. The tilt-pour furnace will require two or more 220-V lines, several 110-V lines, a cooling system if induction heating is used, and an off-gas line under negative pressure. The distillation system will require one 220-V line, a vacuum system, and a condenser cooling unit.

Operation of the remoted equipment with the hot cell's remote handling mechanisms must be possible. Trained personnel to support the facility, operate the equipment, and provide any necessary security will be required. Health physics and safety support must be present to meet NRC, OSHA, and DOT regulations.

Analytical laboratory requirements will be intricate and could probably be best met by the use of a dedicated laboratory. The large number of samples that will be obtained from every experiment will need to be analyzed for essentially all elements. The off-gas, condensates, cover and transport salts, donor and acceptor alloys, and still bottoms will all have to be assayed. Quick analyses (requiring approximately 15 min) will allow much faster optimization of the process and a better understanding of transport mechanisms. Gas chromatography should be the method used for analyzing the off-gases and process/cell atmospheres. Gamma ray and/or atmoic absorption spectroscopy should then be used for analyzing the salts and metals. Both gamma ray and atomic absorption spectroscopy would benefit from computer-assisted data processing. The analytical methods which will be used in the PDPM program at Rocky Flats are summarized in Section g below. Special analytical techniques may be needed to detect elements present in extremely low amounts.

Sample techniques using metal frit filters and pressure differential driving force are being used for both alloy and salt sampling at [ROCKY FLATS]. A similar technique will need to

be developed for hot cell/alpha box use. A method of making composite samples from large specimens will also need to be developed.

All material fed into the process will be accurately weighed and analyzed. The amounts charged initially must compensate for the quantities to be removed by sampling.

The hot cell facility must have the capability of processing and disposing of all wastes generated during the experiments.

f. Equipment Storage and Disposal

Storage space for process equipment may be needed while waiting for fuel receipt, between operating campaigns, while waiting for funding for program expansion, or while dismantling after the initial program. Storage space will be needed for chemical supplies, spare equipment, and the irradiated fuel. Processing and packaging of equipment prior to its disposal will have to conform to NRC and DOT regulations.

g. Analytical Methods for Use in the Rocky Flats PDPM Program

Of four meetings to discuss analytical methods which would be suitable and/or available for use in the PDPM program, the first was on September 15, 1978, and the most recent one was on November 20, 1978. Analytical Laboratory personnel from the product support laboratory process waste laboratories, and the specifications laboratory attended.

The primary purpose of the meetings was to ascertain which analytical techniques have enough resolution to give accurate assays of the fission product concentrations expected in FBR fuel mixed with the alloys and salt used in the salt transport process. Three phases of experimentation were identified. In Phase I, stable isotopes of fission products will be used to determine if partitioning between molten alloys and molten salts occurs as expected. In Phase II (experimental studies beyond FY 1979), the possibility of using isotope tracers at Rocky Flats to augment Phase I will be investigated. Phase III will consist of reprocessing fuel pin(s) by salt transport in a hot cell facility at some site other than Rocky Flats. The recommendations for each phase are given below.

In an additional meeting of laboratory personnel, representative elements of each fission product group were selected. These representative elements were chosen because they have the lowest possible detection limits by the analytical methods available at Rocky Flats and are:

Group	Elements
FP-2	Cs, Ba, Te
FP-3	Y, Nd, Ce
FP-4	Mo, Cd, In, Sn

These representative elements will be used during Phase I. Detection limits and concentration levels needed for 5% accuracy by atomic adsorption are given for all fission product elements in Table A-4. Atomic absorption is agreed to be the most sensitive analytical technique.

Table A-4. Atomic Absorption Guidelines
(All concentrations given in wt %)

Group	Element	Element Concentration for 1% Absorption	Element Concentration for 5% Accuracy
FP-2	Cs	2×10^{-3}	1×10^{-1}
	Rb[a]	1×10^{-3}	5×10^{-2}
	Ba	4×10^{-3}	2×10^{-1}
	Sr	1×10^{-3}	5×10^{-2}
	Sm[b]		1×10^{-1}
	Se	5×10^{-3}	2×10^{-1}
	Te	5×10^{-3}	2×10^{-1}
	Eu[b]		2×10^{-1}
FP-3	Y	2×10^{-2}	1×10^{0}
	La[b]		3×10^{0}
	Pr[b]		3×10^{0}
	Nd[b]		4×10^{-1}
	Gd[b]		3×10^{-1}
	Tb[b]		2×10^{0}
FP-4	Zr	1×10^{-1}	4×10^{0}
	Nb	4×10^{-1}	1×10^{-1}
	Mo	5×10^{-3}	4×10^{-1}
	Tc[a]	3×10^{-2}	3×10^{-1}
	Ru[a]	5×10^{-3}	4×10^{-1}
	Rh[a]	3×10^{-3}	2×10^{-1}
	Pd	3×10^{-4}	1×10^{-1}
	Ag	6×10^{-4}	4×10^{-2}
	Cd	3×10^{-4}	2×10^{-2}
	In	7×10^{-3}	3×10^{-1}
	Sn	4×10^{-2}	2×10^{0}
	Sb	5×10^{-3}	2×10^{-1}

[a]Lamps would need to be purchased. A technetium lamp may be difficult to obtain. Rubidium may require an electrodeless discharge Lamp. Lamps cost approximately $200 each.

[b]Flame emission figures.

The proposed isotopic tracers for use during Phase II are listed in Table A-5. These isotopes were selected on the basis of nonmatching gamma ray emissions, half-life, and availability. The quantities used will be on the order of 1×10^{-9} g. Preliminary approval from HS&E is being sought for their use.

Table A-5. Proposed Isotopic Tracers

Group	Isotope	Half-Life	Comments
FP-2	Cesium-137	20.2 y	already on plant site
	Barium-135M	28 h	make from ^{134}Ba target
	Tellurium-123M	119.7 d	make from ^{122}Te target
FP-3	Yttrium-91	58.6 d	buy from ORNL
	Neodymium-147	11.0 d	make from ^{146}Nd target
	Cerium-141	32.5 d	make from natural Cerium target
FP-4	Molybdenum-99	66.0 h	buy from radiopharmaceutical company or make from 98 Mo
	Cadmium-115m	44.6 d	make from ^{114}Cd target
	Indium-114	49.5 d	make from ^{113}In target
	Tin-113	115.0 d	make from ^{112}Sn target, decays to usable ^{113m}In isotope tracer

Effort on Phase III has consisted of researching the analytical capabilities of various hot cell facilities. A complete list will be made when all data have been received. In general, most facilities are interested in the project but lack the analytical capabilities.

REFERENCES

Amecke

B. Amecke, Contributions to the Reprocessing of Thorium-Uranium Nuclear Fuels with the Salt Transport Method, Dissertation, Technical University of Carolo-Wilhelmina at Braunschweig; ANL-TRANS-1141 (1975).

Ames

L. L. Ames, Controlled Sample Program, Publication No. 1, Characterization of Rock Samples, PNL-2797 (1978).

Arenberg

C. A. Arenberg and P. Jahn, Steam Sintering of Uranium Dioxide, J. Am. Ceram. Soc. 41(5), 179 (1958).

Auge

R. G. Auge, Rocky Flats, private communication with T. D. Santa Cruz (May 1979).

Bailey

R. A. Bailey and G. J. Janz, Experimental Techniques in the Study of Fused Salts, The Chemistry of Non-Aqueous Solvents, Vol. I, J. J. Lagowski, Ed., Academic Press, New York (1966).

Bard

R. J. Bard, J. P. Bertino, and D. L. Bunker, Activating Uranium Dioxide, Ind. Eng. Chem. 53(12), 1003 (1961).

Barr

M. J. Barr, Activation of Some UO_2 Powders by Milling and Oxidation-Reduction, WHAN-FR-8 (1970).

Bates

J. K. Bates, L. J. Jardine, and M. Krumpelt, A Nonaqueous Reprocessing Method for Thorium Based Fuels, ACS/CSJ Chemical Congress, Actinide Separations Symposium, Honolulu (1979).

Bean

C. H. Bean, K. M. Myles, M. Krumpelt, S. Vogler, and M. J. Steindler, Zinc Distillation Process, Argonne National Laboratory Report ANL 79-79, Series I, Vol. 10 (in preparation).

Becker

C. R. Becker and T. S. Soine, Screening Test for Proposed Molten Salt Electrolytes, Hanford Atomic Products Operation, HW-77591 (May 10, 1963).

Belle

J. Belle and B. Lustman, Properties of Uranium Dioxide, WAPD-184 (1957).

Blomeke

J. O. Blomeke, E. Sonder, J. P. Nichols, S. Lindenbaum, R. S. Dillon, E. D. Arnold, and H. F. Soard, An Analysis of Energy Storage and its Effects in the Proposed National Radioactive Waste Repository, ORNL-TM-3403 (1971).

BPNL

Battelle Pacific Northwest Laboratory, Technology, Safety, and Cost of Decommissioning a Reference Nuclear Fuel Reprocessing Plant, NUREG-0278 (1977).

Brewer

L. Brewer, HP-67 Calculator Programs for Thermodynamic Data and Phase Diagram Calculations, LBL-5485 (May 25, 1978).

Brophy

J. H. Brophy, L. A. Shepard, and J. Wulff, Powder Metallurgy, W. Leszynski, Ed., Interscience, New York, p. 113 (1961).

Buttrey

K. Buttrey, O. R. Hillig, P. M. Magee, and E. H. Ottewitte, Liquid Metal Fast Breeder Reactor (LMFBR) Task Force Cycle Study, NAA-SR-MEMO-12604 (1968).

Christian

J. D. Christian, Process Behavior and Control of Ruthenium and Cerium in Controlling Airborne Effluents from a Fuel Cycle Plant, Proceedings of the ANS-AIChE Meeting Aug. 5-6, 1976.

Clayton

J. C. Clayton and S. Aronson, Some Preparative Methods and Physical Characteristics of Uranium Dioxide Powders, J. Chem. Eng. Data 6(1), 43 (1961); also WAPD-178.

Desaj

V. Desaj, C. Aksarnan, and D. R. Morris, J. Chem. Soc., Faraday Trans. I, 71, 1083 (1975).

Desyatnik

V. N. Desyatnik et al., Izv. Vyssh. Uchebn. Zaved. Tsvetn. Metall. 16(6), 86 (1973).

Doi

H. Doi and T. Ito, Significance of Physical State of Starting Precipitate in Growth of Uranium Dioxide Particles, J. Nucl. Mater. 11(1), 94 (1964).

Drossbach

P. Drossbach, Elektrochemie geschmolzener Salze, Verdag von Julius Springer, Berlin, p. 63, (1938).

Eastman

E. D. Eastman, D. D. Cubicciotti, and C. D. Thurmond, The Chemistry and Metallurgy of Miscellaneous Materials, L. L. Quill, Ed., McGraw Hill Company, New York, pp. 6-12 (1950).

Eck

R. Eck, Corrosion of Powder Metallurgy Molybdenum-Tungsten Alloys in Liquid Zinc, European Symposium on Powder Metallurgy, Stockholm, Sweden, June 4-8, 1978 (in German).

Eitel
W. Eitel and B. Lange, Z. Anorg. Allg. Chem. 171, 168-180 (1928); (C.A. 23:16).

Flynn
K. F. Flynn, L. J. Jardine, and M. J. Steindler, Method for Determining Leach Rates of Simulated Radioactive Waste Forms, Radioactive Waste in Geologic Storage, ACS Symposium Series 100, American Chemical Society, Washington, D.C., pp. 115-127 (1979).

Fuhrman
N. Fuhrman, L. D. Stower, Jr., and A. B. Holden, Low-Temperature Sintering of Uranium Dioxide, J. Am. Ceram. Soc. 46(3), 114 (1963).

Gardner
N. R. Gardner, Uranium Dioxide and Other Ceramic Fuels, in Nuclear Reactor Fuel Elements, A. P. Kaufmann, Ed., Interscience Publishers, New York (1962).

Gruen
D. M. Gruen and R. L. McBeth, Inorg. Chem. 8, 2625 (1969).

Herdan
G. Herdan, Small Particle Statistics, Academic Press, London (1960).

Heymann
E. Heymann and E. Fuedlander, Z. Phys. Chem A 148, 177-194 (1930) (C. A. 24:2688).

Hingston
F. J. Hingston, A. M. Posner, and J. P. Quirk, Adsorption of Selenite by Goethite. Adv. Chem. Ser. 79, 82-90 (1968).

Johnson-1964
T. R. Johnson, R. D. Pierce, L. Burris, Jr., and R. K. Steunenberg, Skull Reclamation Process Part 2, Oxidation of Melt Refining Skulls, Argonne National Laboratory Report ANL-6874 (1964).

Johnson-1965
I. Johnson, M. G. Chasanov, and R. M. Yonco, Trans. Met. Soc. AIME 233, 1408 (1965).

Johnson-1966
I. Johnson, K. E. Anderson, and R. A. Blomquist, ASM Trans. Q. 59, 352 (1966).

Johnson-1969
T. R. Johnson, F. G. Teats, and R. D. Pierce, A Method for the Purification of Molten Chloride Salts, Argonne National Laboratory Report ANL-7603 (August 1969).

Kaufman
L. Kaufman and H. Nesor, Treatise on Solid State Chemistry, Vol. 5, Plenum Press, New York, p. 179 (1975).

Knighton-1971
J. B. Knighton, G. J. Bernstein, G. N. Vargo, and R. D. Pierce, Development of a Mixer-Settler for Liquid Metal-Salt Systems, Argonne National Laboratory Report ANL-7810 (June 1971).

Knighton-1978
J. B. Knighton, Radiochemica Acta 25, 181 (1978).

Knighton-1979
J. B. Knighton, Rocky Flats Plant, private communication with M. F. Boyle (May 1979).

Krumpelt
M. Krumpelt, I. Johnson, and J. J. Heiberger, J. Less-Common Met. 18, 35 (1969).

Laughlin
W. C. Laughlin and N. W. Gregory, J. Chem. Eng. Data 20, 137 (1975).

Lawroski
S. Lawroski et al., Chemical Engineering Division Summary Report, January, February, March, 1960, Argonne National Laboratory Report ANL-6145, p. 70 (1960).

Lorenz
R. Lorenz and D. Eitel, Z. anorg Chem. 91, 46-65 (1915) (C.A. 9:1565).

McCurnin
W. R. McCurnin, Manager of Nuclear operations, Energy Systems Group, Canoga Park, California, telephone conversation (April 13, 1979).

McElroy
J. L. McElroy, Quarterly Progress Report Research and Development Activities Waste Fixation Program, October-December 1976, Battelle Pacific Northwest Laboratories Report PNL-2264 (November 1977).

Mendel
J. E. Mendel et al., Annual Report on the Characteristics of High Level Waste Glass, Battelle Pacific Northwest Laboratories Report BNWL-2252 (June 1977).

Moore
R. H. Moore, U.S. patent 2,948,586 (Aug. 1960).

Mullins
L. J. Mullins, Los Alamos Scientific Laboratories, telephone communication with T. D. Santa Cruz (May 1979).

Neal
Colin Neal and V. W. Truesdale, The Sorption of Iodate and Iodide by Riverine Sediments: Its Implications to Dilution Gauging and Hydrochemistry of Iodine, J. Hydrology 31, 281-291 (1976).

Newby
B. J. Newby and D. W. Rhodes, Ruthenium Behavior During Calcination, ICP-1164 (1978).

ORNL-1970
Aqueous Processing of LMFBR Fuels - Technical Assessment and Experimental Program Definition, ORNL-4436 (1970).

ORNL-1973
Voloxidation - Removal of Volatile Fission Products from Spent LMFBR Fuels, J. H. Goode, Ed., ORNL-TM-3723 (1973).

Piret-1950
J. W. Axelson and E. L. Piret, The Crushing of Single Particles of Crystalline Quartz, Ind. Eng. Chem. 42, 665 (April 1950).

Piret-1961
W. J. Kenny and E. L. Piret, Slow Compression Crushing of Single Particles of Glass, AIChE J. 7, 199 (June 1961).

Piret-1962
R. A. Zeleny and E. L. Piret, Dissipation of Energy in Single-Particle Crushing, Ind. Eng. Chem. Process Des. Dev. 1, 37-41 (January 1962).

Porter
J. A. Porter and A. E. Symonds, Jr., Electrowinning Plutonium Metal, Savannah River Laboratory, TID-4500 (February 1966).

Relyea
J. F. Relyea and R. J. Serne, Controlled-Sample Program, Publication Number 2: Interlaboratory Comparison of Batch K_d Values, Battelle Pacific Northwest Laboratory, PNL-2872 (June 1979).

Rickert
P. Rickert, M. G. Seitz, N. Meldgin, S. Fried, A. M. Friedman, and M. J. Steindler, Quarterly Technical Progress Report Transport Properties of Nuclear Wastes in Geologic Media for the period April-June 1979 (1979).

Ringwood
A. E. Ringwood et al., Immobilization of High-Level Nuclear Reactor Wastes in SYNROC, Nature 278, 219-223 (1979).

Rocky Flats
Rocky Flats, private communications (February 1979, March 1979).

Seitz-1978
M. G. Seitz, P. G. Rickert, S. M. Fried, A. M. Friedman, and M. J. Steindler, Studies of Nuclear-Waste Migration in Geologic Media, Annual Report November 1976-October 1977 Argonne National Laboratory Report ANL-78-8.

Seitz-1979
M. G. Seitz, P. G. Rickert, S. M. Fried, A. M. Friedman, and M. J. Steindler, Studies of Nuclear-Waste Migration in Geologic Media, Annual Report October 1977-September 1978. Argonne National Laboratory Report ANL-79-30.

Shappert
L. B. Shappert, A Guide for the Design, Fabrication, and Operation of Shipping Casks for Nuclear Applications, Oak Ridge National Laboratory Report ORNL-NSIC-68 (February 1970).

Slate
S. C. Slate, L. R. Bunnell, W. A. Ross, F. A. Simonen, J. H. Westsik, Jr., Stresses and Cracking in High-Level Waste Glass, Proceedings of the Conference on High-Level Radioactive Solid Waste Forms in Denver, Col., December 19-21, 1978, NUREG/CP-0005, p. 393.

Smith-1975
T. H. Smith and W. A. Ross, Impact Testing of Vitreous Simulated High-Level Waste in Canisters, PNWL-1903 (1975).

Smith-1979
Duane H. Smith and H. F. McDuffie, Molten Salt Processes Applied to Ceramic Fuels, First Annual Report, ORNL/TM-6763 (June 1979).

Steindler-1978A
M. J. Steindler et al., Chemical Engineering Division Fuel Cycle Programs, Quarterly Progress Report October-December 1977, Argonne National Laboratory Report ANL-78-37.

Steindler-1978B
M. J. Steindler et al., Chemical Engineering Division Fuel Cycle Programs Quarterly Progress Report, January-March 1978 Argonne National Laboratory Report ANL-78-68.

Steindler-1979A
M. J. Steindler et al., Chemical Engineering Division Fuel Cycle Section Quarterly Progress Report, July-September 1978, Argonne National Laboratory Report ANL-79-6.

Steindler-1979B
M. J. Steindler et al., Chemical Engineering Division Fuel Cycle Programs, Quarterly Progress Report, October-December 1978, Argonne National Laboratory Report ANL-79-29.

Steindler-1979C
M. J. Steindler et al., Fuel Cycle Program, Quarterly Progress Report, January-March 1979, Argonne National Laboratory Report ANL-79-45.

Stull
D. R. Stull et al., JANAF Thermochemical Tables, 2nd Ed., NSRDS-NBS 37 (1971).

Thompson
M. Thompson and A. Kaye, Trans. Electrochem Soc. 67, 169 (1935).

Thonstead
J. Thonstead, and E. Hove, On the Anode's Overvoltage in Aluminum Electrolysis, Can. J. Chem. 42, 1542 (1964).

Threadgill
W. Threadgill, J. Electrochem. Soc, 11, 1408 (1964).

Toth
T. S. Toth and N. A. Lockington, J. Less-Common Met. 12, 353-365 (1967).

Wade
W. Z. Wade and T. Wolf, The Production of Plutonium Metal by Direct Reduction of the Oxide, UCRL 50403 (1968).

Whitehead
D. S. Whitehead, The Sorption of Iodide by Soils as Influenced by Equilibrium Conditions and Soil Properties, J. Sci. Food Agri. 24, 547-556 (1973).

Yamamoto
A. S. Yamamoto and W. Rostoker, Trans. Am. Soc. Met. 50, 1090 (1958).